INSTITUTE

FOR

COSMIC RAY RESEARCH

UNIVERSITY OF TOKYO

ANNUAL REPORT
(APRIL 2008 – MARCH 2009)

5-1-5, Kashiwanoha, Kashiwa, Chiba 277-8582, Japan

Telephone: (81) 4-7136-3102
Facsimile: (81) 4-7136-3115
WWW URL: http://www.icrr.u-tokyo.ac.jp/

TABLE OF CONTENTS

PREFACE

This report summarizes the scientific activities of the Institute for Cosmic Ray Research (ICRR) of the University of Tokyo in the Japanese FY 2008.

ICRR is an inter-university research institute for studies of cosmic rays. The headquarters of ICRR is located in Kashiwa, Chiba prefecture, Japan. In order to promote various cosmic-ray-related studies efficiently, ICRR has three research divisions; Neutrino and Astroparticle division, High Energy Cosmic Ray division, and Astrophysics and Gravity division. ICRR has 3 observatories in Japan; Kamioka Observatory (Kamioka underground, Gifu prefecture), Norikura Observatory (2770 meters asl, Mt. Norikura, Gifu prefecture), and Akeno Observatory (Yamanashi prefecture). In addition, there are 3 major experimental facilities outside of Japan. They are located in Utah in USA, Yangbajing in Tibet, China, and Woomera in Australia.

More than 300 researchers from various Japanese institutions are involved in the research programs of ICRR. It should be noted that most of the scientific outputs from this institute are the results of the collaborative efforts by many institutions. In order to produce outstanding results, it is very important to carry out an experiment by an international collaboration composed of top-level researchers all over the world. Hence, most of the experimental collaborations that ICRR is involved are international ones. For example, the number of collaborators in the Super-Kamiokande experiment is about 130; among them 60 are from abroad (USA, Korea, China, Poland and Spain).

Many exciting scientific activities are described in this report. One of the highlights is the start of the full operation of the Telescope Array experiment, which is a very large scale cosmic ray experiment to study the highest energy cosmic rays. We hope that this report is useful for the understanding of the current research activities of ICRR. Finally, we appreciate very much the strong support of our colleagues in this research field, the University of Tokyo and the Japanese Ministry of Education, Culture, Sports, Science and Technology. They are indispensable for the continuing, and exciting scientific outcome of ICRR.

Takaaki Kajita,
Director,
Institute for Cosmic Ray Research,
The University of Tokyo

The ICRR building at Kashiwa, Chiba, Japan.

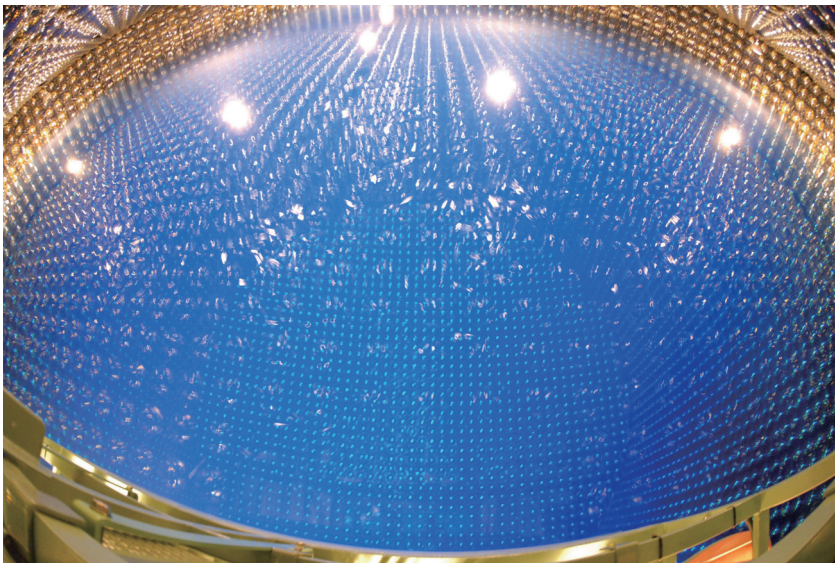

The inner detector of Super-Kamiokande-III during the full reconstruction. The purified water is under filling.

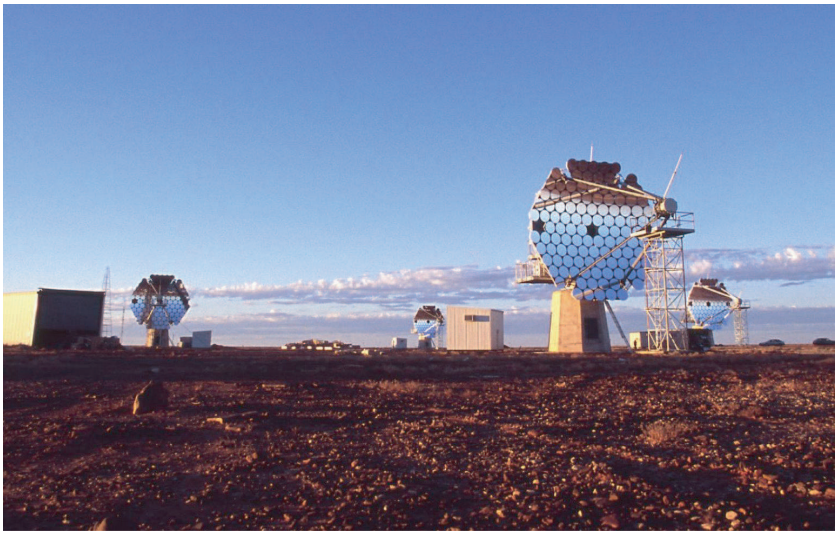

The system of four imaging atmospheric Cherenkov telescopes of 10m diameter of CANGAROO project for detection of very high energy gamma-rays The whole system is in operation since March 2004 in Woomera, South Australia.

Tibet-III air shower array (37000 m^2) at Yangbajing, Tibet (4300 m in altitude).

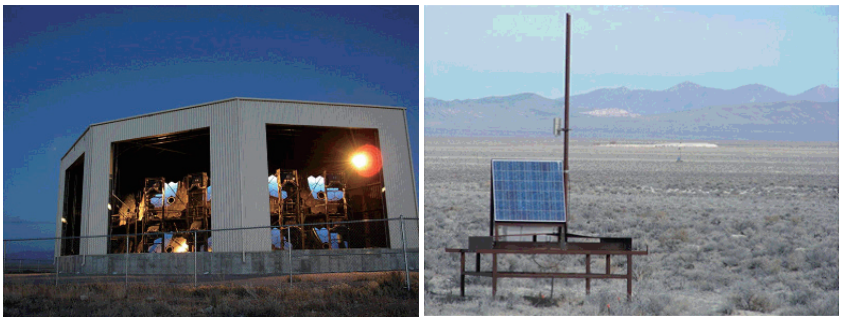

Air fluorescence telescopes (left) and a scintillator surface detector (right) of the Telescope Array experiment in Utah, USA to explore the origin of extremely high energy cosmic rays.

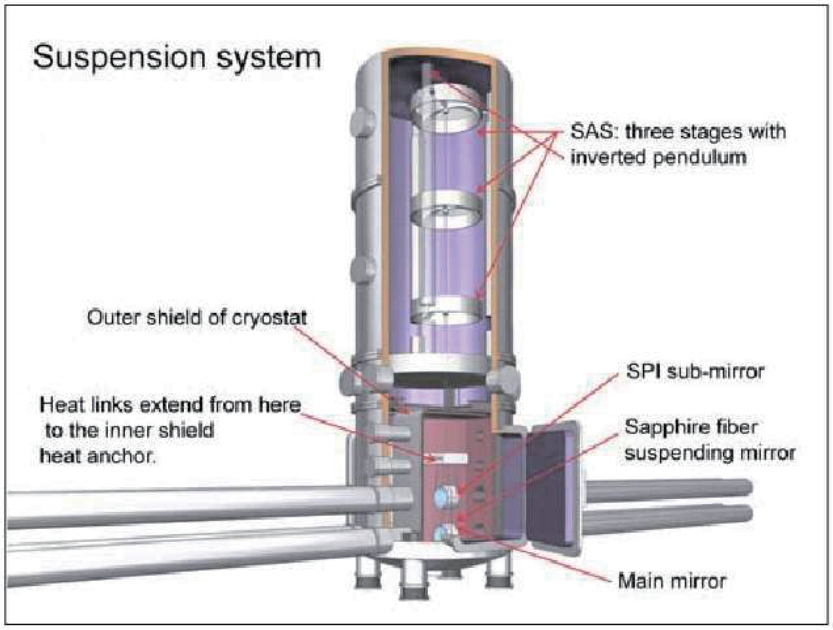

Cryogenic mirror suspension system for Large Scale Cryogenic Gravitational Wave Telescope.

Wide-view telescope of 2.5 m diameter (left telescope) in Arizona, USA for the Sloan Digital Sky Survey project.

A public lecture held by Research Center for Cosmic Neutrinos.

Organization

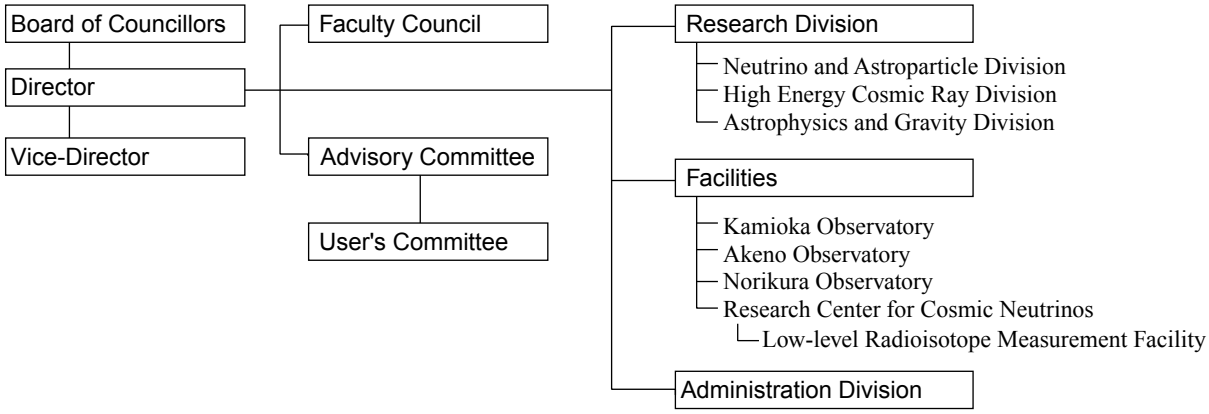

Number of Staff Members in 2008

	Scientific Staff	Technical Staff	Research Fellows	Administrators and Secretaries	
Neutrino and Astroparticle Div.	21	4	4	15	44
High Energy Cosmic Ray Div.	13	8	6	4	31
Astrophysics and Gravity Div.	8	0	3	2	13
Administration	1	0	0	13	14
Total	43	12	13	34	102

FY 2003–2008 Budget

	2003	2004	2005	2006	2007	2008
Personnel expenses	434 874	539 000	465 000	566 000	624 000	632 000
Non-personnel expenses	1 785 449	1 902 000	1 822 000	812 000	1 253 000	1 121 000
Total	2 220 323	2 441 000	2 287 000	1 378 000	1 877 000	1 753 000

(in 1 000 yen)

RESEARCH DIVISIONS

Neutrino and Astroparticle Division

Overview

Super-Kamiokande Experiment

T2K Experiment

XMASS Experiment

High Energy Cosmic Ray Division

Overview

CANGAROO-III Project

TA: Telescope Array Experiment

Tibet ASγ Project

Ashra Project

Astrophysics and Gravity Division

Overview

Gravitational Wave Group

- CLIO Project
- LCGT Project

Sloan Digital Sky Survey

Theory Group

- Neutrino mass, Dark Matter and Baryon Asymmetry via TeV-Scale Physics without Fine-Tuning
- Light Higgs boson scenario in the SUSY seesaw model
- D-term assisted Anomaly Mediation in E6 motivated models
- Precision Measurements of Little Higgs Parameters at the International Linear Collider
- Non-linear evolution of matter power spectrum in modified theories of gravity
- Flavor physics in supersymmetric theories
- Probing reheating temperature of the universe with gravitational wave background
- Direct/indirect detection signatures of non-thermally produced dark matter
- Non-Gaussianity from isocurvature perturbations
- Hilltop Non-Gaussianity
- Cosmic Rays from Dark Matter Annihilation and Big-Bang Nucleosynthesis
- Cosmological Moduli Problem from Thermal Effects
- Neutrino Signals from Annihilating/Decaying Dark Matter in the Light of Recent Measurements of Cosmic Ray Electron/Positron Fluxes
- Upperbound on Squark Masses in Gauge-Mediation Model with Light Gravitino
- A Realistic Extension of Gauge-Mediated SUSY-Breaking Model with Superconformal Hidden Sector
- Non-Gaussianity from Symmetry
- Primordial Curvature Fluctuation and Its Non-Gaussianity in Models with Modulated Reheating
- Exact gravitational lensing by cosmic strings with junctions

NEUTRINO AND ASTROPARTICLE DIVISION

Overview

This division aims to study particle physics that is not accessible within accelerator facilities, with prime interests in physics of neutrinos and proton decay, and astroparticle physics with the use of underground experimental facilities.

Our most important facility is the Super-Kamiokande (SK) detector. It is a 50 kton water Cherenkov detector using 11,129 50 cm-diameter photomultipliers (PMTs) for its inner detector and 1,885 20 cm-diameter PMTs for its outer detector. The data taking of SK started in April 1996. The most important physics results are the discovery of neutrino oscillation in atmospheric neutrinos in 1998 and thereby demonstrating that neutrinos have a finite mass, and the accurate measurement of the solar neutrino flux from the decay of ^{8}B which served to confirm the long-conjectured neutrino oscillation hypothesis in solar neutrinos beyond doubt. The search for nucleon decay at SK gives the current best limit which strongly constrains the grand unification scenario of particle interactions. SK has been monitoring for neutrinos from supernova bursts. If a supernova burst occurs at a distance from the center of our galaxy, SK will be able to detect about 8,000 neutrino events. A high intensity neutrino beam experiment at J-PARC (T2K) is expected to start in 2009 with the SK detector as the far detector of the experiment. High precision measurement of oscillation parameters and the third oscillation pattern (the effect of the mixing angle θ_{13}) will be investigated by T2K.

Another activity of the Neutrino and Astroparticle division is a multi-purpose experiment using liquid xenon aiming at the detection of cold dark matter, neutrino absolute mass using neutrinoless double beta decay, and low energy solar neutrinos. An R&D study for the liquid xenon detector has been performed at the underground laboratory and the construction of the 800 kg detector started in 2007.

Recent progress of research activities in the Neutrino and Astroparticle division is presented here.

Super-Kamiokande experiment

New electronics system

To ensure stable observation for the next 10∼20 years and to improve sensitivity of the detector, the SK electronics system was fully upgraded in September 2008.

Figure 1 shows a picture of our new front-end electronics, QBEE (QTC-Based Electronics with Ethernet). The QBEE is a TKO-standard module which has 24 input channels. Essential components on the QBEE for the analog signal processing and digitization are the QTC (Charge-to-Time Converter) ASIC [1] and the multi-hit TDC. The QTC detects PMT signals by individual built-in discriminators and drives output timing signals whose width represents the integrated charge of the PMT signal. Timing information on both edges

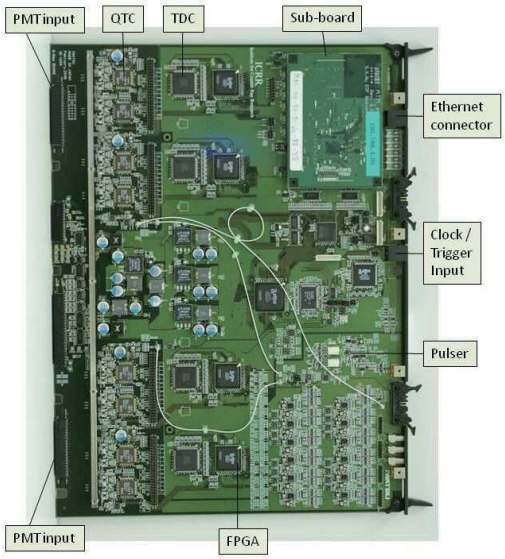

Fig. 1. New front-end electronics, QBEE. PMT signals are fed through the backplane (left side). The Ethernet cable for the data readout and the board control is connected at the front panel (right side) as well as the UTP cable for the 60MHz system clock input.

of a QTC output signal is digitized by the AMT-3 multi-hit TDCs. An FPGA then reads and processes the data stored in the TDC internal buffer continuously by a unit of 17μsec. The QBEE realizes high-speed signal processing by combining the pipelined components like the QTC, TDC and FPGA. The QBEE has an on-board calibration pulser which is used for monitoring and correcting the charge measurement by the QTCs under possible ambient temperature changes.

The high-speed QTC was developed as a custom ASIC in CMOS 0.35μm technology. Figure 2 shows a picture of the internal circuit of the QTC chip. The QTC has three input channels per chip. Each channel has three gain ranges: Small, Medium, and Large. The gain ratio of three ranges, which can be adjusted by external resistor networks, is set to $1{:}\frac{1}{7}{:}\frac{1}{49}$. The overall charge dynamic range of the QTC is 0.2-2500pC, which is about 5 times wider than that of the previous front-end electronics used in SK. The width of the charge integration gate in the QTC is set to 400nsec. The charge integration circuits are triggered by the input PMT signal itself (self-triggering scheme). To reduce charge leakage, the PMT signal to be integrated is delayed by a second-order voltage-controlled voltage source (VCVS) low-pass filter (LPF) in the QTC. Soon after the end of the charge gate, the discharging timer operates for ∼350nsec Input signals within ∼250nsec after the discharge gate are ignored. In total, processing time for one input signal is ∼1000nsec.

The charge and timing resolutions of the QBEE for the single p.e. level signals are 10% and 0.3nsec, respectively,

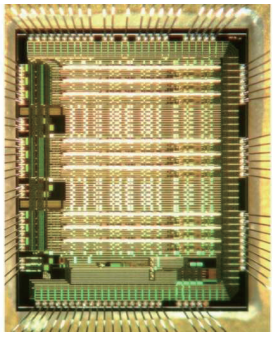

Fig. 2. The internal circuit of the QTC ASIC.

both better than the intrinsic resolutions of the 20-inch PMTs in SK. The QBEE achieves good charge linearity over a wide dynamic range. The charge nonlinearity (i.e. deviation from a linear fitted function) is within $\pm 1\%$ and satisfies our requirements. The discriminators in the QTC can be operated with a -0.3mV threshold, equivalent to 1/10p.e.s, without suffering from intrinsic electrical noise or channel crosstalk.

A total of 553 QBEEs are used in SK, 472 for the inner detector PMTs, 80 for the outer detector PMTs, 1 for a special use to record the flash timings of light sources for various detector calibrations. All the QBEEs operate synchronized by a common 60MHz master clock, which is generated by the MCLK module (see Fig. 3). The MCLK module also generates a 17μsec-cycle periodic trigger for the TDCs on the QBEE. The combination of the periodic TDC trigger and the high-speed signal processing by the QBEEs enables us to record every hit of all the PMTs, including hits by PMT's dark current. This "record every hit" data acquisition is one of the most prominent features of the new electronics system. In the previous system, event triggers were issued when the number of hit PMTs exceeded a certain threshold and only the PMT signals in a 1.3μsec window around the event trigger were processed by front-end electronics. To achieve the "record every hit" data acquisition, the speed of data readout from the front-end electronics and subsequent data processing by the online PC system is also important.

We adopted an Ethernet technology for data readout from the QBEE. The network interface sub-board attached to the QBEE has an FPGA network firmware called SiTCP and gives a 100BASE-TX data transfer. In the previous electronics system, 20 front-end electronics modules shared a TKO bus for data readout and the transfer speed of a TKO bus was about 4MB/sec. The Ethernet enables a parallel readout from the QBEEs. The measured data throughput of a QBEE achieves 11.75MB/sec, which is almost the theoretical limit of the 100BASE-TX and fast enough to realize the "record every hit" data acquisition. In addition, implementing the digital readout on the ethernet daughterboard suppresses readout noise compared to backplane readout, and allows us to achieve a low single photo electron threshold.

The data processed by the QBEEs are collected by 20 Front-end PCs via Ethernet cables and network switches. The hit data are then sorted in time order and sent to the Merger PCs. A software-trigger program is running on the Merger PC to extract an event from all the hit data of all the PMTs. A basic condition of the software-trigger is based on the number of hit PMTs in a certain time window. The special conditions triggered by an external signal input are also prepared for detector calibrations. The software-triggered event data are collected by the Organizer PC and recorded on a disk. A large amount of the data taken by the "record every hit" scheme are successfully processed by the parallel distributed processing in the online system.

The data-taking by the new electronics system started on September 6th, 2008. The present phase of the experiment after the electronics system replacement is called SK-IV. The SK-IV detector performance/sensitivity is much improved for various observations. For example, the result of a test using a high-rate flashing light pulser shows that the SK-IV can take the data from a supernova neutrino burst up to a rate of 6 million events/10sec with no data loss. This limit is about 100 times as large as that of the previous SK phases and is about 1000 times as large as an expected event rate in case of a supernova at the galactic center. The detection of $\mu \to e$ decays is very important to classify interactions in neutrino oscillation analyses or nucleon decay searches. Figure 4 shows the decay time distribution of the $\mu \to e$ decay events. The detection efficiency after 1μsec from the parent muon event timing reaches almost 100%. The high-speed front-end electronics with a better impedance matching to the PMT signal cable gives a better detection efficiency for $\mu \to e$ decays in SK-IV.

Fig. 3. The MCLK module. The 60MHz master clock and 17μsec-cycle periodic trigger are produced as LVDS signals from the RJ45 jack on the front-panel.

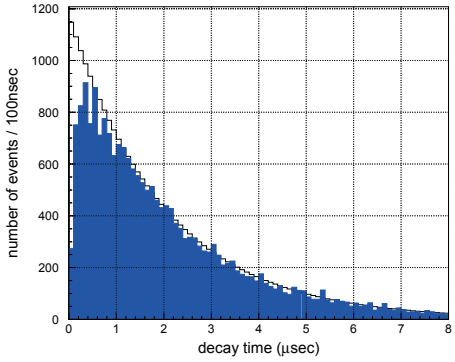

Fig. 4. Decay time of the $\mu \to e$ decay events. The curve shows the number of electrons by muon decays which is estimated by the muon lifetime and the total number of stopping muon events. The hatched histogram shows the detected $\mu \to e$ decay events.

The "record every hit + software-trigger" system will also enable us to detect a delayed signal by the 2.2MeV γ-ray after the neutron capture, which was not feasible with the previous electronics system, because the signal by a 2.2MeV γ-ray is too faint for a hardware trigger. Tagging of neutrons using a delayed 2.2MeV γ-ray signal will help us to reduce background events in a search for supernova relic neutrino events.

The SK-IV observation has been very stable. We hope to achieve brand-new results using the data taken by the new electronics system soon.

Atmospheric neutrinos

Cosmic ray interactions in the atmosphere produce neutrinos. The prediction of the absolute flux has an uncertainty of at least $\pm 20\,\%$. However, the flavor ratio of the atmospheric neutrino flux, $(\nu_\mu + \bar{\nu}_\mu)/(\nu_e + \bar{\nu}_e)$, has been calculated to an accuracy of better than $5\,\%$. Another important feature of atmospheric neutrinos is that the fluxes of upward and downward going neutrinos are expected to be nearly equal for $E_\nu >$(a few GeV) where the geomagnetic effect on primary cosmic rays is negligible.

SK-I observed 11,866 fully-contained (FC) events and 898 partially-contained (PC) events during 1489 days of data taking and SK-II observed 6684 FC events and 430 PC events during 804 days. FC events deposit all of their Cherenkov light in the inner detector, while PC events have exiting tracks which deposit some Cherenkov light in the outer detector. The neutrino interaction vertex was required to have been reconstructed within the 22.5 kiloton fiducial volume, defined to be > 2 m from the PMT wall.

The FC events were classified into "sub-GeV" ($E_{vis} <$ 1330 MeV) and "multi-GeV" ($E_{vis} > 1330$ MeV) samples. Among FC events, single-ring events are identified as e-like or μ-like based on a Cherenkov ring pattern. The momentum resolution of SK-II is slightly worse than SK-I. This is because the number of ID PMTs in SK-II is about half that of SK-I. However, the performance of the vertex reconstruction, the ring counting, and the particle identification in SK-II are almost the same as in SK-I. Some fraction of the multi-ring events is also subdivided into e-like and μ-like events using the event pattern of the most energetic Cherenkov ring in each event.

Energetic atmospheric ν_μ's passing through the Earth interact with rock surrounding the detector and produce muons via charged current interactions. These neutrino events are observed as upward going muons. Upward going muons are classified into two types. One is "upward through-going muons" which have passed through the detector, and the other is "upward stopping muons" which come into and stop inside the detector. The mean neutrino energy of upward through-going muons and upward stopping muons is $\sim$100 GeV and $\sim$10 GeV, respectively. SK-I observed 1856 upward through-going muons and 458 upward stopping muons during 1646 day livetime exposure and SK-II observed 889 and 228 events during 828 days, respectively.

The zenith angle distributions for each samples compared with atmospheric neutrino M.C. predictions are shown in Fig. 5. The prediction is based on the recent precise measure-

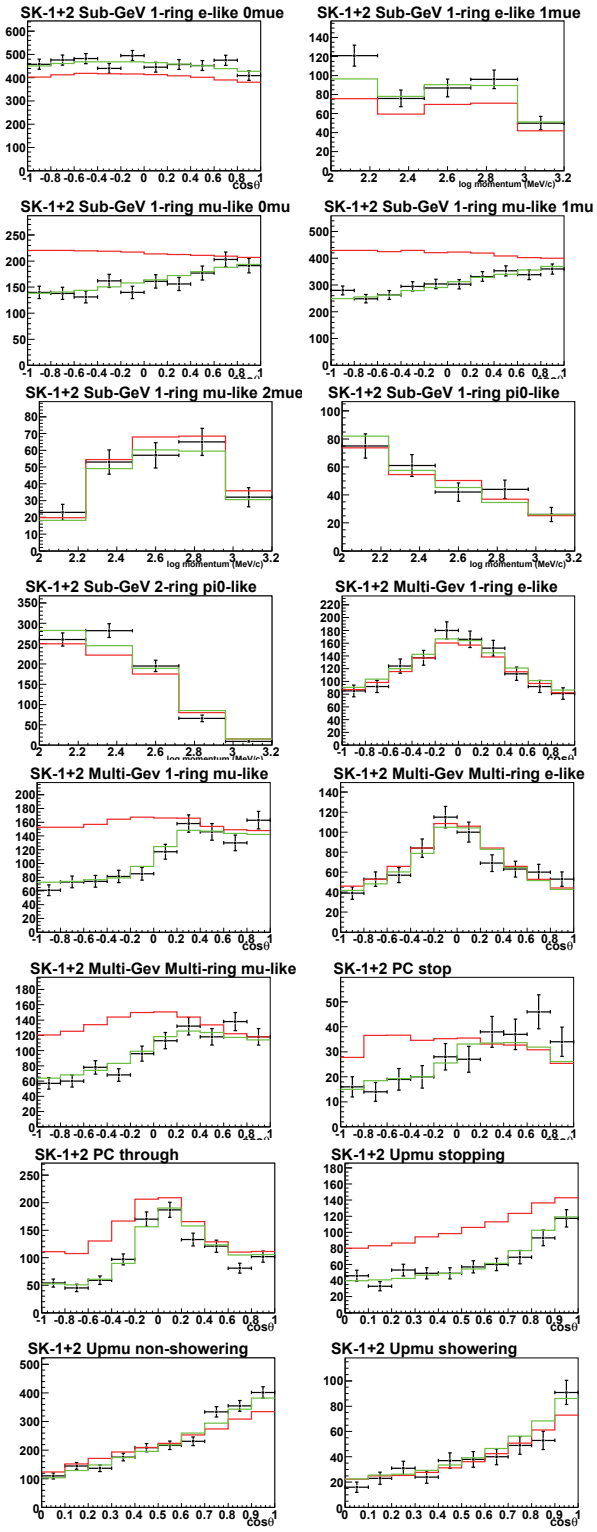

Fig. 5. The zenith angle distributions for each data sample. cosΘ =1 means down-going particles. The red histograms show the MC prediction without neutrino oscillation. The green histograms show the Monte Carlo prediction for $\nu_\mu \leftrightarrow \nu_\tau$ oscillations with $\sin^2 2\theta = 1.0$ and $\Delta m^2 = 2.1 \times 10^{-3}\mathrm{eV}^2$.

ments of primary cosmic rays by BESS, AMS and a three dimensional calculation of the neutrino flux by Honda *et al*. The hadronic interaction model of cosmic rays is also improved in the calculation. The μ-like data from SK exhibit a strong up-down asymmetry in zenith angle (Θ) while no significant asymmetry was observed in the e-like data. The data were compared with the Monte Carlo expectation without neutrino oscillations and the best-fit expectation for $\nu_\mu \leftrightarrow \nu_\tau$ oscillations. The oscillated Monte Carlo reproduced the zenith angle distributions of the data well.

We carried out a neutrino oscillation analysis using the entire SK-I and II atmospheric neutrino data set. Figure 6 shows the allowed neutrino oscillation parameter regions for $\nu_\mu \leftrightarrow \nu_\tau$ oscillations. The best fit oscillation parameters are $\sin^2 2\theta = 1.0$ and $\Delta m^2 = 2.1 \times 10^{-3}\mathrm{eV}^2$. The allowed oscillation parameter range is $\sin^2 2\theta > 0.95$ and $\Delta m^2 = (1.7 - 2.7) \times 10^{-3}\mathrm{eV}^2$ at 90 % C.L.

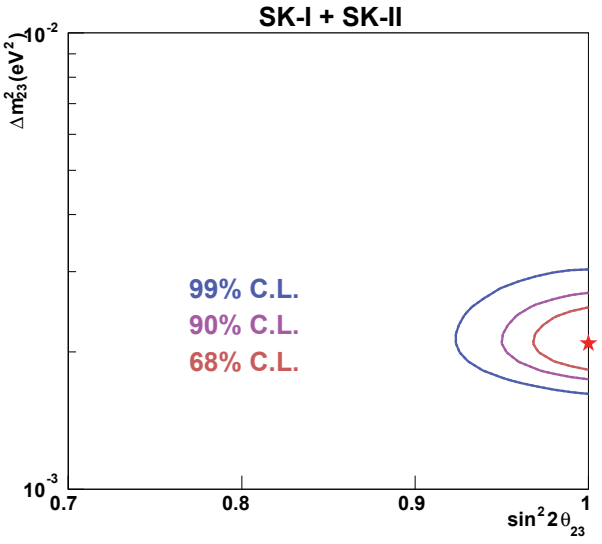

Fig. 6. Allowed region of $\nu_\mu \rightarrow \nu_\tau$ neutrino oscillation parameters obtained by SK using contained atmospheric neutrino events and upward-going muon events.

The atmospheric neutrino data is well described by neutrino oscillations as shown above. In this case, the survival probability of a ν_μ is given by a sinusoidal function of L/E, where L is the travel distance. E is the neutrino energy. However, the sinusoidal L/E dependence of this survival probability of ν_μ has not yet been directly observed. We used a selected sample of these atmospheric neutrino events, those with good resolution in L/E, to search for an oscillation maximum in the L/E distribution.

The neutrino energy, E, was estimated from the total energy of charged particles observed in the inner detector. The flight length of neutrinos, L, which ranges from approximately 15 km to 13,000 km depending on the neutrino zenith angle, was estimated from the reconstructed neutrino direction. The neutrino direction was taken to be along the total momentum vector of all observed particles. Since the correlation between the neutrino directions and the directions of observed particles is taken into account in the Monte Carlo simulations, we applied the same analysis techniques to both real events and

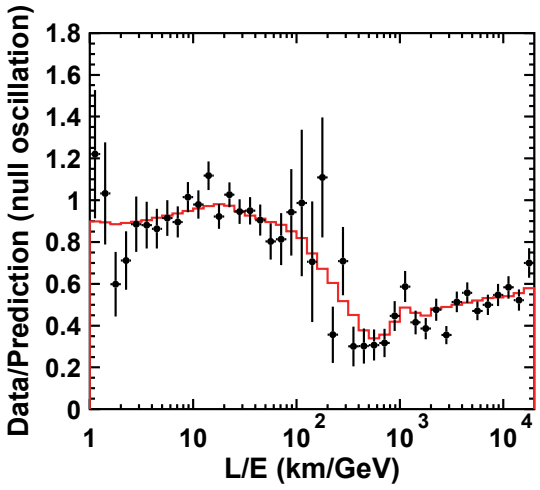

Fig. 7. Ratio of the data to the MC events without neutrino oscillation (points) as a function of the reconstructed L/E together with the best-fit expectation for 2-flavor $\nu_\mu \leftrightarrow \nu_\tau$ oscillations (red line). The error bars are statistical only.

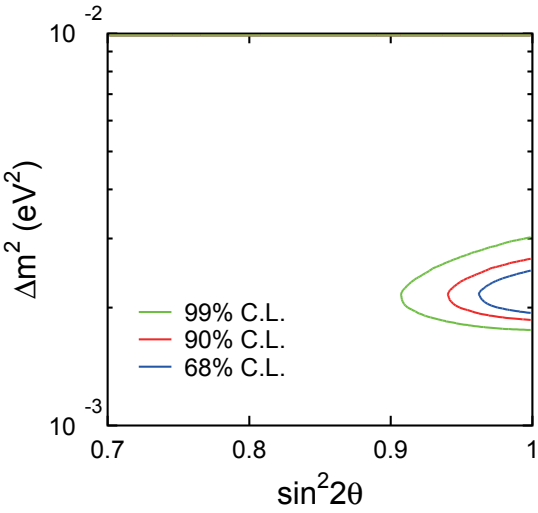

Fig. 8. 68, 90 and 99 % C.L. allowed oscillation parameter regions for 2-flavor $\nu_\mu \leftrightarrow \nu_\tau$ oscillations obtained in the L/E analysis.

Monte Carlo events. We applied a cut to reject low energy or horizontal-going events since they have either large scattering angles or large $dL/d\Theta_{\mathrm{zenith}}$.

Figure 7 shows the observed L/E distribution of the ratio of data events to unoscillated MC events. In the figure, a dip which corresponds to the first oscillation maximum, is observed around $L/E = 500\,\mathrm{km/GeV}$. The distribution was fit assuming $\nu_\mu \leftrightarrow \nu_\tau$ oscillations. The best-fit expectation shown in the figure corresponds to $(\sin^2 2\theta, \Delta m^2) = (1.00, 2.2 \times 10^{-3}\mathrm{eV}^2)$. Figure 8 shows the contour plot of the allowed oscillation parameter regions. This result is consistent with that of the oscillation analysis using zenith angle distributions. The observed L/E distribution gives the first direct evidence that the neutrino survival probability obeys the sinusoidal function predicted by neutrino flavor oscillations.

Another interest is an observation of ν_τ in the atmospheric neutrinos since there has not yet been evidence for appear-

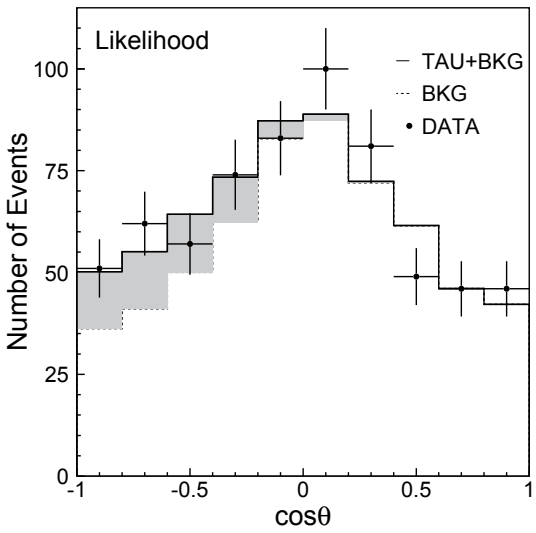

Fig. 9. The zenith angle distribution for tau candidate events in the likelihood analysis. The dashed histogram (background neutrinos) and the solid line (excess of ν_τ) show the best fit for the data.

ance of ν_τ charged current interactions due to $\nu_\mu \leftrightarrow \nu_\tau$ oscillations. We have performed a search for the ν_τ appearance by using the SK-I atmospheric neutrino data [2]. The analysis is based on two statistical methods: a likelihood analysis and a neural network. Since τ's produced in the Super-K detector would immediately decay into many hadrons, the event pattern would be similar to that of high-energy multi-ring ν_e events. Using the statistical difference in τ-like and background events, we have derived variables to select an enriched sample of ν_τ charged current events in the atmospheric neutrino data. The differences appear in the energy spectrum, the number of charged pions in the final state, and in the fraction of lepton energy with respect to neutrino energy. We optimized a combination of the variables and defined a likelihood function so that the signal to noise ratio becomes maximal. We also use the neural network for the analysis. Before these analyses, we applied pre-selection cuts on: (1) fiducial volume, (2) multi-GeV, and (3) the most energetic ring is *e*-like.

After the pre-selection cuts based on the likelihood and neural network, we fit the zenith angle distribution of the ν_τ enriched sample to a combination of the expected ν_τ and the atmospheric neutrinos (ν_μ and ν_e) including oscillations at $\sin^2 2\theta = 1.0$ and $\Delta m^2 = 2.1 \times 10^{-3}\mathrm{eV}^2$. Fig. 9 shows the fitted zenith angle distribution. Using τ selection efficiencies estimated by Monte Carlo study, we concluded the number of tau events during the SK-I exposure is $138 \pm 48^{+14.8}_{-31.6}$ with the likelihood analysis and $134 \pm 48^{+16.0}_{-27.2}$ with the neural network while 78.4 ± 26 and 8.4 ± 27 are expected for each analysis. Thus the fitted results are found to be consistent with pure $\nu_\mu \leftrightarrow \nu_\tau$ oscillations and ν_τ appearance.

Two flavor neutrino oscillations successfully describe the SK atmospheric neutrino data. However, contributions by electron neutrino oscillations have not been observed yet. We extended our neutrino oscillation analysis in order to treat three neutrino flavors. For the analysis, $\Delta m^2_{23} \sim \Delta m^2_{13} \equiv \Delta m^2 >> \Delta m^2_{12}$ was assumed. If the parameter θ_{13} in the

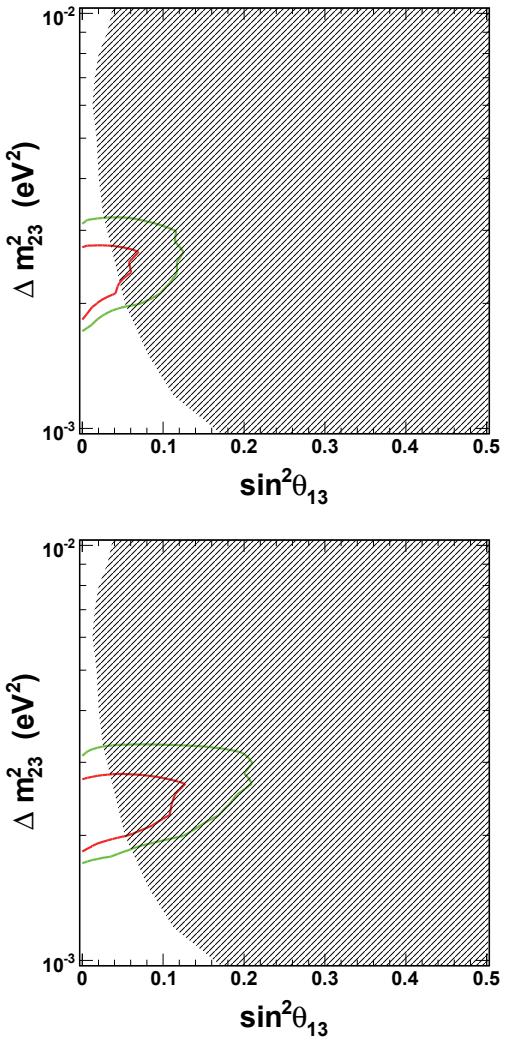

Fig. 10. The allowed region for (Δm^2, $\sin^2\theta_{13}$) for the normal (upper figure) and inverted (lower figure) hierarchy. We assumed positive Δm^2. The red and blue contours correspond to allowed regions obtained by this analysis. The hatched region corresponds to 90% C.L. excluded area by CHOOZ experiment.

mixing matrix of lepton sector (MNS matrix) is finite, neutrino oscillations among $\nu_\mu \leftrightarrow \nu_e$ may be observed. Moreover, the mixing parameter is affected by potentials caused by matter and oscillations are expected to be resonantly enhanced around 5 GeV. Therefore, we can expect an increase of upward-going Multi-GeV *e*-like events. Fig. 10 shows the result of the three-flavor neutrino oscillation analysis. Though there was no significant excess of electrons, we set an upper limit on θ_{13}. More statistics are needed to improve sensitivity [3].

We also studied deviations of $\sin^2\theta_{23}$ from 0.5 assuming $\theta_{13} = 0$. If the contribution of 1-2 parameters ($\Delta m^2_{12}, \sin^2\theta_{13}$) are considered, the enhancement (or reduction) of low energy ν_e flux is expected in the case of $\theta_{23} < (>)\pi/4$. The oscillation analysis was performed with and without 1-2 oscillation parameters. Figure 11 shows $\chi^2 - \chi^2_{min}$ distributions as a function of $\sin^2\theta_{23}$ for oscillations with 1-2 parameters (solid line) and without 1-2 parameters (dotted line). There was no sig-

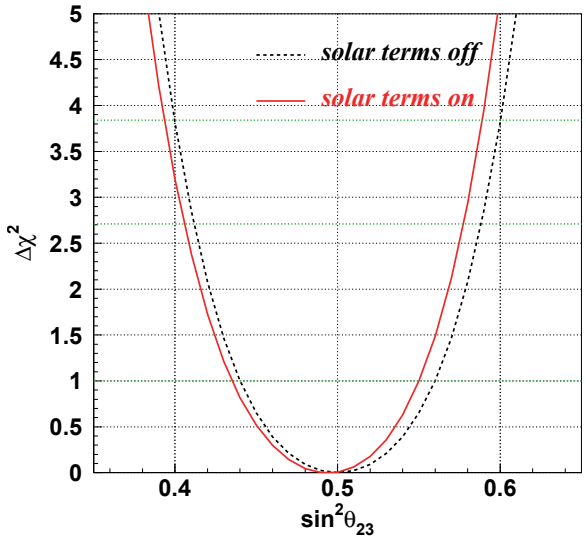

Fig. 11. $\chi^2 - \chi^2_{min}$ distributions as a function of $sin^2\theta_{23}$ for oscillations with 1-2 parameters (solid line) and without 1-2 parameters (dotted line).

nificant discrepancy of θ_{23} from $\pi/4$. $\sin^2\theta_{23}$ is constrained too $0.44 \geq \sin^2\theta_{23} \geq 0.55$ at one σ level.

In addition to neutrino oscillations, several attempts are proposed to explain the atmospheric neutrino problem. We tested the possibility of $\nu_\mu - \nu_\tau$ oscillation + non standard neutrino-matter interactions, flavor changing neutral current and lepton non universality. We obtained no evidence of NSI signal, we set 90% C.L. limits for the NSI parameters, $|\varepsilon_{\mu\tau}| < 1.1 \times 10^{-2}$, $-4.9 \times 10^{-2} < \varepsilon_{\tau\tau} - \varepsilon_{\mu\mu} < 4.9 \times 10^{-2}$, $|\varepsilon_{e\tau}| < 0.16$ and $-0.05 < \varepsilon_{\tau\tau} < 0.06$.

We performed several studies to search for astrophysical sources of high energy neutrinos using the Super-Kamiokande-I neutrino induced upward-going muon data. The data set consists of 2359 events with a minimum energy 1.6 GeV, of which 1892 are through-going and 467 stop within the detector. No statistically significant evidence for point sources or any diffuse flux from the galactic plane is found. The 90 % C.L. upper limits on upward-going muon flux from astronomical sources which are located in the southern hemisphere and always under the horizon for Super-Kamiokande are $(1 \sim 4) \times 10^{-15}\mathrm{cm}^{-2}\mathrm{s}^{-1}$[4] [5].

Solar neutrinos

SK detects solar neutrinos through neutrino-electron scattering, $\nu + e \rightarrow \nu + e$, with which the energy, direction and time of the recoil electron are measured. Due to its large fiducial mass of 22.5 kilotons, SK gives the most precise measurement of the solar neutrinos' flux with accurate information of the energy spectrum and time variations. For this precision experiment precise calibrations are performed for the energy scale, energy resolution, angular resolution and the vertex position resolution using a LINAC and ^{16}N radioisotope generated by a DT neutron generator.

In this year, we have started to improve SK-III data analysis. We have locate a 0.5nsec order problem in the timing calibration, then fixed the 10cm level vertex shift. This will

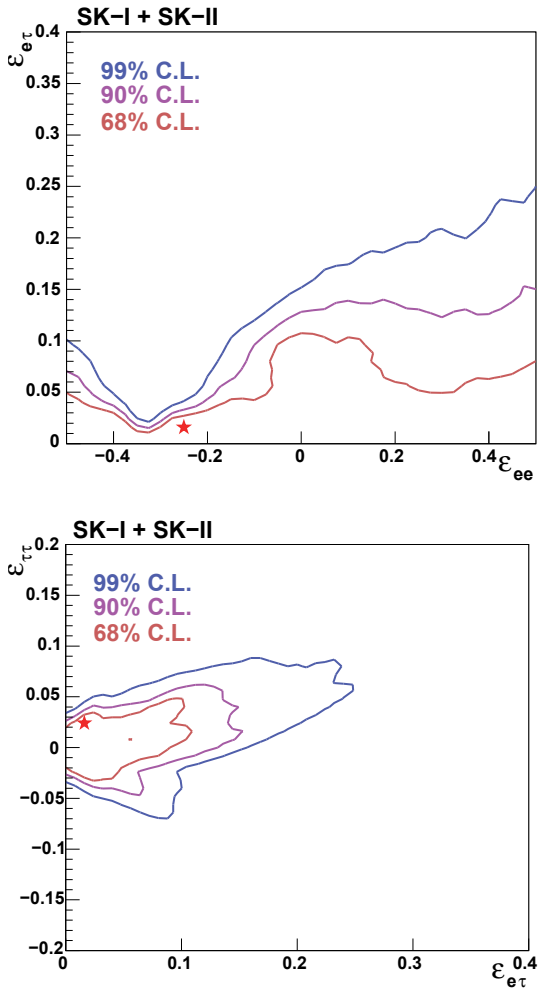

Fig. 12. Allowed NSI parameters region for ε_{ee}*v.s.*$\varepsilon_{e\tau}$ (top) and $\varepsilon_{e\tau}$*v.s.*$\varepsilon_{\tau\tau}$ (bottom).

reduce the systematic error on solar neutrino flux by the vertex shift. The water quality during SK-III period are also studied precisely, then obtained water absorption parameter as a function of time. The data reduction cuts are also under optimizing to SK-III data.

We have also lowered energy threshold of SK-III detector from 5.0MeV to 4.5MeV on April 16. These are total energy of recoil electrons. Figure 13 shows the low-energy data reduction steps from April 16, 2008 until the end of SK-III (August 17, 2008). SK-III shows a lower event rate in the central 13.3kt in the final data sample, though the event rates in SK-III are consistent with those in SK-I in the 22.5kt fiducial volume.

Figure 14 shows the angular distributions of the final data sample in the central 13.3kton region. The background rates in the 5.0-5.5MeV region have been improved in SK-III, though the signal rate is consistent. We are planning to summarize the SK-III solar neutrino results in 2009.

SK-IV has been started in September. The software trigger system is used in SK-IV, so essentially there is no trigger threshold. Since the current data acquisition computer power is limited, we are currently accumulating the solar neutrino

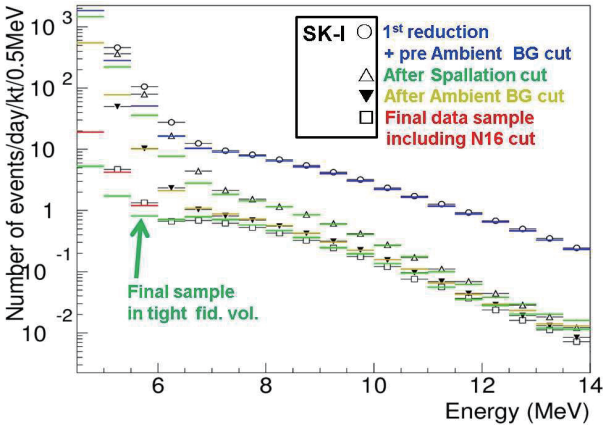

Fig. 13. The data reduction steps in SK-III during April 16 and August 17 in 2008. The colored lines are from SK-III, and the black plots are from SK-I. The tight fiducial volume cut to select central 13.3kt is applied to the data below 6.0MeV. The 22.5kton fiducial volume is applied above 6.0MeV.

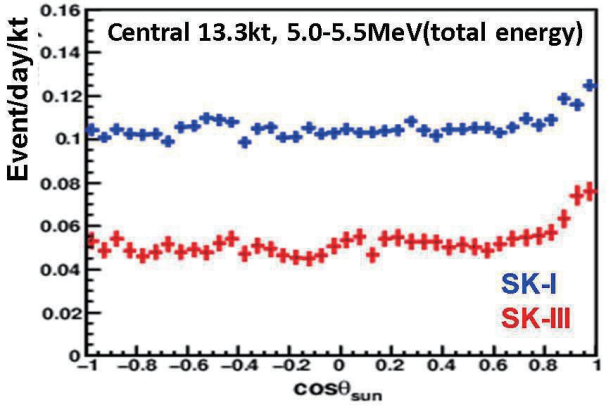

Fig. 14. The angular distribution in the central region of the SK detector. The blue and red plots correspond to SK-I and SK-III, respectively. The vertical and horizontal length are 23.6m and $R^2 \leq 180m^2$, and the fiducial volume is 13.3kton in these plots.

data with the same energy threshold level as SK-III. Now, we are trying to introduce the new computer system to achieve 100% event selection efficiency at 3.5MeV in electron total energy.

Search for nucleon decay

Proton decays and bound neutron decays (nucleon decays in general) is the most dramatic prediction of Grand Unified Theories in which three fundamental forces of elementary particles are unified into a single force. Super-Kamiokande (SK) is the world's largest detector to search for nucleon decays and it has accumulated data of 91.7 kt·yrs (SK-I) and 49.2 kt·yrs (SK-II) resulting in 141 kt·yrs data in total. Various nucleon decay modes have been looked for in SK but we have found no significant signal excess so far.

A proton decay into one positron and one neutral pion ($p \to e^+\pi^0$) is one of the most popular decay modes. This decay mode is mediated by super-heavy gauge bosons and discovery of the signal would give us the information of the mass of the gauge mesons. To discriminate the signal from the atmospheric neutrino background, we reconstruct the number of particles (Cherenkov rings) and reconstruct the total visible energy corresponding to parent proton mass and total momentum corresponding to the proton's Fermi momentum. The signal efficiency and the estimated atmospheric neutrino background for SK-I are 44.9% and 0.20 events in 91.7 kt·yrs. Even with about one half (19%) of the photocoverage area in SK-II, we achieved high detection efficiency of signals (43.7%) and low background levels (0.11 events in 49.2 kt·yrs). The BG rate was confirmed by an artificial neutrino beam by using 1-kton water Cherenkov detector [6]. Because there are no candidate events in SK-I and SK-II data, we obtained a lower limit on the partial lifetime of the proton; $\tau/B_{p\to e^+\pi^0} > 8.2 \times 10^{33}$ years at 90% confidence level [7].

Moreover, we have performed extensive search for nucleon decays into a charged lepton (e^+ or μ^+) and a meson (π^0, π^-, η, ρ^0, ρ^-, or ω). Among these decay modes, we have observed two candidate events for $p \to \mu^+\eta$ with the expected background of 0.45 events in the exposure of SK-I + SK-II. In other modes, we have observed at most one event while expected background is in the order of 0.1. Figure 15 shows obtained upper limits on the partial proton lifetime.

In addition, we looked for SUSY favored decay modes which include K mesons in the final state, $p \to \bar{\nu}K^+$, $n \to \bar{\nu}K^0$, $p \to \mu^+K^0$, and $p \to e^+K^0$. In $p \to \bar{\nu}K^+$ search, we looked for 236 MeV/c monochromatic muons from the decay of K^+. Figure 16 shows the comparison between data and fitting results of the muon momentum distribution for single-ring μ-like events. We observed no excess of signal. In other modes, there are no significant signal excess. Therefore we conclude that there is no evidence of nucleon decays and we calculated partial lifetime limits taking into account systematic uncertainties. Obtained limits are 2.3×10^{33}, 1.3×10^{32}, 1.3×10^{33} and 1.0×10^{33} years at 90% confidence level for $p \to \bar{\nu}K^+$, $n \to \bar{\nu}K^0$, $p \to \mu^+K^0$, and $p \to e^+K^0$ modes, respectively.

We also looked for neutron-antineutron oscillation (conversion) in the water that violates Baryon number by 2. The

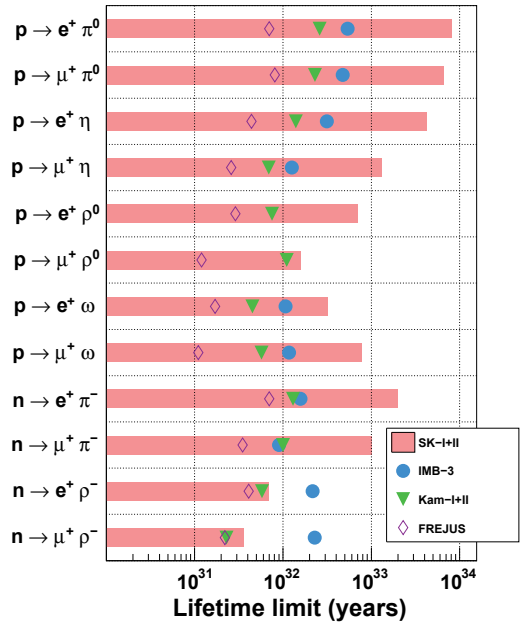

Fig. 15. The lifetime limits on the partial lifetime of protons.

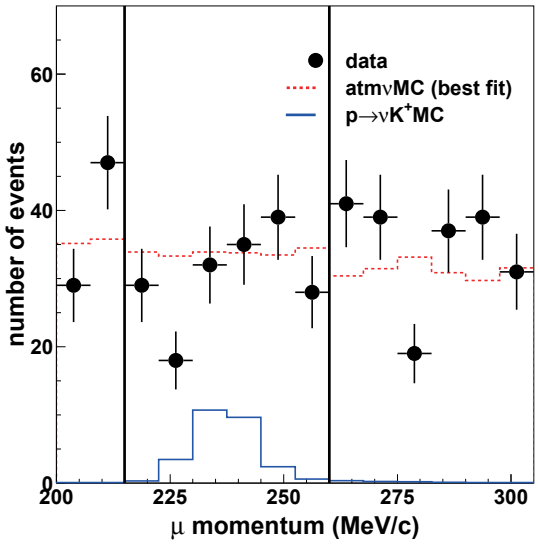

Fig. 16. The comparison between data and fitting results of the muon momentum distribution for single-ring μ-like events. The filled circles show data with statistical errors. The solid line shows $p \to \bar{\nu}K^+$ MC. The dashed line shows the best fitted atmospheric neutrino MC with free normalization.

antineutron annihilates with a nearby nucleon (proton or neutron) producing multiple secondary pions and gammas which emit isotropic Cherenkov photons with a visible energy of 1 GeV. In the full SK-I data, the number of observed candidates is 23 events while expected backgrounds is 24. We have set the upper limit on the neutron-antineutron conversion rate to 1.99×10^{32} years at 90% confidence level. This limit gives the upper limit on the oscillation time of a free neutron as 2.49×10^8 sec at 90% confidence level and can be compared with the reactor experiment limit of 0.86×10^8 sec.

Supernova neutrinos

Kamiokande and IMB observed neutrino burst from supernova 1987a. Those observations confirmed that the energy release by neutrinos is about several$\times 10^{53}$erg. Super-Kamiokande is able to detect several thousand neutrino events if it happens near the center of our galaxy. Until now, no clear neutrino burst from a supernova was observed in Super-Kamiokande.

Currently, we have been improving the the Supernova Relic Neutrino (SRN) search in SK. The SRN is the diffuse supernova neutrino background from all the supernovae in the past. It is expected that the SRN would become dominant in 18–40MeV energy region, though they haven't been observed yet.

In SK detector, we have applied the special data selections to enhance the SRN candidates. The energy region was 18–82MeV, and the fiducial volume was 22.5kton. All the cut criteria are under retuning, including the fiducial volume cut and the energy threshold.

Bibliography

[1] H. Nishino *et al.*, "High-Speed Charge-to-Time Converter ASIC for the Super-Kamiokande Detector' ', To be submitted to Nucl. Inst. and Meth. A.

[2] Super-Kamiokande Collaboration, "A measurement of atmospheric neutrino flux consistent with tau neutrino appearance", Submitted to Phys. Rev. Lett., hep-ex/0607059.

[3] Super-Kamiokande Collaboration, "Three flavor neutrino oscillation analysis of atmospheric neutrinos in Super-Kamiokande", Phys. Rev. D 774 (2006) 032002.

[4] Super-Kamiokande Collaboration, "High energy neutrino astronomy using upward-going muons in Super-Kamiokande-I' ' Astrophys. J. 652, (2006) 198.

[5] Super-Kamiokande Collaboration, "Search for Diffuse Astrophysical Neutrino Flux Using Ultrahigh Energy Upward-going Muons in Super-Kamiokande-I." Astrophys. J. 652, (2006) 206.

[6] S. Mine *et al.* [K2K Collaboration], "Experimental study of the atmospheric neutrino backgrounds for proton decay to positron and neutral pion searches in water Cherenkov detectors," Phys. Rev. D **77**, 032003 (2008) [arXiv:0801.0182 [hep-ex]].

[7] H. Nishino *et al.* [Super-Kamiokande Collaboration], "Search for Proton Decay via $p \to e^+\pi^0$ and $p \to \mu^+\pi^0$ in a Large Water Cherenkov Detector," Phys. Rev. Lett. **102**, 141801 (2009) [arXiv:0903.0676 [hep-ex]].

T2K Experiment

[Spokesperson : T. Kobayashi]

High Energy Accelerator Research Organization, Japan, Tsukuba 305-0801

In collaboration with the members of:
ICRR, University of Tokyo, Japan; Kyoto University, Japan; KEK, High Energy Accelerator Research Organization, Japan; Kobe University, Japan; Osaka City University, Japan; Hiroshima University, Japan; Tohoku University, Japan; University of Tokyo, Japan; Miyagi Edu. University, Japan; Chonnam National University, Korea; Seoul National University, Korea; Dongshin University, Korea; Gyeongsang National University, Korea; Kyungpook National University, Korea; Sejong University, Korea; Sungkyunkwan University, Korea; Boston University, USA; Brookhaven National Lab, USA; Colorado State University, USA; Duke University, USA; Louisiana State University, USA; Stony Brook University, USA; University of California at Irvine, USA; University of Colorado, USA; University of Pittsburgh, USA; University of Rochester, USA; University of Washington, Seattle, USA; TRIUMF, Canada; University of Alberta, Canada; University of British Columbia, Canada; University of Regina, Canada; University of Toronto, Canada; University of Victoria, Canada; York University, Canada; University of Oxford, UK; Imperial College London, UK; Lancaster University, UK; Queen Mary, University of London, UK; Sheffield University, UK; STFC/Rutherford Appleton Laboratory/Daresbury Laboratory, UK; The University of Liverpool, UK; University of Warwick, UK; Universitat Autonoma de Barcelona IFAE, Spain; IFIC University of Valencia, Spain; INRM, Russia; CEA/DAPNIA Saclay, France; IPN Lyon (IN2P3), France; LLR Ecole polytechnique (IN2P3), France; LPNHE-Paris, France; RWTH Aachen University, Germany; INFN Sezione di Roma, Italy; Napoli University, Italy; Padova University, Italy; Rome University, Italy; ETHZ, Swiss; University of Geneva, Swiss; University of Warsaw, Poland; A. Soltan Institute for Nuclear Studies, Poland; H.Niewodniczanski Institute of Nuclear Physics, Poland; Technical University, Poland; University of Silesia, Poland; Wroclaw University, Poland; Institute for Nuclear Research, Russia;

The K2K experiment established the method of the accelerator-based long baseline neutrino oscillation experiment and successfully confirmed the neutrino oscillation phenomena. Meanwhile, several experiments have measured 2 out of 3 neutrino mixing angles and 2 mass differences using accelerator, atmospheric, solar and reactor neutrinos. However, one mixing angle, θ_{13}, has not been measured and has only been found to be small. The experimental sensitivity of the θ_{13} measurement is still limited by statistics and thus, there is a chance to measure the value with a much more intense neutrino beam. Furthermore, if θ_{13} is large enough, it may be possible to search for CP violation in the lepton sector and to measure the CP phase, δ, which is one of the last parameters of the neutrino oscillation. Therefore, several next generation experiments, which utilize high intensity neutrino beams, have been planned for the further investigation of the neutrino oscillations. The Tokai to Kamioka long baseline neutrino oscillation experiment (T2K) is one of the new generation experiments. The intense neutrino beam is produced by using a new high intensity proton synchrotron accelerator at the J-PARC site in Tokai village. As a far detector to study neutrino oscillation phenomena, the T2K experiment utilizes Super-Kamiokande(SK), which is located at 295 km from the beam production target.

In the design of the neutrino beam line for T2K, the concept of off-axis beam [1] is introduced. With this method, it is possible to efficiently produce a low energy neutrino beam with narrow energy spread from the high energy proton beam. Also, it is possible to tune the peak energy by changing the direction of the beam direction. Based on this concept, the direction of the neutrino beam is intentionally shifted from the direction of the SK detector by a few degrees and also the direction of the beam is tunable. The initial peak position of the neutrino beam energy is adjusted to ~ 650 MeV by setting the off-axis angle to $\sim 2.5^\circ$ to maximize the neutrino oscillation effects at the SK detector. The generated neutrino beam is primarily ν_μ with a small contamination of ν_e, which is estimated to be $\sim 0.4\%$ at the flux peak. The T2K neutrino beam is expected to be almost two orders of magnitude more intense compared to the K2K neutrino beam. The construction of the beamline facility for the T2K experiment has been completed in spring of 2009 and the physics run is expected to start by the end of FY2009.

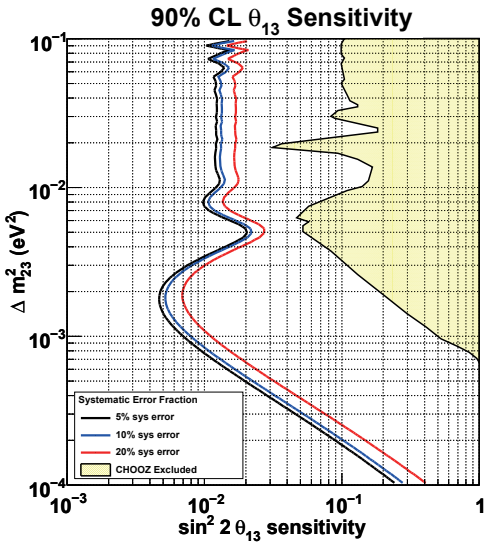

Fig. 1. Expected sensitivity to θ_{13} by T2K (750 kW beam, 5 years of running) as a function of Δm^2_{23} compared with current best limit by the CHOOZ reactor experiment.

As described, one of the motivations of this experiment

*1 Long Baseline Neutrino Oscillation Experiment BNL E889 proposal, (1995).

is to measure the neutrino oscillation parameter θ_{13}, which is only known to be small ($\sin^2 2\theta_{13} \lesssim 0.1$) by the previous experiments. It is of great interest to know the value of a nonzero θ_{13} or how close to zero θ_{13} is. The T2K experiment will try to measure θ_{13} using the electron neutrino appearance channel and there is a possibility to be the first experiment to observe the neutrino oscillation signature with the appearance channel.

Figure 1 shows T2K's expected sensitivity to θ_{13} as a function of Δm^2_{23}. The shaded region is the excluded region by the CHOOZ experiment. As shown in this figure, the T2K experiment has more than one order of magnitude better sensitivity compared to the current best limit.

If the measured θ_{13} is large enough, it will be possible to investigate CP violation in the lepton sector with further extension of this experiment.

Another major purposes of this experiment are precise measurements of θ_{23} and Δm^2_{23}. Owing to the high statistics, the precisions of these parameters are expected to be almost one order of magnitude better than before. So far, θ_{23} mixing is known to be very large and almost maximal from the Super-Kamiokande, K2K and the MINOS experiments. If $\sin^2 2\theta_{23} = 1$, it may suggest an underlying new symmetry.

To achieve the expected precision, we have been working to improve the SK detector, to understand the detector and to improve the analysis methods. In the following sections, some of the works are described briefly.

Detector Upgrade

The reconstruction work of Super-Kamiokande was completed in 2006 and all the PMTs were installed just as in SK-I. It will help the T2K experiment in search for the electron neutrino appearance, to distinguish the π^0 backgrounds from the ν_e signal more efficiently.

In summer 2008, the electronics and the DAQ systems were replaced and newly developed ADC/TDC modules called QBEE were installed. The new QBEE boards consist of the custom analog ASIC chips and the multi-hit TDC chips. This new system allows us to observe the T2K neutrino events with good stability and accuracy.

The trigger system of the new DAQ system is software based and the T2K neutrino beam induced events are stored using the beam extraction timing from the accelerator. With this scheme, it is possible to record all the PMT hit information around the beam arrival timing as the T2K events. In order to make this system work, the beam timing is required to be transferred within a few seconds. This time, we have prepared the dedicated network line from the J-PARC accelerator to the Kamioka site to transfer the necessary timing information as soon as the protons are extracted. This system has been tested using the dummy timing information for several months. As a result, the typical latency to transfer the beam timing was measured to be less than several tens of ms, which is much shorter than the 3 second allowance, and the trigger system was confirmed to work as designed.

Precise Detector Calibration

The response of the far detector, SK, must be well understood in order to maximize the sensitivities to oscillation parameters such as θ_{13}, θ_{23}, and Δm^2_{23}. In the electron appearance search, single π^0 production backgrounds can fake single-ring electron signals when one of the two γ rings is not identified. Even if a small portion of ν_μ induced events are mis-identified as electrons, it will be a serious background. Therefore, we have started to study the ring identification and the particle identification capabilities of the detector very carefully. It is also important to reduce the uncertainty in the absolute energy scale measurement (2.5%) in order to achieve a Δm^2_{23} measurement with $\sim$ a few% accuracy. Moreover, further calibration of the fundamental properties such as the charge and timing responses of each PMT, the light attenuation and scattering in water, and the light reflection by the detector materials are indispensable.

Software Upgrade

All measurements of the physical quantities of an event, such as the vertex position, the number of Cherenkov rings, the momentum, the particle type and the number of the decay electrons, are automatically performed based on the reconstruction algorithms. The analysis software can be shared with the one for the atmospheric neutrino analysis. However, the energy region in our interest for the T2K experiment is limited and thus, there is room to optimize the software for the particular analysis for the T2K experiment. This work has started, especially in the π^0 rejection studies.

Also, the R&D work of the possible near detector to measure the left right symmetry of the neutrino beam has been started in RCCN in order to investigate the feasibility of the future extension.

Bibliography

[1] Y. Itow *et al.*, The JHF-Kamioka neutrino project, (2001), hep-ex/0106019.

XMASS experiment

XMASS is a multi-purpose experiment using liquid xenon that aims at the detection of cold dark matter, search for neutrinoless double beta decay, and detection of low energy solar neutrinos. Construction of a one-ton liquid xenon detector (100 kg fiducial volume) was approved in 2007 and will be done in 2009. This detector is expected to search for dark matter with a sensitivity that is improved by a factor of 100 over that in existing experiments.

Liquid xenon detectors

There are three motivations for developing liquid xenon detectors.

1. Astronomical observations suggest that there is dark matter (non-luminous particles with mass) in the universe. One of the most likely candidates for dark matter is a weakly interacting massive particle (WIMP), such as the lightest supersymmetric particle. The recoil of a xenon nucleus due to an interaction with dark matter will produce scintillation light in liquid xenon.

2. The Super-Kamiokande experiment shows that neutrinos have mass. However, we do not yet know their absolute mass or whether they are Majorana or Dirac type. The Xenon nuclei with mass number 136 is the double beta nuclei best suited for this research.

3. The energy spectrum of solar neutrinos has been measured only above 5 MeV by SK and SNO and that of low-energy solar neutrinos (pp, ^{7}Be neutrinos, etc.) has not yet been measured. A 10-ton liquid xenon detector will be able to detect pp neutrinos and ^{7}Be neutrinos by detecting ν+e scattering, at a rate of 10 and 5 events/day, respectively.

For all these purposes, background caused by gamma rays outside the liquid xenon must be suppressed. The key idea in reducing background is that gamma rays can be absorbed by liquid xenon itself (self-shielding). A sphere of liquid xenon absorbs low energy gamma rays from the outside within the outer 10-20 cm thick layer and realizes a low background radiation in the central volume. WIMPs and neutrinos, however, interact throughout the detector. Therefore, if the vertices of the events can be reconstructed, WIMPs and neutrinos can be observed in a low background environment by extracting only events observed deep inside the detector. The event reconstruction can be accomplished by observing photons with many photo multipliers mounted outside the fiducial volume. Liquid xenon has the following advantages to realize this idea:

- With the high atomic number of xenon ($Z = 54$) and the high density of liquid xenon ($\sim 3\,\mathrm{g/cm^3}$), external gamma-rays can be absorbed within a short distance from the detector wall (self-shielding).
- A large light yield of 42,000 photons/MeV, which is as good as a NaI(Tl) scintillator, enables good event reconstruction as well as detection of small energy signals such as dark matter recoil.
- The 175-nm-wavelength scintillation light of liquid xenon can be detected by a photomultiplier tube (PMT) comprising a bi-alkaline photocathode with a quartz window.
- Purification is easier than with other materials (e.g. distillation is possible).
- Isotope separation is possible. It is possible to enrich ^{136}Xe for double beta decay or deplete ^{136}Xe for solar neutrino measurements.

We have been studying liquid xenon detectors since 2000. A 3 kg fiducial volume liquid xenon detector has been developed for R&D study and test data obtained. Event reconstruction, self-shielding and low internal activity have been confirmed. The description of the one-ton liquid xenon detector in the following sections represents the first phase of this project. The detector aims to detect cold dark matter particles with improved sensitivity by a factor of 100. The second phase of the XMASS project requires a larger detector with more than 10-tons of liquid xenon. The detector is intended for a detailed study of dark matter, and detection of low energy solar neutrinos. The search for neutrinoless double beta decay with the 10-ton detector needs additional efforts in the reduction of background activity in a few MeV energy regions.

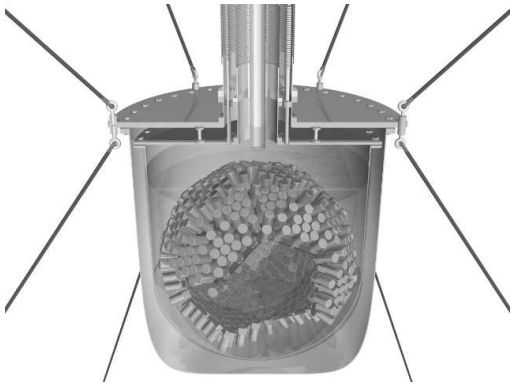

Fig. 1. The central part of the proposed one-ton liquid xenon detector intended for dark matter search. The detector has a sensitivity of $10^{-45} \sim 10^{-44}\mathrm{cm}^2$ in cross section, which is two orders of magnitude better than the current best limit in the world.

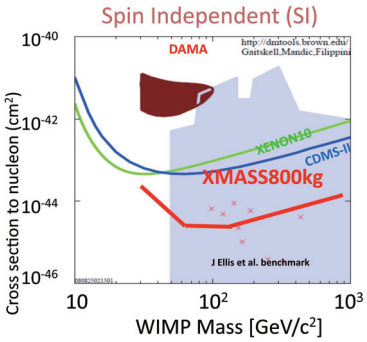

Fig. 2. Expected sensitivity of the proposed one-ton liquid xenon detector. See http://dmtools.berkeley.edu/

One-ton detector

We plan to make the one-ton detector to search for dark matter down to $10^{-45} \sim 10^{-44}\mathrm{cm}^2$ in cross section which is two orders of magnitude better than the current best limit in the world. Figure 1 shows the central part of the detector. Its background and sensitivity were evaluated by Monte Carlo simulations which were validated by the current experimental results. The advantages of our detector design are as follows:

1. Extension of the detector is straightforward because the target substance is liquid.
2. The energy threshold is as low as 5 keV since the photo electron yield is high.
3. Purification of the target substance is easy because xenon is naturally in a gas phase.
4. It is possible to use pulse shape analysis to select nuclear recoil events.

The expected sensitivity for particle dark matter is better than the current experimental limits by two orders of magnitude. Figure 2 shows the expected sensitivity of the one-ton detector.

Construction of the one-ton detector

The construction of the one-ton detector started in 2007 and is to be completed by 2009. Important progress related to the construction has been made.

Fig. 3. A water tank (left side) for shielding from gamma ray and neutrons. The liquid xenon detector will be located at the center of the tank.

Construction of radiation shield

Ambient gamma rays and neutrons are serious sources of background, and pure water is one of the best materials for reducing it. We designed a liquid xenon detector immersed in the cylindrical water tank shown in Fig. 3. It is 10 m in diameter and 11 m high. Its construction completed and an inner structure for supporting the detector is going to be done. A water purification system will be prepared by the summer in 2009.

Mass production of PMTs

The central part of this detector is shown in Fig. 1. The PMTs (shown as many cylinders) are one of the main components of this part. The PMTs consists of a hexagonal photo cathode to maximize the photo sensitive area of the detector. They are specially developed and designed for this experiment since the scintillation wavelength is very short (175 nm) and the operating temperature is low (-100C). In addition, the PMT materials including base parts were carefully selected and evaluated with a low background germanium detector. Production of 650 PMTs started at the end of fiscal year 2008, and is to be completed by the end of summer in 2009.

Detail design of the liquid xenon vessel

In the Fig. 1, PMT holder and liquid xenon vessel are also shown. Copper was chosen as their material because of its purity and high atomic number. Detail design of holder and vessel was done and ready for construction.

Development of a distillation tower

Radioactive contamination in xenon contributes background for dark matter signals. ^{85}Kr in xenon is one potential source of radioactive contamination. In order to reduce krypton contamination, a distillation system was developed which is able to process 6 kg Xe/hour and achieve better than 10^{-5} reduction in krypton concentration. This system will be tested in early summer in 2009.

Recirculation system for liquid xenon

We may need to purify liquid xenon before or during detector operation to reduce possible contamination. One example is water vapor which absorbs scintillation light. Another example is radon gas which is a source of background. To reduce such contaminations, we have constructed and tested a recirculation system with the 3 kg fiducial volume liquid xenon detector. At present, reduction of water vapor in liquid xenon has been observed but no clear reduction of radon contamination observed. Some other candidates of filters will be tested in 2009.

References

1. Y. Suzuki et al., “Low energy solar neutrino detection by using liquid xenon”, Aug. 2000, hep-ph/0008296.
2. S. Moriyama, “XMASS EXPERIMENT I”, Proceedings of the International Workshop on Technique and Application of Xenon Detectors, Kashiwa, Japan, 3-4 Dec. 2001.
3. Y. Suzuki, “XMASS”, presentation at the Identification of Dark Matter (IDM2008), Stockholm, Sweden, 18-22 August 2008.
4. M. Yamashita,“XMASS experiment”, presentation at the 16th YKIS Conference, Progress in Particle Physics 2008, Kyoto, Japan, 16-19 February 2009.

HIGH ENERGY COSMIC RAY DIVISION

Overview

Three major research activities of the High Energy Cosmic Ray Division are the study of very high energy gamma rays by the CANGAROO group, extremely high energy cosmic rays by the Telescope Array (TA) group, and very high energy cosmic rays and gamma rays by the Tibet ASγ Collaboration. It is particularly worth noting that TA started full operation in the spring of this fiscal year. Other activities, such as experiments utilizing the Akeno observatory, the Norikura observatory, the Mt. Chacaltaya observatory (jointly operated with Bolivia), and the emulsion-pouring facilities are closely related to inter-university joint research programs. Also an all-sky high resolution air-shower detector (Ashra) has been installed on the Hawaii island.

The CANGAROO project (Collaboration of Australia and Nippon for a GAmma-Ray Observatory in the Outback) is a set of large imaging atmospheric Cherenkov telescopes to make a precise observation of high-energy air showers originated by TeV gamma rays. It started as a single telescope with a relatively small mirror (3.8 m in diameter) in 1992. In 1999 a new telescope with a 7-m reflector has been built, and now it has a 10-m reflector with a fine pixel camera. The main purpose of this project is to explore the violent, non-thermal universe and to reveal the origin of cosmic rays. An array of four 10-m telescopes has been completed in March 2004 so that more sensitive observations of gamma rays are realized with its stereoscopic imaging capability of Cherenkov light. Several gamma-ray sources have been detected in the southern sky and detailed studies of these sources are now ongoing.

At the Akeno observatory, a series of air shower arrays of increasing geometrical sizes were constructed and operated to observe extremely high energy cosmic rays (EHECRs). The Akeno Giant Air Shower Array (AGASA) was operated from 1991 to January 2004 and covered the ground area of 100 km^2 as the world largest air shower array. In 13 years of operation, AGASA observed a handful of cosmic rays exceeding the theoretical energy end point of the extra-galactic cosmic rays (GZK cutoff) at 10^{20} eV. The Telescope Array (TA), a large plastic scintillator array with air fluorescence telescopes, has been constructed in Utah, USA, which succeeds AGASA and measures the EHECRs with an order of magnitude larger aperture than that of AGASA to unveil the origin of super-GZK cosmic rays discovered by AGASA. The full-scale TA has just started taking data as the largest array viewing the northern sky.

An air shower experiment aiming to search for celestial gamma-ray point sources started in 1990 with Chinese physicists at Yangbajing (Tibet, 4,300 m a.s.l.) and has been successful. This international collaboration is called the Tibet ASγ Collaboration. An extension of the air shower array was completed in 1995 and an emulsion chamber has been combined with this air shower array since 1996 to study the primary cosmic rays around the knee energy region. After successive extensions carried out in 1999, 2002 and 2003, the total area of the air shower array amounts to 37,000 m^2. The sun's shadow in cosmic rays affected by the solar magnetic field was observed for the first time in 1992, utilizing its good angular resolution at multi-TeV energy region. From this experiment with better statistics, we expect new information to be obtained on the large-scale structure of the solar and interplanetary magnetic field and its time variation due to the 11-year-period solar activities.

A new type of detector, called Ashra (all-sky survey high resolution air-shower detector), has been developed and the first-phase stations have been installed near the Mauna Loa summit in the Hawaii Island. It will monitor optical and particle radiation from high-energy transient objects with a wide field-of-view. The optical system is under tuning and real observation will start soon.

CANGAROO-III Project

[Spokespersons : R.W. Clay, M. Mori, and T. Tanimori]

Collaboration list:
Institute for Cosmic Ray Research, University of Tokyo, Chiba, Japan; School of Chemistry and Physics, University of Adelaide, Australia; Mt Stromlo and Siding Spring Observatories, Australian National University, Australia; Australia Telescope National Facility, CSIRO, Australia; Department of Radiological Sciences, Ibaraki Prefectural University of Health Sciences, Ibaraki, Japan; Faculty of Science, Ibaraki University, Ibaraki, Japan; School of Allied Health Sciences, Kitasato University, Kanagawa, Japan; Department of Physics, Konan University, Hyogo, Japan; Department of Physics, Kyoto University, Kyoto, Japan; Solar-Terrestrial Environment Laboratory, Nagoya University, Aichi, Japan; National Astronomical Observatory of Japan, National Institutes of Natural Sciences, Tokyo, Japan; Department of Physics, Tokai University, Kanagawa, Japan; Department of Physics, Yamagata University, Yamagata, Japan; Faculty of Management Information, Yamanashi Gakuin University, Yamanashi, Japan; Faculty of Medical Engineering and Technology, Kitasato University, Kanagawa, Japan; Department of Physics, Hiroshima University, Hiroshima, Japan; Department of Basic Physics, Tokyo Institute of Technology, Tokyo, Japan; Institute of Particle and Nuclear Studies, High Energy Accelerator Research Organization (KEK), Ibaraki, Japan [1].

Status of the Project

CANGAROO is the acronym for the Collaboration of Australia and Nippon (Japan) for a GAmma Ray Observatory in the Outback. The collaboration started in 1992 with a single Imaging Atmospheric Cherenkov Telescope (IACT) of 3.8 m diameter called CANGAROO-I in the desert area near Woomera, South Australia (136°47′E, 31°06′S, 160 m a.s.l.).

As its third-generation experimental setup, the CANGAROO-III stereoscopic IACT system has been in operation since March 2004 with four IACTs of 10 m diameter. Stereoscopic observations of atmospheric Cherenkov light images produced by particle showers caused by high-energy particles bombarding the earth allow effective discrimination of gamma rays from charged cosmic rays which are the overwhelming backgrounds. Three of the four telescopes (called T2, T3 and T4 in the order of construction) have been used in observations since 2005 as the first telescope, completed in 2000 and having been used as CANGAROO-II, has degraded and is equipped with a different electronics system from the others. A stereoscopic triggering system was installed at the beginning of 2005 and has been working properly, rejecting most single muon events, which are the major background component at low energies. We are continuing observations of various candidates of celestial gamma-ray emitters on moonless, clear nights.

In February 2008, a considerable number of segment mirrors of T4, corresponding to about 10% of the total mirror area, were blown off by heavy storm. Part of them was fixed and put back to the telescope in March 2008. Since May 2008, two of the four telescopes (T3 and T4) have been used in observations as the reflectivity of T2 mirrors has degraded seriously. The T3 and T4 mirrors were cleaned using tap water in May 2008 and their reflectivities calibrated using muon ring events were improved by more than 10%.

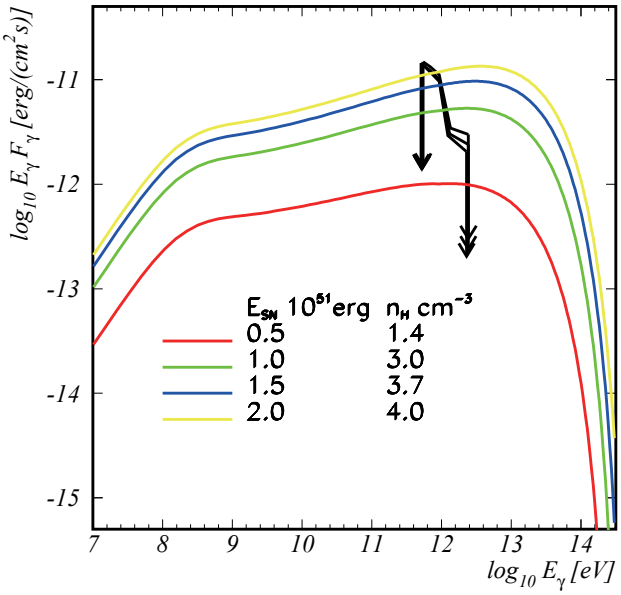

Fig. 1. Spectral energy distributions for Kepler's SNR. The black lines with arrows at both ends are the 2σ flux upper limits obtained by CANGAROO-III. The colored curves are spectra predicted from hadronic models by Berezhko et al. (2006), obtained assuming the distance to Kepler's SNR to be 4.8 kpc and varying the supernova explosion energy and the ambient matter density.

CANGAROO-III Results

In 2008, CANGAROO-III papers of five celestial objects were published in journals: the blazar PKS 2155–304 [2], the pulsar wind nebula MSH 15–52 [3], Kepler's supernova remnant [4], the unidentified TeV source HESS J1804–216 [5], and the Galactic Plane [6]. One paper of the clusters of galaxies Abell 3667 and Abell 4038 was also submitted to a journal [7]. Results of relatively recent papers are summarized below.

Kepler's Supernova Remnant [4]

Kepler's supernova remnant (SNR) is 400 years old and both younger (Cas A) and older (RX J0852.0–4622, RX J1713.7–3946, etc.) SNRs are known to be TeV gamma-ray sources. Therefore, one might expect a similar level of TeV gamma-ray emission also from Kepler's SNR, if the SNR age is a dominant factor in cosmic-ray acceleration.

CANGAROO-III observed Kepler's SNR in April 2005 for an effective observation time of 874 min. No statistically significant gamma-ray signal has been detected from the SNR and we have estimated 2σ flux upper limits corresponding to the 10–30% Crab level. They are plotted in Figure 1 together with model predictions obtained by Berezhko et al. (2006)[2] considering a reasonably wide range of possibilities for the distance of the SNR (3.4–7.0 kpc), the supernova explosion energy ($(0.5–2.0)\times10^{51}$ erg), and the ambient matter density (0.4–6.0 cm^{-3}). Limitations on the allowed parameter range in the model were discussed in comparison with the flux upper limits.

*2 Berezhko, E. G., Ksenofontov, L. T., & Völk, H. J. 2006, A&A, **452**, 217

HESS J1804–216 [5]

A Galactic plane survey was performed in 2004 by the H.E.S.S. IACTs with a flux sensitivity of 0.02 Crab for gamma rays above 200 GeV. Fourteen new gamma-ray sources were detected at significance levels above 4σ, and 11 of the sources either have no counterpart or possible counterparts with significant positional offsets. HESS J1804–216 is one of the brightest, and its spectrum is softest in this survey; the flux is about 0.25 Crab above 200 GeV with a photon index of 2.72 ± 0.06. In addition, with a size of $\sim 22'$, it is one of the most extended TeV gamma-ray sources.

We observed HESS J1804–216 with the CANGAROO-III IACTs from May to July in 2006. We detected very high energy gamma rays above 600 GeV at the 10σ level in an effective exposure of 76 hr. We obtained a differential flux of $(5.0\pm1.5_{\rm stat}\pm1.6_{\rm sys})\times10^{-12}(E/1\,{\rm TeV})^{-\alpha}\,{\rm cm}^{-2}\,{\rm s}^{-1}\,{\rm TeV}^{-1}$ with a photon index α of $2.69\pm0.30_{\rm stat}\pm0.34_{\rm sys}$, which is consistent with that of the H.E.S.S. observation in 2004. We also confirmed the extended morphology of the source. By combining our result with multiwavelength observations, we discussed the possible counterparts of HESS J1804–216 and the radiation mechanism based on leptonic and hadronic processes for a SNR and a pulsar wind nebula (PWN). An example is shown in Figure 2 for the leptonic model for the PWN of PSR B1800–21 with a time-dependent rate of electron-injection.

Galactic Plane [6]

The Galactic Plane is known to be a very bright source of gamma rays in the GeV energy band. Its gamma-ray spa-

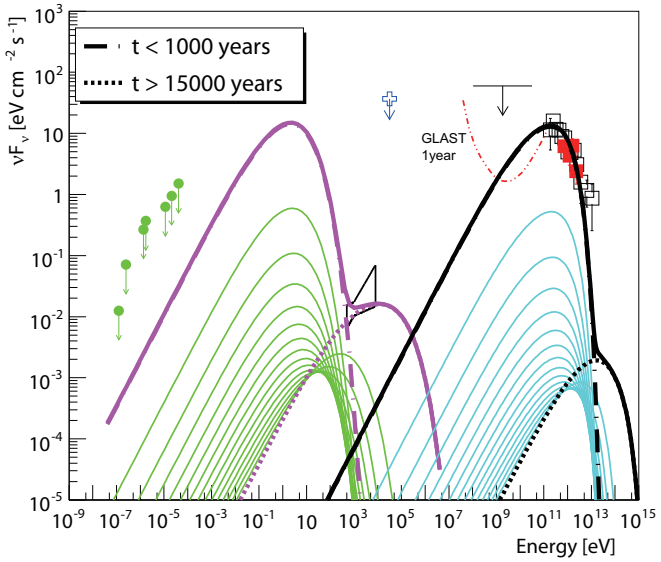

Fig. 2. Spectral energy distribution and the leptonic model curves for the pulsar wind nebula of PSR B1800–21 with a time-dependent rate of electron-injection with an age $\tau = 16$ kyr, an initial spin-down timescale $\tau_0 = 700$ yr, a braking index of the pulsar $n_{\rm br} \sim 1.6$, a spectral index of injected electrons $\Gamma_e = 1.5$, and a magnetic field $B = 8\,\mu$G. The right-hand curves show the inverse Compton component, and the left-hand curves show the synchrotron emissions. The dot-dashed curves show the spectra produced by old electrons ($t < 1000$ yr), and the dotted curves show the spectra produced by young electrons ($t > 15000$ yr). The thin solid curves represent their medium per 1000 yr ($1000 < t < 15000$ yr), and the thick solid curves show their total.

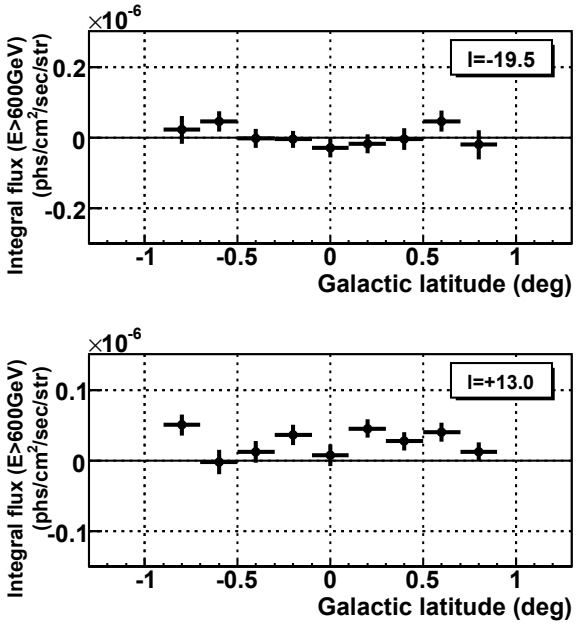

Fig. 3. The latitude profiles of the flux intensity for $\ell = -19°.5$ and $\ell = +13°.0$, obtained by projecting two-dimensional excess count maps onto $\ell = $ const. lines. The raw count profile was divided by the acceptance and the solid angles for each projection bin. The bin size in the latitude direction was selected to be $0°.2$. Vertical bars represent fitting errors in each data subset.

tial profile and spectrum across the entire galactic plane were measured by satellite experiments such as SAS-II, COS-B, and CGRO. Among these, the EGRET detector on the CGRO was sensitive to GeV gamma-rays, and the observations using this detector provided the detailed spatial and spectral characteristic features of gamma-ray emission from the Galactic Plane up to 30 GeV. Above this energy, some models of the diffuse gamma-ray emission predict very hard spectra, extrapolations of which are detectable at TeV energies by using the current generation of IACTs.

In 2004, we searched for very high energy (VHE) gamma-ray emission from the Galactic Plane using the CANGAROO-III stereoscopic IACT system. Two different longitude regions of $\ell = -19°.5$ and $\ell = +13°.0$ on the Galactic Plane were observed in July and August 2004 for 8.0 hr and 5.9 hr, respectively. We analyzed events that triggered three telescopes aiming to measure the diffuse emission component. No significant signal associated with the Galactic Plane was found from either of the regions (Figure 3). Assuming that the gamma-ray spectrum is described by a single power-law for energies ranging between a few GeV and TeV, lower limits of the power-law spectral indices were found to be 2.2 for both of the regions with a 99.9% confidence level (CL). This result is consistent with the other VHE measurements and constrains a hypothesis in which a very hard (~ 2.0) cosmic ray electron spectrum was introduced to explain the EGRET GeV anomaly.

Clusters of Galaxies [7]

Clusters of galaxies are candidate sites for the origin of ultra high energy (UHE) cosmic rays because accretion and merger shocks in clusters may accelerate particles to high energies, A prediction was presented for gamma-ray emission from a cluster of galaxies at a detectable level with the current generation of IACTs. The gamma-ray emission is produced via inverse Compton (IC) upscattering of cosmic microwave background (CMB) photons by electron-positron pairs generated by collisions of UHE cosmic rays in the cluster.

We observed two southern clusters of galaxies, Abell 3667 and Abell 4038, searching for VHE gamma-ray emission with the CANGAROO-III telescope system in 2006. The ON-source observation times are 29.7 hr and 23.6 hr for Abell 3667 and Abell 4038, respectively. The analysis showed no significant excess around these clusters (significance maps shown in Figure 4), yielding upper limits on the gamma-ray emission. From a comparison of the upper limit for the northwest radio relic region of Abell 3667 with a model prediction, we derived a lower limit for the magnetic field of the region of $\sim 0.1\,\mu$G. This shows the potential of gamma-ray observations in studies of the cluster environment. We also discussed the flux upper limit from cluster center regions with a model of gamma-ray emission from neutral pions produced in hadronic collisions of cosmic-ray protons with the intra-cluster medium (Figure 5). The derived upper limits of the cosmic-ray energy densities within this framework are $\sim 20\,{\rm eV\,cm^{-3}}$ for Abell 3667 and $\sim 40\,{\rm eV\,cm^{-3}}$ for Abell 4038, which are an order of magnitude higher than that of our Galaxy.

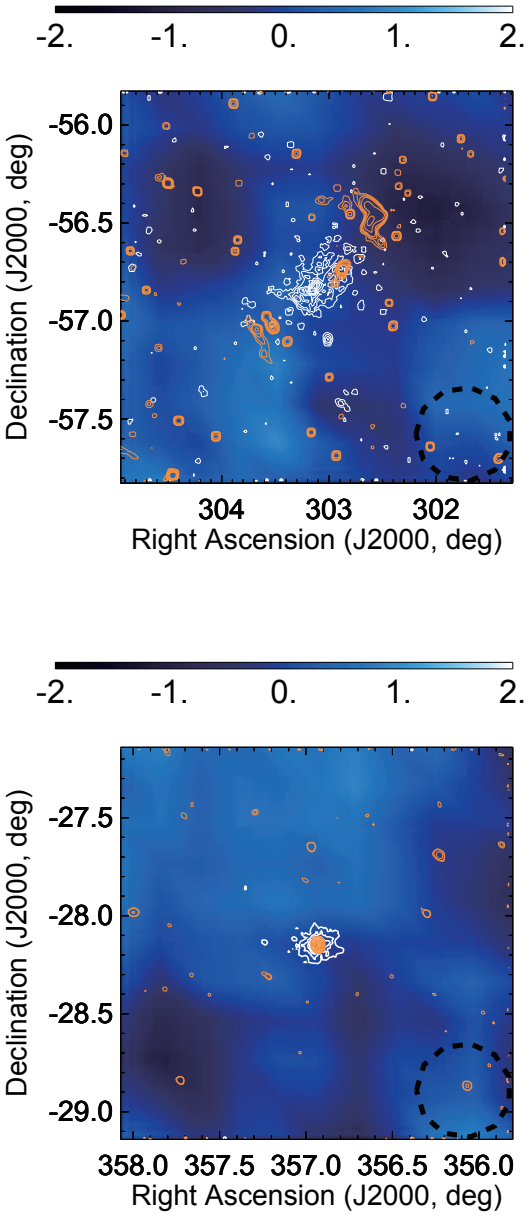

Fig. 4. Two-dimensional significance maps around the clusters. The map centers correspond to the position of the cD galaxy of each cluster, and at each point a smoothing algorithm within $0^\circ.6 \times 0^\circ.6$ was applied. Contours of other wavelengths (X-ray and radio) are over-plotted. The top panel is for Abell 3667, where the white contours show *ROSAT* hard-band data and orange contours show SUMSS 843 MHz radio data. The bottom panel is for Abell 4038, where white contours show *ROSAT* hard-band data and orange contours show VLA 1.4 GHz radio data. Our point-spread function is also shown at the bottom-right corner.

CANGAROO-II Observations of SS 433/W 50 [8]

SS 433 is a close proximity binary system consisting of a compact star and a normal star. It is located at the center of the SNR W 50. Jets of material are directed outwards from the vicinity of the compact star symmetrically to the east and west. Non-thermal hard X-ray emission is detected from lobes

*[3] Aharonian, F. A., et al. 2006, Nature, **440**, 1018

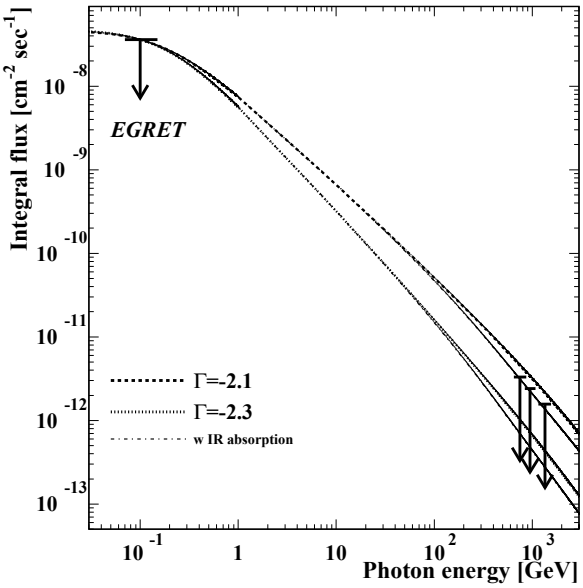

Fig. 5. Gamma-ray flux upper limits for the cluster core region of Abell 4038 with the gamma-ray emission spectrum via π^0-decay process, normalized to the EGRET upper limit. The EGRET upper limit is indicated by the arrow at 100 MeV, and the lines are the gamma-ray spectrum from the proton power-law indices of $\Gamma = -2.1$ and -2.3 with an energy cutoff of 200 TeV. The gamma-ray absorption effect by IR photons are represented by dot-dashed lines, where the P0.4 model in Aharonian et al. (2006)[3] is adopted.

lying on both sides. Shock accelerated electrons are expected to generate sub-TeV gamma rays through the IC process in the lobes.

CANGAROO-II observed the western X-ray lobe region in August and September 2001, and in July and September 2002. The total observation times are 85.2 hr for ON source and 80.8 hr for OFF source. In the ON-source observations, the tracking position was set at "*p*1" indicated in Figure 6, from which the hardest power-law X-ray spectrum was ob-

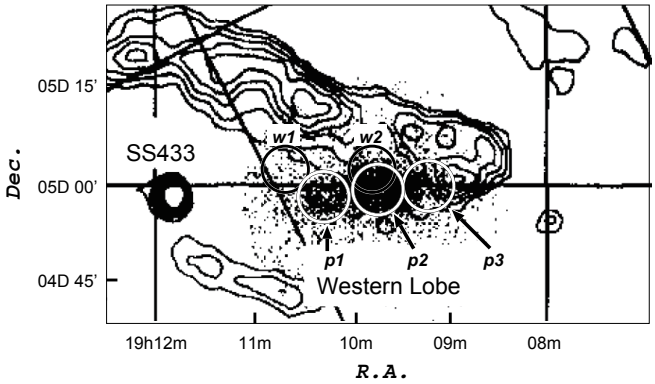

Fig. 6. 4.75 GHz radio contour map of W 50 overlaid on X-ray images of the western X-ray lobe (dots) obtained by *ASCA*. Solid white circles show the regions reported by the *ASCA* team in 2000. We label these regions "*p*1", "*p*2" and "*p*3". Solid black circles show the regions reported by the *ROSAT* & *ASCA* team in 1997, which are labeled "*w*1" and "*w*2".

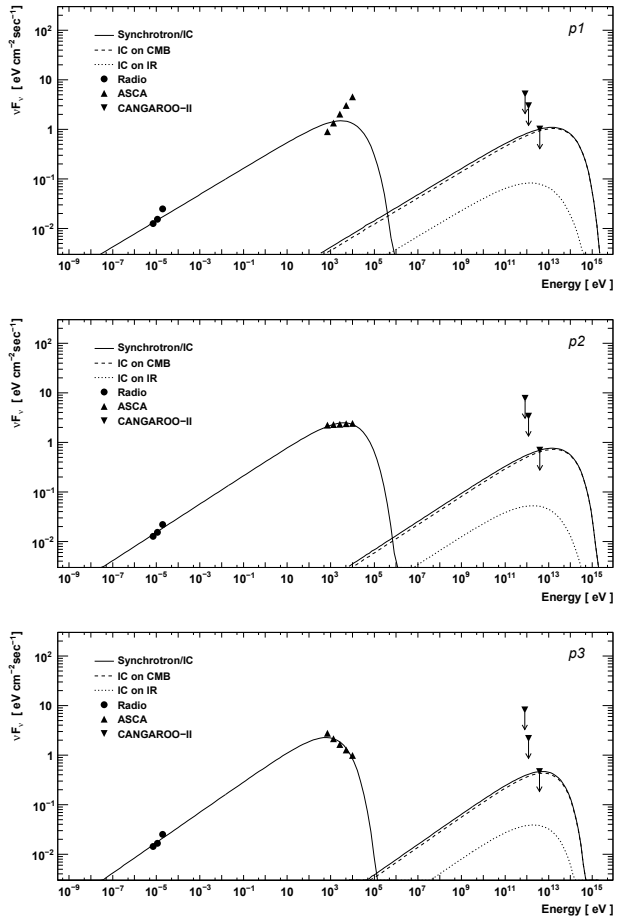

Fig. 7. Synchrotron/IC model fitting to the spectral energy distributions at "$p1$" (top), "$p2$" (middle) and "$p3$" (bottom). The X-ray fluxes are from *ASCA* and the radio fluxes are calculated from the result of the Effelsberg 100 m telescope for each frequency. The 99% CL upper limit fluxes of this work are shown by down-arrows. The thick solid lines represent the synchrotron/IC spectra. Two components (CMB and IR) of IC are shown by the dashed lines and the dotted lines, respectively.

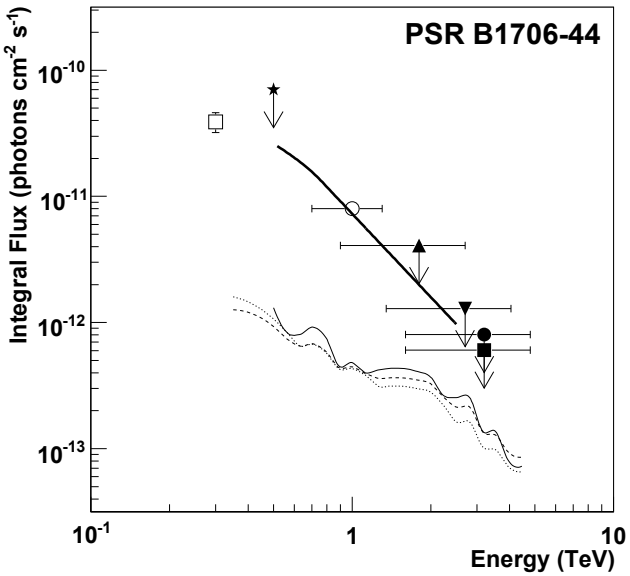

Fig. 8. Integral gamma-ray fluxes from PSR B1706–44 obtained using the CANGAROO-I data. The 95% CL upper limits to the integral flux from PSR B1706–44 obtained from the 1993, 1993 + 1994, 1997, and 1998 data are indicated by the filled circle, filled square, filled triangle, and filled upside-down triangle, respectively. The open circle indicates the integral flux estimated by Kifune et al. (1995)[4] using the 1993 data. The horizontal bars represent the systematic errors of the threshold energies. The 99% CL upper limit curves obtained by H.E.S.S. are indicated by the thin solid, dashed, and dotted lines. The thick solid line is the integral spectrum converted from the preliminary CANGAROO-II result (Kushida et al. 2003[5]). The open square and filled star indicate the results from the Durham group and BIGRAT, respectively.

tained by *ASCA*. No significant excess of sub-TeV gamma rays has been found at 3 regions ("$p1$", "$p2$" and "$p3$" shown in Figure 6) of the western X-ray lobe of the SS 433/W 50 system. The 99% CL upper limits to the fluxes of gamma rays at energies greater than 850 GeV have been derived as 1.5, 1.3, and 0.79 in unit of 10^{-12} photons cm^{-2} s^{-1} for "$p1$", "$p2$" and "$p3$", respectively. The synchrotron/IC model has been applied to the multiwavelength spectrum together with radio and X-ray data (Figure 7). Lower limits to the magnetic field strengths have been estimated to be 4.3 μG for the brightest X-ray emission region ("$p2$") and 6.3 μG for the far end from SS 433 in the western X-ray lobe ("$p3$").

Reanalysis of CANGAROO-I Data [9]

Old CANGAROO-I data have been reanalyzed for PSR B1706–44, SN 1006, and the Vela pulsar region in response to the results reported for these sources by the H.E.S.S. Collaboration. Although detections of TeV gamma-ray emission from these sources were claimed by CANGAROO more than 10 years ago, upper limits to the TeV gamma-ray signals from PSR B1706–44 and SN 1006 derived by H.E.S.S. are about an order of magnitude lower. The H.E.S.S. group detected strong diffuse TeV gamma-ray emission from Vela but with a morphology differing from the CANGAROO result.

In the reanalysis, in which gamma-ray selection criteria have been determined exclusively using gamma-ray simulations and OFF-source data as background samples, no significant TeV gamma-ray signals have been detected from compact regions around PSR B1706–44 or within the northeast rim of SN 1006. The upper limits to the integral gamma-ray fluxes at the 95% CL have been estimated for the 1993 data of PSR B1706–44 to be $F(> 3.2 \pm 1.6\,\mathrm{TeV}) < 8.03 \times 10^{-13}$ photons cm^{-2} s^{-1}, for the 1996 and 1997 data of SN 1006 to be $F(> 3.0 \pm 1.5\,\mathrm{TeV}) < 1.20 \times 10^{-12}$ photons cm^{-2} s^{-1} and $F(> 1.8 \pm 0.9\,\mathrm{TeV}) < 1.96 \times 10^{-12}$ photons cm^{-2} s^{-1}, respectively. These results are plotted in Figure 8 and Figure 9 together with the other previous results.

The reanalysis did result in a TeV gamma-ray signal from the Vela pulsar region at the 4.5σ level using 1993, 1994, and 1995 data. The excess was located at the same posi-

*3 Kifune, T. et al. 1995, ApJL, **438**, L91
*5 Kushida, J. et al. 2003, 28th ICRC (Tsukuba), **4**, 2493

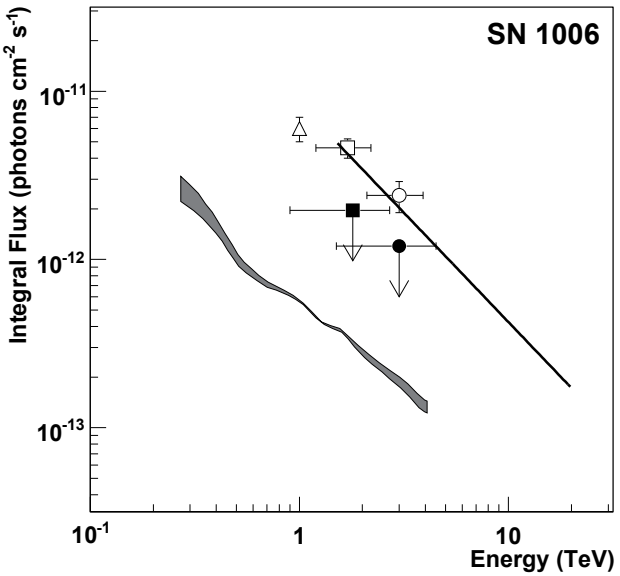

Fig. 9. Integral gamma-ray fluxes from the NE rim of SN 1006 obtained using the CANGAROO-I data. The 95% CL upper limits to the integral fluxes are indicated by the filled circle (1996 data with the selection criteria optimized for the $0^\circ.3$ offset) and the filled square (1997 data). The open circle and open square are the integral fluxes estimated by Tanimori et al. (1998)[6]using the 1996 and 1997 data, respectively. The thick solid line is the integral spectrum converted from the CANGAROO-I differential spectrum (Tanimori et al. 2001[7]). The horizontal bars represent the systematic errors of the threshold energies. The 99.9% CL upper limits obtained by H.E.S.S. are indicated by the gray band for a range of assumed photon indices (2 to 3). The open triangle indicates the preliminary CANGAROO-II result (Hara et al. 2001[8]).

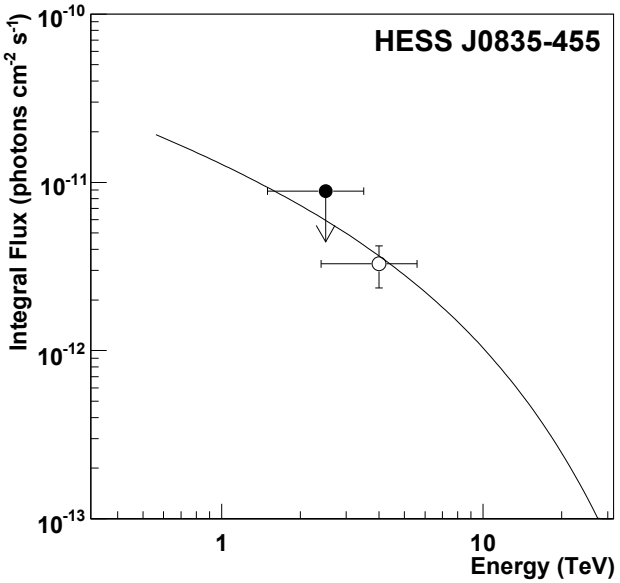

Fig. 10. Integral gamma-ray fluxes from the Vela pulsar region ($0^\circ.8$ radius centered on HESS J0853–455) obtained from the CANGAROO-I data. The open circle represents the integral flux from the 1993 to 1995 data and the filled circle represents the 95% CL upper limit to the flux from the 1997 data. The horizontal bars represent the systematic errors of the threshold energies. The solid line is the integral spectrum converted from the differential spectrum of HESS J0853–455 measured by H.E.S.S. assuming a power law with an exponential cutoff.

tion, $0^\circ.13$ to the southeast of the Vela pulsar, as that reported in the original analysis. We have investigated the effect of the acceptance distribution in the field of view of the 3.8 m telescope, which rapidly decreases toward the edge of the field of the camera, on the detected gamma-ray morphology. The expected excess distribution for the 3.8 m telescope has been obtained by reweighting the distribution of HESS J0835–455 measured by H.E.S.S. with the acceptance of the 3.8 m telescope. The result is morphologically comparable to the CANGAROO excess distribution, although the profile of the acceptance-reweighted H.E.S.S. distribution is more diffuse than that of CANGAROO. The integral gamma-ray flux from HESS J0835–455 has been estimated for the same region as defined by H.E.S.S. from the 1993–1995 data of CANGAROO to be $F(>4.0\pm1.6\,\mathrm{TeV}) = (3.28\pm0.92)\times 10^{-12}\,\mathrm{photons\,cm^{-2}\,s^{-1}}$, which is statistically consistent with the integral flux obtained by H.E.S.S. as shown in Figure 10.

Other Activities

A light-weight and cost-effective metal mirror has been developed for replacing current mirrors used in the CANGAROO-III telescopes or for the next generation Cherenkov telescopes. A sample mirror of 20 cm diameter was made grinding its surface and is currently checked for performance. Methods of surface coating have also been investigated. For upgrading photomultiplier tube (PMT) cameras of the CANGAROO-III telescopes, a super bialkali PMT, new preamplifiers, and Cockcroft-Walton breeder circuits for PMTs have been tested or developed. Compact data acquisition circuits utilizing analog memory cells (AMCs) have been developed for recording Cherenkov light signals with higher time resolution (~ 1 GHz) and lower power consumption. Cheap implementation of a GPS compass module has been developed for auto calibrations of the telescope attitude. Its calibration accuracy should be better than $0^\circ.1$ in principle. This technology will be important in the next generation observatory of many (~ 100) IACTs, dramatically reducing time and effort of manually tuning their rotation axes.

*5 Tanimori, T. et al. 1998, ApJL, **497**, L25
*6 Tanimori, T. et al. 2001, 27th ICRC (Hamburg), **6**, 2465
*8 Hara, S. et al. 2001, 27th ICRC (Hamburg), **6**, 2455

Bibliography

[1] Collaboration website: `http://vesper.icrr.u-tokyo.ac.jp/`.

[2] Y. Sakamoto et al., *Astrophys. J.*, **676**, 113 (2008).

[3] T. Nakamori et al., *Astrophys. J.*, **677**, 297 (2008).

[4] R. Enomoto et al., *Astrophys. J.*, **683**, 383 (2008).

[5] Y. Higashi et al., *Astrophys. J.*, **683**, 957 (2008).

[6] M. Ohishi et al., *Astropart. Phys.*, **30**, 47 (2008).

[7] R. Kiuchi et al., *Astrophys. J.*, **704**, 240 (2009).

[8] Sei. Hayashi et al., *Astropart. Phys.*, **32**, 112 (2009).

[9] T. Yoshikoshi et al., *Astrophys. J.*, **702**, 631 (2009).

TA: Telescope Array Experiment

Spokespersons:

M. Fukushima / ICRR, University of Tokyo
P. Sokolsky / Dept. of Physics, University of Utah

Collaborating Institutions:

Chiba Univ., Chiba, Japan; Chungnam Nat. Univ., Daejeon, Korea; Ehime Univ., Matsuyama, Japan; Ewha W. Univ., Seoul, Korea; Hiroshima City Univ., Hiroshima, Japan; Hanyang Univ., Seoul, Korea; ICRR, Univ. of Tokyo, Kashiwa, Japan; INR, Moscow, Russia; Kanagawa Univ., Yokohama, Japan; KEK/IPNS, Tsukuba, Japan; Kinki Univ., Higashi-Osaka, Japan; Kochi Univ., Kochi, Japan; Musashi Inst. of Tech., Tokyo, Japan; Nat. Inst. of Rad. Sci., Chiba, Japan; Osaka City Univ., Osaka, Japan; Pusan Nat. Univ., Pusan, Korea; Rutgers Univ., Piscataway, NJ, USA; Saitama Univ., Saitama, Japan; Tokyo Inst. of Tech., Tokyo, Japan; Tokyo Univ. of Science, Noda, Japan; Univ. of Denver, Denver, CO, USA; Univ. of Utah, Salt Lake City, UT, USA; Univ. of Yamanashi, Kofu, Japan; Waseda Univ., Tokyo, Japan;
Yonsei Univ., Seoul, Korea

Overview of TA

The TA project was proposed in 2000 [1] to investigate the origin of super-GZK cosmic rays by employing a large array of fluorescence telescopes with about 100 times larger acceptance than AGASA. The HiRes experiment, however, presented an energy spectrum indicating the GZK-cutoff in the 27th ICRC and the result was later published [2].

With contradictory results on the existence of GZK cutoff appearing, it became urgent to understand the experimental bias in the energy and the acceptance determination of super-GZK cosmic rays. We initiated constructing a composite detector with AGASA-like ground array and TA fluorescence telescopes [3]. We call it as the phase-1 TA (ph-1 TA). We expect simultaneous measurement of the same EHECRs by the detectors of two different types will sort out the systematics of two methods. It will guide us to a reliable determination of the primary energy and the acceptance of EHECRs.

The phase-1 TA consists of a large plastic scintillator array and three stations of air fluorescence telescopes overlooking the array from periphery as shown in Fig.1. The ground array will give an aperture of about 1900 km^2 sr for zenith angles below 60°, which is approximately an order of magnitude larger than that of AGASA. The fluorescence telescope will have a stereoscopic aperture of about 860 km^2 sr with 10% duty factor at 10^{20} eV. The telescope will also supply information on the primary particle species by measuring the longitudinal shower profile. It is located in the West Desert of Utah, 140 miles south of Salt Lake City (lat. 39.3°N, long. 112.9°W, alt. ∼1400 m). The construction was completed in 2007, and TA is fully operating from March 2008.

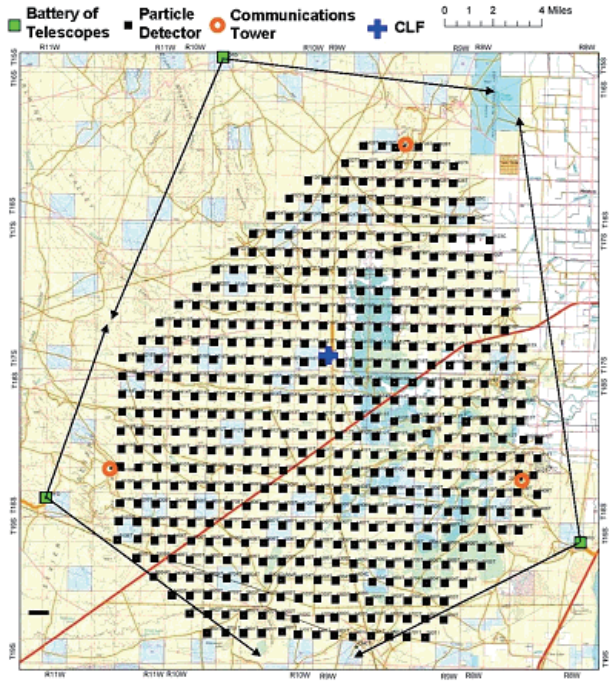

Fig. 1. Detector Arrangement of the ph-1 TA. The locations of 507 surface detectors are indicated by filled black boxes. The three fluorescence telescope stations are marked by filled green boxes. The three communication towers are marked by orange circles. The central laser facility is marked by a blue cross.

Ground Array of the ph-1 TA

The ground detector array consists of 507 plastic scintillators on a grid of 1.2 km spacing. It covers the ground area of about 700 km^2. The trigger efficiency is ∼100% for cosmic rays with energies more than 10^{19} eV with zenith angle less than 45°.

The counter is composed of two layers of plastic scintillator overlaid on top of each other. The scintillator (CIMS-G2; CI Kogyo Ltd.) is 1.2 cm thick, 3 m^2 large and is read out by 104 wave length shifter fibers installed in grooves on the surface. Both ends of the fibers are bundled and optically connected to the photomultiplier (9124SA; Electron Tubes Ltd.).

The signal from each PMT is continuously digitized with a 12-bit flash ADC with 50 MHz sampling. When both of the PMTs record more than 1/3 of the muon signal (Level-0 trigger), wave forms are stored with a time stamp supplied by the GPS (M12+ Timing Oncore Receiver; Motorola, Inc.). This rate of local buffering is less than 1 kHz. For the event timing, we took a GPS timing (PPS; pulse per second) prior to the event occurrence and a fractional time of one second is added using clock frequency of 50 MHz DAQ system. The absolute location and the altitude of each SD is measured by the GPS of each SD electronics operated in '3D fix mode' before the commissioning period. The accuracy is expected to be better than 0.3m in horizontal direction and better than 0.5m in altitude. After the commissioning period, the GPS is changed to 'position hold mode'. The relative timing between remotely separated counters will be better than ±20 ns

by the GPS, which is sufficient to supply good resolution for the determination of the arrival direction.

When both of the PMT signals exceed a trigger threshold of three muons (Level-1 trigger), the timing is recorded in a local trigger list. The content of the list is transmitted to a branch DAQ board by the wireless LAN at 1 Hz. The list contains less than 100 events for normal counters. To cover communication in the whole surface detector array, the array is divided into three regions. The branch DAQ board is installed on a communication tower built at the periphery of the array for each region. Each surface detector is assigned to one of the three branch DAQ boards on the tower. A colinear antenna which is indirectional in azimuth is connected to each branch DAQ board. An air shower event is identified by the branch DAQ firmware by requiring clustered hits (at least three adjacent counters) with a coincidence timing within 8μsec (Level-2 trigger). The trigger rate of air shower events taken at each tower is around 0.003 Hz.

When an air shower trigger is generated in a branch DAQ board, a command is sent to all counters, and relevant counters storing the event within $\pm 32\mu$sec respond by transmitting the wave form data to the branch DAQ board. We employ a commercially produced wireless transmitter using 2.4 GHz spread spectrum technology, and we use the speed of 2 Mbps. The dead-time-less DAQ operation is aimed with the high transmission speed together with a large buffering memory at each counter. The data in a branch DAQ board on the tower are transmitted to an industrial PC board inside a cabinet at the tower site. The data taken in the PC board at the tower sites are then transmitted via 5.7GHz wireless communication network and stored in a mass storage at the Cosmic Ray Center in DELTA which is located to the east of the TA site. Fig.2 shows an air shower event taken with surface detectors.

We have been taking data for the whole ground array since March 2008. We have 507 surface detectors in the field after we deployed remaining four counters in November 2008. Since three DAQ sub-arrays were operated independently, there was inefficiency of shower trigger around the boundaries of neighboring DAQ sub-arrays. We installed cross-boundary trigger between neighboring regions to make the Level-2 trigger efficiency uniform inside the whole region except the border of the array in November 208. One of the three tower PCs was defined as a central PC and trigger information from two other tower PCs is transmitted to the central PC via tower-to-tower wireless LAN communication. We do not have inefficiency of Level-2 trigger around the boundaries of DAQ sub-arrays now.

We developed a real-time system that works in the background to monitor a variety of information for SD calibration and maintenance. The gain of the whole SD system is determined by the histogram of the penetrating 'muon' signals accumulated locally at the SD. Pulse charges of about 420k muons are histogrammed locally at the SD and sent out every 10 minutes for the recording. A typical result of the energy deposit histogram of the 'muon' signals fit with the MC is shown in Fig. 3. Here COSMOS MC is used for air shower simulation and GEANT4 is used for detector simulation.

We are developing a new air shower full MC simulation system for the precise measurement of ultra-high energy cosmic rays based on parallel computing COSMOS MC using a PC cluster. We estimate energy of ultra-high energy cosmic rays by using total energy deposited at a certain distance from the shower core. We define S(800) as the total energy deposited in the SD which is located at a distance of 800m from the shower core. Fig. 4 shows zenith angle dependence of S(800) obtained for 10^{20}eV proton using a QGSJET2 hadron

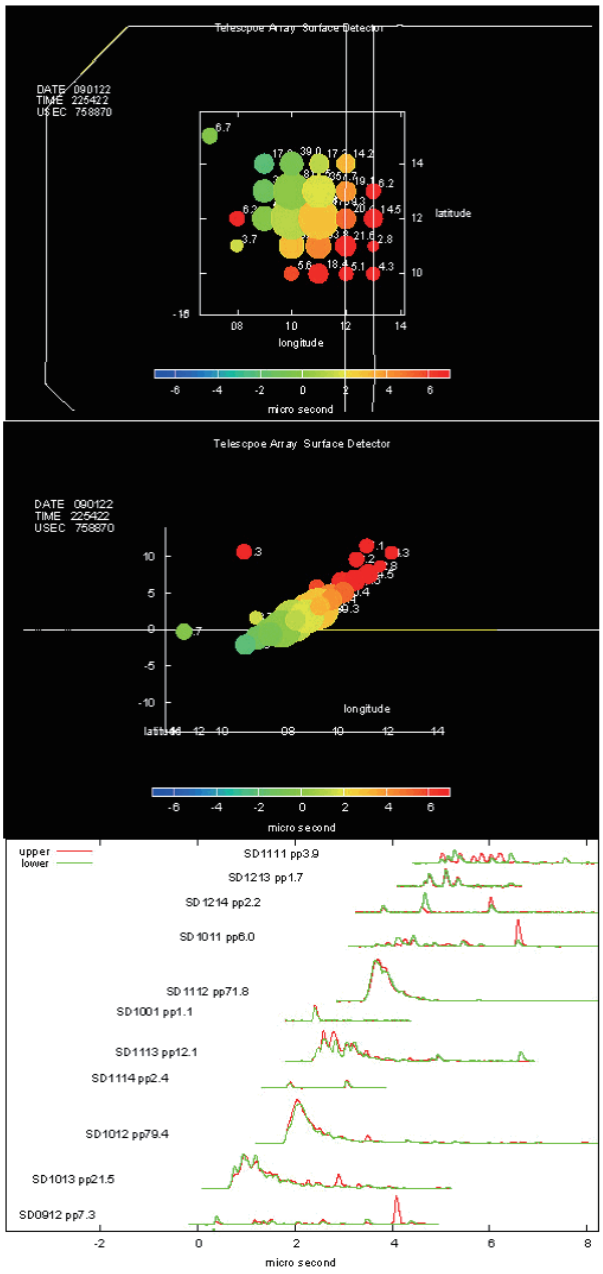

Fig. 2. Air Shower Event Observed with Surface Detectors. The top panel shows charge map of surface detectors which observed more than 1/3 of a muon signal. The horizontal axis and vertical axis represent longitude and latitude in detector ID, respectively. The radius of the circle is proportional to the logarithm of the energy deposition. The color bar shows triggered timing in micro second. The middle panel shows timing map. The vertical axis is triggered timing and the horizontal axis is the distance in detector ID. The bottom panel shows wave form distributions from the detectors. Red lines show upper layer scintillator signal and green lines show lower layer's signal.

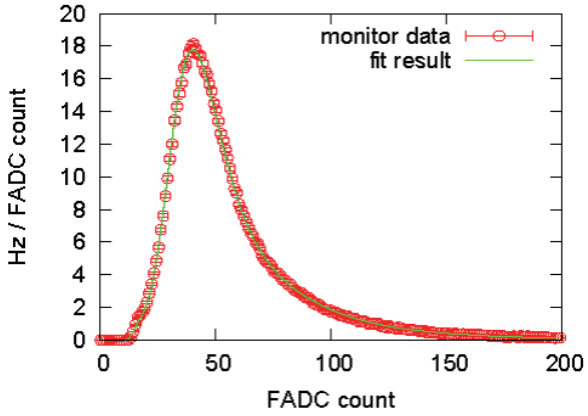

Fig. 3. An example of the energy deposit histogram of the 'muon' signals. Open circles are the measured spectrum and the solid curve is expected energy deposit by the simulation.

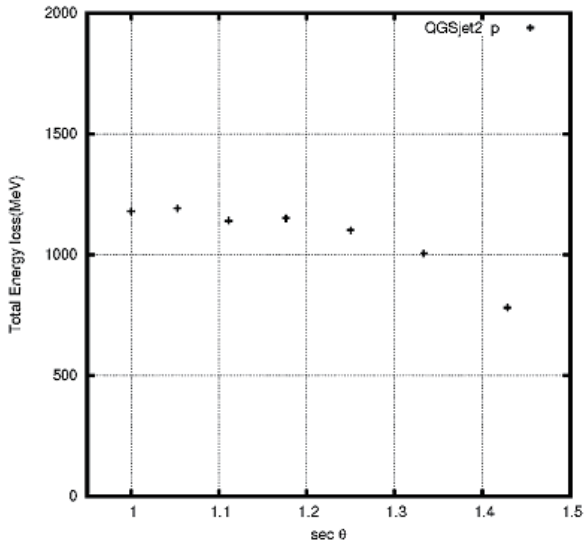

Fig. 4. Zenith angle dependence of the energy deposition S(800) in case of 10^{20}eV primary proton with QGSJET2 interaction model. We average the azimuth angle dependence of S(800) from the shower core.

interaction model.

Fluorescence Telescope

The ph-1 TA has three fluorescence stations. The fluorescence station in the southeast is called the Black Rock Mesa (BRM) site. The southwestern station is called the Long Ridge (LR) site and the station in the north is called the Middle Drum (MD) site.

Twelve reflecting telescopes are installed at each of the BRM and LR stations and cover the sky of 3°-34° in elevation and 108° in azimuth looking toward the center of the ground array.

The air shower image is detected by a mosaic PMT camera on the focal plane. A set of 16×16 PMTs (Hamamatsu 6234) with a hexagonal window is used for one camera. Each PMT covers 1.1°×1.0° patch of the sky.

A signal from the PMT is amplified by a factor of 50 by

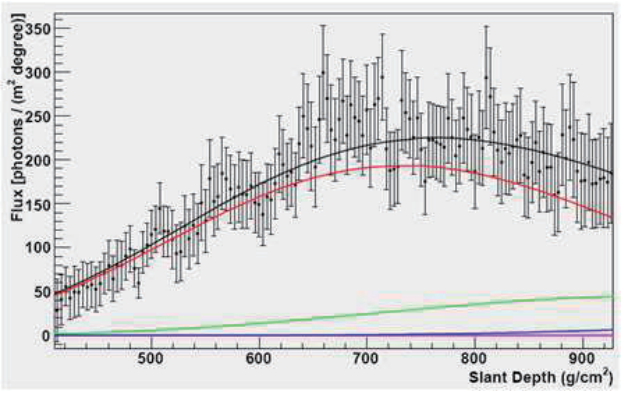

Fig. 5. Flux of light from an air shower event by the fluorescence telescope. Flux of light from data is shown together with expected light from total contribution, fluorescence, direct Cherenkov, Rayleigh-scattered Cherenkov and aerosol-scattered Cherenkov by black, red, pink, green and blue curves, respectively.

the pre-amplifier and is sent to a Signal Digitizer and Finder (SDF). The SDF module receives the signal with a shaping filter and digitizes it with a 12-bit, 40 MHz FADC. Consecutive four samplings are added by the following FPGA. A trace of fluorescence signal is searched in pipeline at the FPGA employing a sliding sum algorithm for every 25.6 μs of the time window. The dc component from the night sky background is estimated every 1 ms and is subtracted.

The result of the "hit" search by the SDF is reported to a Track Finder (TF) in the same VME crate and an air shower track is searched in one camera. A track is found when five or more adjacent PMTs are fired. A looser track definition is applied to a camera-crossing event. The results of all TF modules are concentrated to a Central Trigger Decision (CTD) module and the decision of data acquisition is made. The wave form data stored in the SDF memory are read out to "a camera PC" in parallel. Data are transferred from the camera PCs and collected to a storage PC by Ethernet during the daytime. Fig.5 shows an example of the flux of light from an air shower event observed by the fluorescence telescope.

The calibration of the telescope sensitivity is important for the measurement of energy. Characterizing parameters of each component such as the mirror reflectivity, filter transmission, PMT quantum efficiency and the electronics gain were measured piece by piece at the production or in situ [8]. The relative gain of all PMTs were adjusted in situ by the Xenon Flasher installed at the center of the mirror. The light from the flasher is diffused and filtered by BG3. The Xenon Flasher supplies a light pulse of good uniformity (<3%) to all PMTs in a camera.

There are three "standard" PMTs installed in a camera. The efficiency and the gain of the standard PMT are calibrated before installing to a camera and their values are transmitted to other PMTs by the Xenon Flasher calibration. A tiny YAP ($YAlO_3$:Ce) scintillator with 50 Bq ^{241}Am source is embedded in the BG3 filter of the standard PMT. The calibration of the standard PMT will be monitored by the YAP pulser.

For the calibration of the standard PMT, we developed a light source using a Rayleigh scattering of nitrogen laser

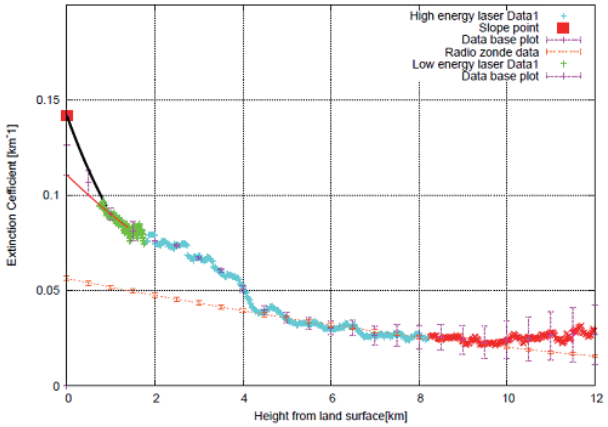

Fig. 6. The extinction coefficient as a function of the height from the ground. The results from vertical LIDAR shots are shown by the blue line and the green line for high energy shots and low energy shots, respectively. The black line is the exponential curve connected between the data at 0 km obtained by the slope method and the data obtained at the lowest height. The red dot line shows the extinction coefficient of pure Rayleigh scattering calculated from radiosonde data measured at Elko in Nevada where 340 km apart from the TA site.

(337 nm) in the nitrogen atmosphere. The power of laser is measured pulse by pulse to an accuracy of 5% and the known cross section of Rayleigh scattering is applied to calculate the intensity of the scattered light.

A LIDAR (LIght Detection And Ranging) system located at the Black Rock Mesa station is used for the atmospheric monitoring. It consists of a pulsed Nd:YAG laser (the third harmonic, 355 nm) and a telescope attached to an alto-azimuth mount and sharing the same optical axis. The laser can be shot to any direction and the back-scattered light is received by the telescope to analyze the extinction coefficient along the path of the laser. Fig. 6 shows an example of the extinction coefficient as a function of the height from the ground.

We also built a laser shooting facility (Central Laser Facility: CLF) in the middle of the array. The intensity of the laser shot is monitored to 5% accuracy and the Rayleigh scattering at high altitude can be considered as a "standard candle" observable at all stations. The comparison of the received light gives a reliable information for the difference and the change of atmospheric conditions. The CLF operation started in December 2008. Fig. 7 shows examples of CLF laser tracks.

For monitoring the cloud in the night sky, we installed an infra-red CCD camera (IR camera) at the Black Rock Mesa station, and take data of the night sky every hour during FD observation. The camera measures sky temperature in a field of view (FOV) of $25.8^\circ \times 19.5^\circ$ and digitizes in 320×236 pixels. The camera is mounted on a steering table and its orientation is changed in elevation and azimuthal directions via PC control. Fig. 8 show examples of pictures of the IR camera for a clear and a partly-cloudy skies, and the distribution of pixel data D. The pixel data $D = 1100$ corresponds to $\sim 20^\circ$C and $D = 1200$ to $\sim 0^\circ$C. We developed a statistical analysis method to judge the sky condition by defining the (clear/cloudy) flag of the IR images from the distribution of the pixel data and the thresholds. We found that most of the sky seen from the station is covered with clouds if there is a cloud in one direction in the FOV of the camera. Therefore this information obtained from the IR camera can be used for the FD data selections.

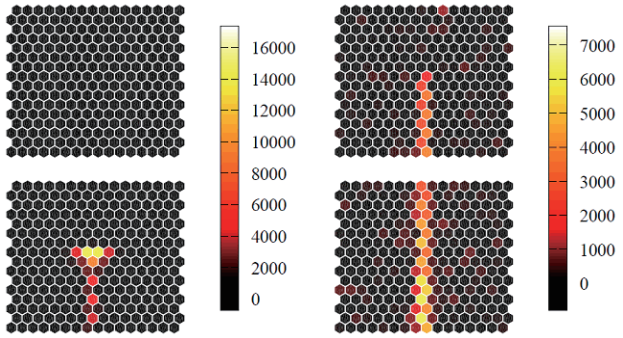

Fig. 7. Examples of CLF laser tracks. (left) the laser beam was blocked around the middle of the lower view by the cloud. (right) the laser shot image was taken at a clear night. Color bars show ADC counts.

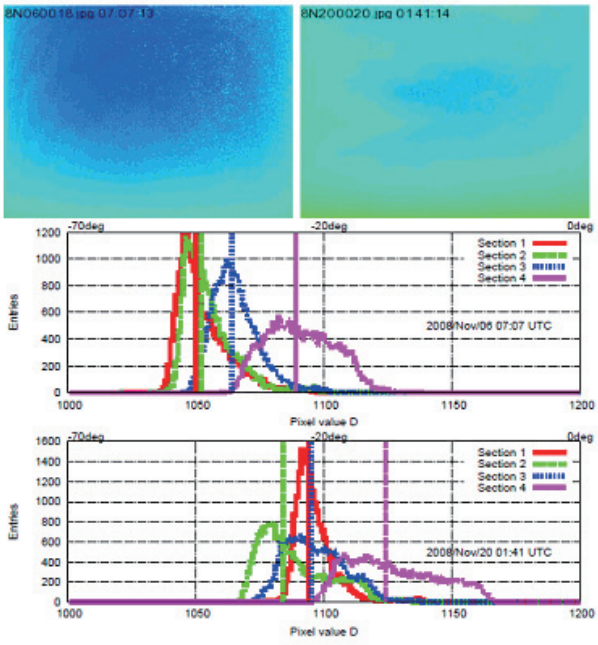

Fig. 8. Examples of IR pictures and distributions of the pixel data D of a clear and a partly cloudy skies (for lower elevation angle, 10.5°.). The vertical line for each distribution is the median D50

In order to confirm the absolute energy scale of the fluorescence detector in situ, we plan to operate a compact electron linear accelerator (TA-LINAC) about 100 m away from the fluorescence station and inject an electron beam vertically up into the atmosphere. A beam of 10^9 electrons with energy of 40 MeV and a duration of 1 μs well simulates a shower energy deposition of $\sim 4 \times 10^{16}$ eV 100 m away from the station, which corresponds to a shower of $\sim 4 \times 10^{20}$ eV 10 km away. The calibration is obtained by comparing the observed fluorescence signal with the expected energy deposition calculated by the GEANT simulation [9]. The accelerator was designed with a collaboration of KEK accelerator physicists and was assembled in KEK. We finished testing the basic performance of the accelerator in KEK by the end of 2008. The

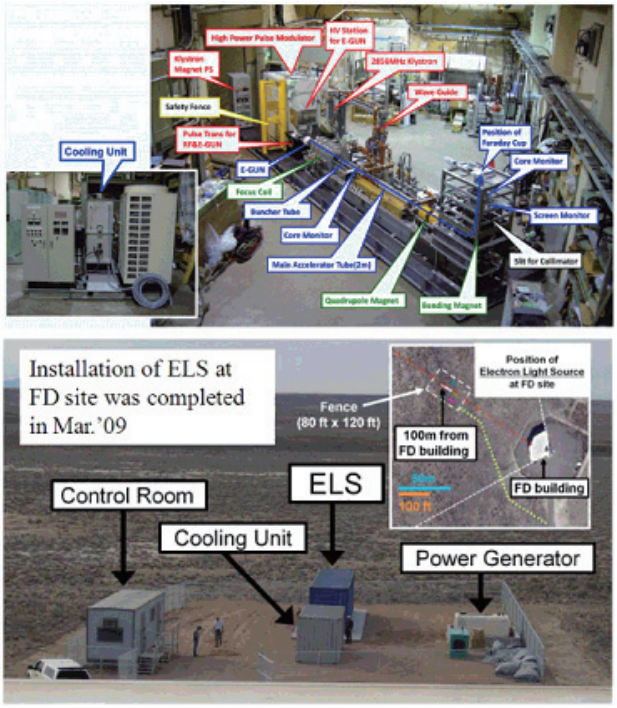

Fig. 9. Electron Linac. (top) the linac which was assembled in KEK, and (bottom) the one which was installed at the FD site.

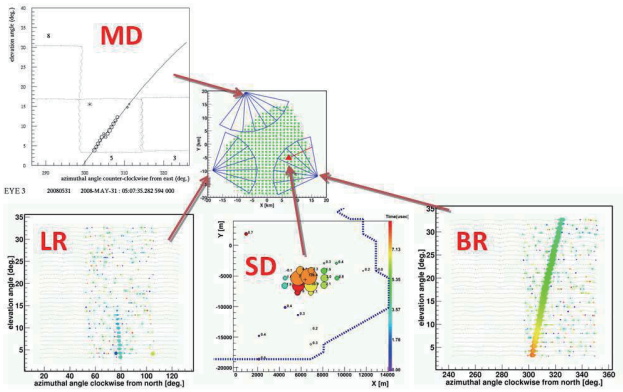

Fig. 10. An example of an air shower event which was observed simultaneously by surface detectors and three FD stations.

main accelerator part was installed in a 40-feet commercial container. We transported the accelerator system from Japan, and deployed it to the BRM site in March 2008. Fig. 9 shows the pictures of the completed TA-LINAC in KEK and the installed one at the FD site.

The Middle Drum FD station was constructed using refurbished equipment from the old HiRes-I observatory at Dugway in Utah. HiRes mirrors are 20% smaller in area than the mirrors in the BRM and LR FD stations. The MD fluorescence detector also observes at elevation angles from 3 to 31 degrees.

Three FD stations are fully operated from November of 2007. Fig. 10 show an example of an air shower event which was observed simultaneously by surface detectors and three FD stations.

Prospects

The construction of the ph-1 TA was completed in 2007 by the collaboration of Japanese, Korean, and American physicists. The Japanese fund for ph-1 TA was approved in 2003 by the Grants-in-Aid for Scientific Research (Kakenhi) of Priority Areas. The US fund is supported by the US National Science Foundation (NSF) through awards PHY-0307098 and PHY-0601915 (University of Utah) and PHY-0305516 (Rutgers University). The US proposal includes a construction of TALE, a Low Energy extension of TA down to 10^{17} eV, to investigate the modulation of CR composition and spectrum expected by the galactic to extra-galactic transition of CR origins.

The Auger group calibrated the ground array energy estimator $\rho(1000)$, the muon density 1000 m away from the shower center, by the measurement of shower energy from the fluorescence telescope. The Auger group and the HiRes group published the results of energy spectrum, which are consistent with GZK cutoff [4, 5] with their energy scales determined by the method of fluorescence telescope.

For the anisotropy, the Auger group claimed there is a correlation between the arrival directions of the highest energy cosmic rays and the positions of AGN [6] while the HiRes group reported that no correlations have been found [7].

For composition in EHE region, the Auger data suggests a change to a heavier composition while HiRes data is consistent with constant elongation rate which stays with proton.

The energy measurement of ph-1 TA therefore is less sensitive to the unknown composition of the primary cosmic rays and the details of hadronic interactions at EHE, whereas its sensitivity to the composition determination using the muon content is limited. It is our belief that the characteristic features of ph-1 TA, the sampling of electromagnetic shower energy, the unique calibration of fluorescence generation, usage of HiRes-I telescopes in TA site, and the measurement in the Northern Hemisphere, will make an essential contribution to the understanding of the intricate problem of GZK cutoff, anisotropy, and composition of EHECRs.

Bibliography

[1] The Telescope Array Project: Design Report, July, 2000.

[2] T.Abu-Zayyad et al., Phys. Rev. Lett. 92 (2004) 151101; T.Abu-Zayyad et al., Astropart. Phys. 23 (2005) 157.

[3] M.Fukushima et al., Proc. of 28th ICRC, Tsukuba, 2 (2003) 1025; S.Kawakami et al., Proc. of 28th ICRC, Tsukuba, 2 (2003) 1033; F.Kakimoto et al., Proc. of 28th ICRC, Tsukuba, 2 (2003) 1029; M.Fukushima, Proc. of APPI2003 workshop, KEK Proceedings 2003-6.

[4] R.U. Abbasi *et al.* (HiRes Collaboration), Phys. Rev. Lett. 100 (2008) 101101.

[5] J. Abraham *et al.* (Pierre Auger Collaboration), Phys. Rev. Lett. 101 (2008) 061101.

[6] J. Abraham *et al.* (Pierre Auger Collaboration), Astropart. Phys. 29 (2008); J. Abraham *et al.* (Pierre Auger Collaboration), Science 318 (2007) 939;

[7] R.U. Abbasi *et al*. (HiRes Collaboration), Astropart. Phys. 30 (2008) 175-179.

[8] H. Tokuno *et al*., Nucl. Instr. and Meth. A601 (2009) 364-371.

[9] T. Shibata *et al*., Ncul. Instr. and Meth. A597 (2008) 61-66.

Tibet ASγ Project

Experiment

The Tibet air shower experiment has been successfully operated at Yangbajing (90°31′ E, 30°06′ N; 4300 m above sea level) in Tibet, China since 1990. It has continuously made a wide field-of-view (approximately 2 steradian) observation of cosmic rays and gamma rays in the northern sky.

The Tibet I array was constructed in 1990 and it was gradually upgraded to the Tibet II by 1994 which consisted of 185 fast-timing (FT) scintillation counters placed on a 15 m square grid covering 36,900 m^2, and 36 density (D) counters around the FT-counter array. Each counter has a plastic scintillator plate of 0.5 m^2 in area and 3 cm in thickness. All the FT counters are equipped with a fast-timing 2-inch-diameter photomultiplier tube (FT-PMT), and 52 out of 185 FT counters are also equipped with a wide dynamic range 1.5-inch-diameter PMT (D-PMT) by which we measure up to 500 particles which saturates FT-PMT output, and all the D-counters have a D-PMT. A 0.5 cm thick lead plate is put on the top of each counter in order to increase the counter sensitivity by converting gamma rays into electron-positron pairs in an electromagnetic shower. The mode energy of the triggered events in Tibet II is 10 TeV.

In 1996, we added 77 FT counters with a 7.5 m lattice interval to a 5,200 m^2 area inside the northern part of the Tibet II array. We called this high-density array Tibet HD. The mode energy of the triggered events in Tibet HD is a few TeV.

In the late fall of 1999, the array was further upgraded by adding 235 FT-counters so as to enlarge the high-density area from 5,200 m^2 to 22,050 m^2, and we call this array and further upgraded one Tibet III. In 2002, all of the 36,900 m^2 area was covered by the high-density array by adding 200 FT-counters more. Finally we set up 56 FT-counters around the 36,900 m^2 high density array and equipped 8 D-counters with FT-PMT in 2003. At present, the Tibet air shower array consists of 761 FT-counters (249 of which have a D-PMT) and 28 D-counters as in Fig. 1.

The performance of the Tibet air shower array has been well examined by observing the Moon's shadow (approximately 0.5 degree in diameter) in cosmic rays. The deficit map of cosmic rays around the Moon demonstrates the angular resolution to be around 0.9° at a few TeV for the Tibet III array. The pointing error is estimated to be better than 0°.011, by displacement of the shadow's center from the apparent center in the north-south direction, as the east-west component of the geomagnetic field is very small at the experimental site. On the other hand, the shadow center displacement in the east-west direction due to the geomagnetic field enables us to spectroscopically estimate the energy scale uncertainty less than ±12 %.

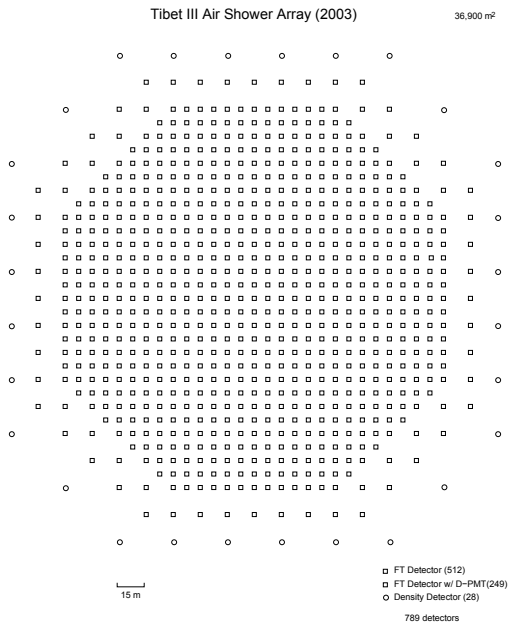

Fig. 1. Schematic view of the Tibet III array.

Thanks to high statistics, the Tibet air shower experiment introduces a new method for energy scale calibration other than the conventional estimation by the difference between the measured cosmic-ray flux by an air shower experiment and the higher-energy extrapolation of cosmic-ray flux measured by direct measurements by balloon-borne or satellite experiments.

Physics Results

Our current research theme is classified into 4 categories:

(1) TeV celestial gamma-ray point/diffuse sources,

(2) Chemical composition and energy spectrum of primary cosmic rays in the knee energy region,

(3) Cosmic-ray anisotropy in the multi-TeV region with high precision,

(4) Global 3-dimensional structure of the solar and interplanetary magnetic fields by observing the Sun's shadow in cosmic rays.

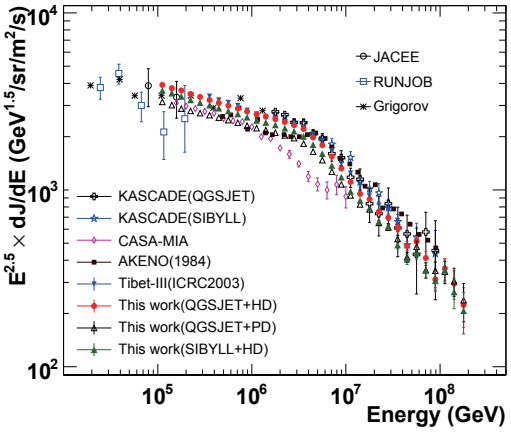

Fig. 2. From [1]. The differential energy spectra of all particles obtained by the present work using mixed composition models compared with other experiments. For the following references; JACEE (Asakimori et al. 1998),RUNJOB (Apanasenko et al. 2001), Grigorov (Grigorov et al. 1971), KASCADE (Antoni et al. 2005), CASA-MIA (Glasmacher et al. 1999), AKENO(1984) (Nagano et al. 1984), Tibet-III(ICRC2003) (Amenomori et al. 2003a), see [1].

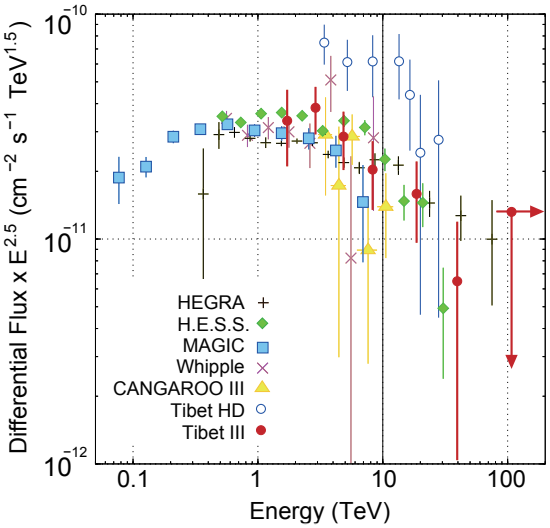

Fig. 3. From [3]. Differential energy spectrum of γ-rays from the Crab Nebula obtained using the data collected from 1999 November to 2005 November with the Tibet-III array in comparison with the results from IACTs. For more detail and references, see [3].

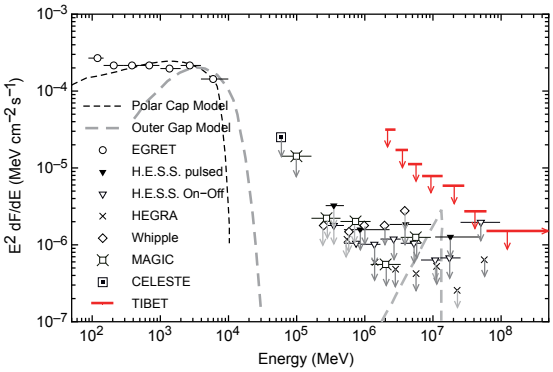

Fig. 4. From [3]. Upper limits on the pulsed γ-ray flux from the Crab pulsar observed by the Tibet-III array (arrows with thick solid line), together with results from other experiments. The long-dashed curve and dashed curve represent the fluxes expected from the outer gap and polar cap models, respectively. For more detail and references, see [3].

We will introduce a part of the results obtained in this fiscal year.

As shown in Fig. 2, we obtain an updated all-particle energy spectrum of primary cosmic rays in a wide range from 10^{14} eV to 10^{17} eV using 5.5×10^7 events collected in the period from 2000 November through 2004 October by the Tibet-III air-shower array located at 4300 m above sea level (atmospheric depth of 606 g/cm^2). The size spectrum exhibits a sharp knee at a corresponding primary energy around 4 PeV. This work uses increased statistics and new simulation calculations for the analysis. We performed extensive Monte Carlo calculations and discuss the model dependences involved in the final result assuming interaction models of QGSJET01c and SIBYLL2.1 and primary composition models of heavy dominant (HD) and proton dominant (PD) ones. Pure proton and pure iron primary models are also examined as extreme cases. The detector simulation was also made to improve the accuracy of determining the size of the air showers and the energy of the primary particle. We confirmed that the all-particle energy spectra obtained under various plausible model parameters are not significantly different from each other as expected from the characteristics of the experiment at the high altitude, where the air showers of the primary energy around the knee reaches near maximum development and their features are dominated by electromagnetic components leading to the weak dependence on the interaction model or the primary mass. This is the highest-statistical and the best systematics-controlled measurement covering the widest energy range around the knee energy region.

The Tibet-III air shower array, consisting of 533 scintillation detectors, has been operating successfully at Yangbajing in Tibet, China since 1999. Using the dataset collected by this array from 1999 November through 2005 November, we obtained the energy spectrum of γ-rays from the Crab Nebula[3], expressed by a power law as $(dJ/dE) = (2.09 \pm 0.32) \times 10^{-12}(E/3\ \mathrm{TeV})^{-2.96\pm0.14}\mathrm{cm}^{-2}\mathrm{s}^{-1}\mathrm{TeV}^{-1}$ in the energy range of 1.7 to 40 TeV. As shown in Fig. 3, this result is consistent with other independent γ-ray observations by imaging air Cherenkov telescopes.

We also search for gamma rays from the Crab pulsar with 33 ms periodicity and find no significant signal. Accordingly, we set flux upper limits on the pulsed gamma-ray flux, as shown in Fig. 4.

In this analysis, we carefully checked and tuned the performance of the Tibet-III array using data on the Moon's shadow in comparison with a detailed Monte Carlo simulation. The shadow is shifted to the west of the Moon's apparent position as an effect of the geomagnetic field, although the extent of this displacement depends on the primary energy positively charged cosmic rays. This finding enables us to estimate the systematic error in determining the primary energy from its shower size. This error in our experiment is estimated to be less than $\pm12\%$ including uncertainties in the chemical

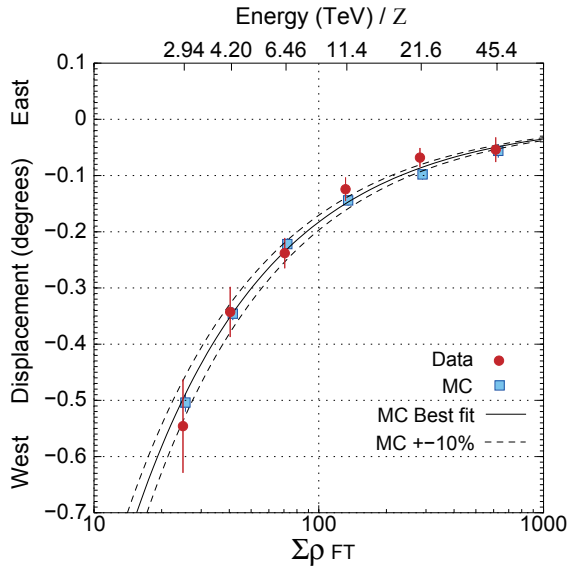

Fig. 5. From [3]. Dependence of shower size on the displacement of the Moon's shadow in the east-west direction. The filled circles show the experimental data, and open squares represent the MC simulation. The solid curve is fitted to the MC events, and dashed curves show a ±10% deviation from the solid curve, respectively. The upper scale indicates the logarithmic mean of E/Z (TeV / Z) in each $\sum\rho_{\rm FT}$ bin. For more detail, see [3].

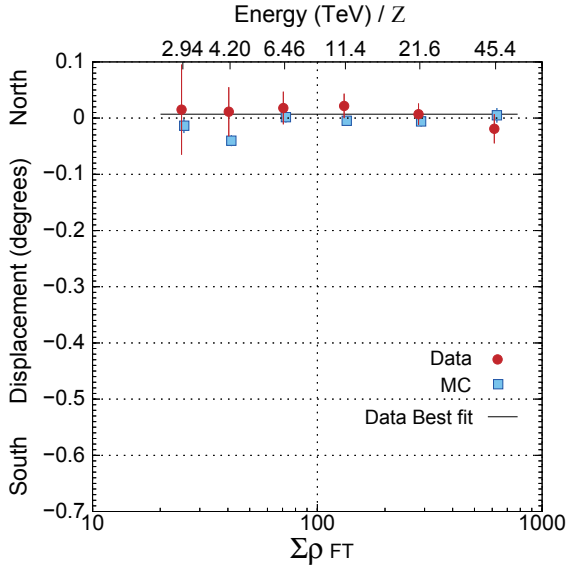

Fig. 6. From [3]. Dependence of shower size on the displacement of the Moon's shadow in the north-south direction. The filled circles and open squares represent experimental data and the MC simulation, respectively. The solid line denotes the fitting to the experimental data assuming a constant function, resulting in $0^\circ.008 \pm 0^\circ.011$. The upper scale indicates the logarithmic mean of E/Z (TeV/Z) in each $\sum\rho_{\rm FT}$ bin. For more detail, see [3].

composition of primary cosmic rays and in the hadronic interaction models, as is shown in Fig. 5. This energy scale estimation is the first attempt among cosmic-ray experiments at ground level. The systematic pointing error is also estimated to be smaller than $0^\circ.011$, as shown in Fig. 6. The deficit rate and position of the Moon's shadow are shown to be very stable within a statistical error of ±6% year by year. This guarantees the long-term stability of point-like source observation with the Tibet-III array. These systematic errors are adequately taken into account in our study of the Crab Nebula.

The solar activity in Cycle 23 gradually changes to final minimum phase. The Sun's shadow generated by multi-TeV cosmic-ray particles has been continuously observed with the Tibet-II and Tibet-III air shower array in 1996 through 2008 during almost whole period of the Solar Cycle 23. We have shown that the Sun's shadow is strongly affected by the solar and interplanetary magnetic fields changing with the solar activity. We present yearly variation of the Sun's shadow above 10 TeV in association with the Solar Cycle 23, in unit of deficit significance in Fig. 7 and in unit of deficit intensity in Fig. 8, respectively. We observe the solar minimum still continue in 2008, as is indicated by the corresponding sunspot number observation. We keep an eye on the Sun's shadow next year to see whether it will still remain at high significance or not.

Other Activities

This group has developed and completed several automatic measuring systems that are powerful for analyzing cosmic ray tracks or air shower spots, that is, automatic microdensitometers, precise coordinate-measuring systems and image scanners controlled by a computer. Enormous data recorded on nuclear emulsion plates or X-ray films are rapidly

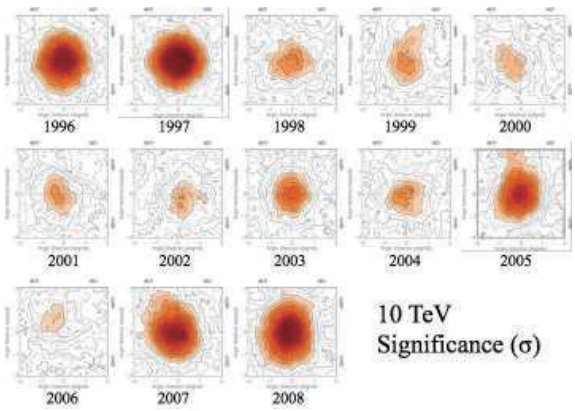

Fig. 7. Observed yearly variation of the Sun's shadow depth (significance map.

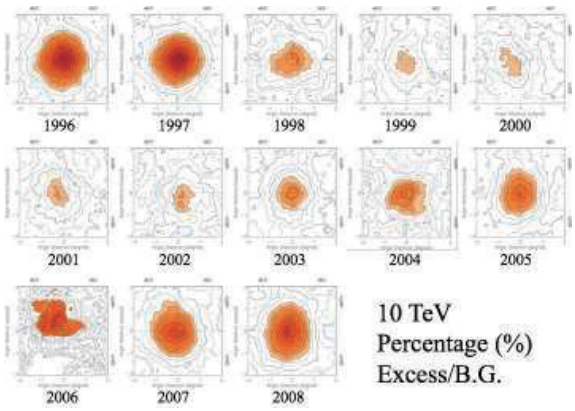

Fig. 8. Observed yearly variation of the Sun's shadow depth, (intensity map).

and precisely measured by the use of these measuring systems.

The emulsion-pouring facilities can meet the demands for making any kind of nuclear emulsion plates which are used for cosmic ray or accelerator experiments. The thermostatic emulsion-processing facilities are operated in order to develop nuclear emulsion plates or X-ray films. Using these facilities, it is also possible to make and develop emulsion pellicles in 600 μm thickness each. In this way, these facilities are open to all the qualified scientists who want to carry out joint research program successfully.

Future Plans

(1) Gamma-ray astronomy in the 100 TeV region

We have a plan to construct a large ($\sim 10,000$ m$^2 \times 1.5$m deep) underground (~ 2.5 m soil+concrete overburden) water Cherenkov muon detector array (Tibet MD) around an extended version (Tibet AS, $\sim$83,000 m^2) of Tibet III. By Tibet AS + MD, we aim at background-free detection of celestial point-source gamma rays in the 100 TeV region (10 TeV – 1000 TeV) with world-best sensitivity and at locating the origins of cosmic rays accelerated up to the knee energy region in the northern sky. The measurement of cut off energies in the energy spectra of such gamma rays in the 100 TeV region may contribute significantly to understanding of the cosmic-ray acceleration limit at SNRs. Search for extremely diffuse gamma-ray sources by Tibet AS + MD, for example, from the galactic plane or from the Cygnus region may be very intriguing as well. Above 100 TeV, the angular resolution of Tibet AS with 2-steradian wide field of view is 0.2° and the hadron rejection power of Tibet MD is 1/10000. The proposed Tibet AS + MD, demonstrated in Fig. 9, has the world-best sensitivity in the 100 TeV region, superior to HESS above 10-20 TeV and to CTA above 30-40 TeV.

Then, how many unknown/known sources do we expect to detect by Tibet AS + MD, assuming the energy spectra of the gamma-ray sources extend up to the 100 TeV region? Eleven of the HESS new 14 sources discovered by the galactic plane survey in the southern sky would be detected by Tibet AS + MD, if it were located at the HESS site. As no extensive search has been done by an apparatus with sensitivity comparable to HESS (1 % in unit of RX J1713.7-3946/50-hour observation) in the northern sky, we expect to discover some 10 new gamma-ray sources in the northern sky. In addition to unknown point-like sources, we expect to detect established sources in the 100 TeV region: TeV J2032+4130, HESS J1837-069, Crab, some new Milagro sources, Mrk421, Mrk501 are sufficiently detectable and Cas A, HESS J1834-087,LS I+63 303, IC443 and M87 are marginal.

Furthermore, our integral flux sensitivity to diffuse gamma rays will be the world-best as well. The diffuse gamma rays from the Cygnus region reported by the Milagro group and also diffuse gamma-rays from the galactic plane will be clearly detected. Diffuse gamma-rays of extragalactic origin may be an interesting target as well.

In fall, 2007, a prototype underground muon detector, composed of two 52m^2 water pools, was successfully constructed in Tibet to demonstrate the technical feasibility, cost estimate, validity of our Monte Carlo simulation, as is shown in Figs. 10 and 11. Single muon peak is clearly observed in the prototype muon detectors. Preliminary analysis indicates that our MC simulation reproduces real data quite reasonably. Detailed comparison is under way.

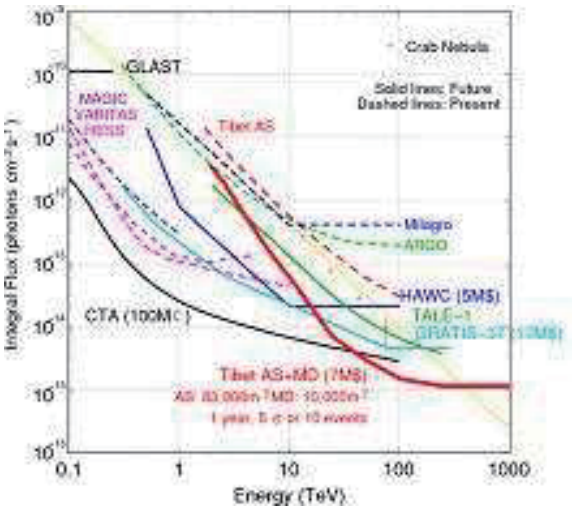

Fig. 9. Tibet AS + MD (red curve) integral flux sensitivity (5σ or 10 events/1yr) for a point source.

Fig. 10. Prototype muon detector viewed from outside, just before being covered with soil.

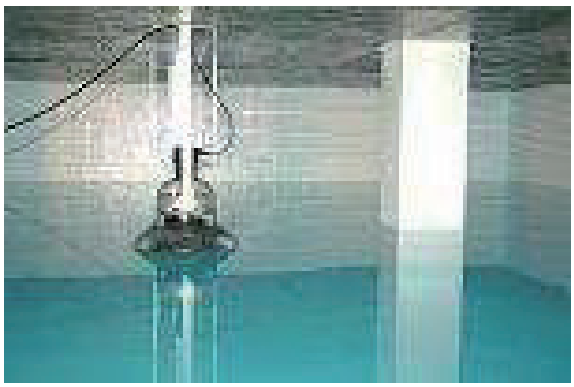

Fig. 11. Prototype muon detector viewed from inside.

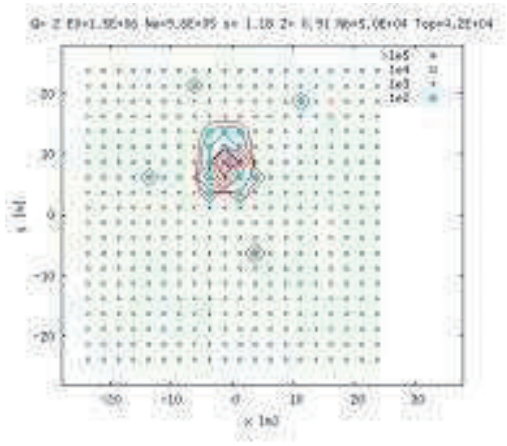

Fig. 12. Illustration of YAC array.

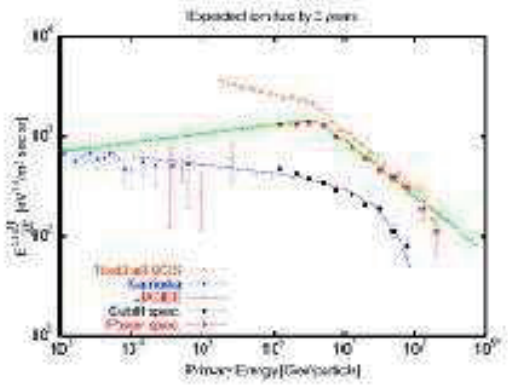

Fig. 13. Expected cosmic-ray iron energy spectra with Tibet AS + YAC.

(2) Chemical composition of primary cosmic rays making the knee in the all-particle energy spectrum

We have measured the energy spectra of primary cosmic-ray protons, heliums, all particles around the knee energy region. The main component responsible for making the knee structure in the all particle energy spectrum is heavier nuclei than helium. The next step is to identify the chemical component making the knee in the all particle energy spectrum. We have a plan to install an air shower core detector array (1000 to 5000 m^2 in area) around the center of Tibet III, as is illustrated in Fig. 12 to distinguish the heavy component making the knee by measuring the difference in lateral distribution of energetic air shower cores.

This will be the first experiment to selectively measure the energy spectrum of the heavy component in the knee energy region and will demonstrate that the knee of the all particle energy spectrum is really composed of heavy nuclei. Figure 13 shows the expected energy spectra of cosmic-ray iron nuclei depending on theoretical models. Tibet AS + YAC has a strong model discrimination power.

Tibet ASγ collaboration

ICRR, Univ. of Tokyo, Kashiwa, Chiba 277-8582

In collaboration with the members of:
Hirosaki Univ., Hirosaki, Japan; Saitama Univ., Urawa, Japan; IHEP, Beijing, China; Yokohama National Univ., Yokohama, Japan; Hebei Normal Univ., Shijiazhuang, China; Tibet Univ., Lhasa, China; Shandong Univ., Jinan, China; South West Jiaotong Univ. Chengdu, China; Yunnan Univ., Kunming, China; Kanagawa Univ., Yokohama, Japan; Faculty of Education, Utsunomiya Univ., Utsunomiya, Japan; ICRR, Univ. of Tokyo, Kashiwa, Japan; Konan Univ., Kobe, Japan; Shibaura Inst. of Technology, Saitama, Japan; Department of Physics, Shinshu Univ., Matsumoto, Japan; Center of Space Science and Application Research, Beijing, China; Tsinghua Univ., Beijing, China; Waseda Univ., Tokyo, Japan; NII, Tokyo, Japan; Sakushin Kakuin Univ., Utsunomiya, Japan; AMNC, Utsunomiya Univ., Utsunomiya, Japan; Tokyo Metropolitan Coll. of Industrial Technology, Tokyo, Japan; Shonan Inst. of Technology, Fujisawa, Japan; RIKEN, Wako, Japan; School of General Education, Shinshu Univ. Matsumoto, Japan.

Bibliography

Papers in refereed journals

[1] "The all-particle spectrum of primary cosmic rays in the wide energy range from 10^{14} eV to 10^{17} eV observed with the Tibet-III air-shower array", M. Amenomori *et al.*, ApJ **678** 1165–1179, (2008).

[2] "The energy spectrum of all-particle cosmic rays around the knee region observed with the Tibet-III air-shower array", M. Amenomori *et al.*, Advances in Space Research, **42** 467–472, (2008).

[3] "Multi-TeV Gamma-Ray Observation from the Crab Nebula Using the Tibet-III Air Shower Array Finely Tuned by the Cosmic-Ray Moon's Shadow", M. Amenomori *et al.*, ApJ **692** 61–72, (2009).

Papers in conference proceedings

[4] "Analysis of primary cosmic ray proton and helium components at the knee energy region with the Tibet hybrid experiment", M. Amenomori *et al.* (The Tibet ASγ Collaboration), Proceedings of the 30th International Cosmic Ray Conference, Merida, Mexico, 3-11 July 2007, vol.**2**, 117–120, (2008).

[5] "Chemical composition of cosmic rays at the knee measured by the Tibet air-shower-core detector", M. Amenomori *et al.* (The Tibet ASγ Collaboration), Proceedings of the 30th International Cosmic Ray Conference, Merida, Mexico, 3-11 July 2007, vol.**2**, 121–124, (2008).

[6] "Future plan for observation of cosmic gamma rays in the 100 TeV energy region with the Tibet air shower array : physics goal and overview", M. Amenomori *et al.* (The Tibet ASγ Collaboration), Proceedings of the 30th

International Cosmic Ray Conference, Merida, Mexico, 3-11 July 2007, vol.**2**, 353–356, (2008).

[7] "Future plan for observation of cosmic gamma rays in the 100 TeV energy region with the Tibet air shower array : simulation and sensitivity", M. Amenomori *et al.* (The Tibet ASγ Collaboration), Proceedings of the 30th International Cosmic Ray Conference, Merida, Mexico, 3-11 July 2007, vol.**2**, 357–360, (2008).

[8] "A search for 100 TeV celestial gamma rays with the Tibet air shower array and a future prospect", M. Amenomori *et al.* (The Tibet ASγ Collaboration), Proceedings of the 30th International Cosmic Ray Conference, Merida, Mexico, 3-11 July 2007, vol.**2**, 575–578, (2008).

[9] "Seven-year observation of multi-TeV gamma rays from the Crab Nebula with the Tibet air shower array", M. Amenomori *et al.* (The Tibet ASγ Collaboration), Proceedings of the 30th International Cosmic Ray Conference, Merida, Mexico, 3-11 July 2007, vol.**2**, 799–802, (2008).

[10] "Search for pulsed multi-TeV gamma rays from the Crab pulsar with the Tibet III air shower array", M. Amenomori *et al.* (The Tibet ASγ Collaboration), Proceedings of the 30th International Cosmic Ray Conference, Merida, Mexico, 3-11 July 2007, vol.**2**, 783–786, (2008).

[11] "Gamma-hadron separation of parent particles of air showers above several 10 TeV energies using Tibet-III air-shower array", M. Amenomori *et al.* (The Tibet ASγ Collaboration), Proceedings of the 30th International Cosmic Ray Conference, Merida, Mexico, 3-11 July 2007, vol.**2**, 583–583, (2008).

[12] "Study of discrimination between cosmic gamma rays and protons at multi-TeV energies with the Tibet air shower array", M. Amenomori *et al.* (The Tibet ASγ Collaboration), Proceedings of the 30th International Cosmic Ray Conference, Merida, Mexico, 3-11 July 2007, vol.**3**, 1493–1493, (2008).

[13] "The cosmic ray all-particle spectrum in the wide energy range from 10^{14} eV to 10^{17} eV observed with the Tibet-III air shower array", M. Amenomori *et al.* (The Tibet ASγ Collaboration), Proceedings of the 30th International Cosmic Ray Conference, Merida, Mexico, 3-11 July 2007, vol.**4**, 103–106, (2008).

[14] "Zenith angle dependence of the size spectrum of air showers around the knee observed with the Tibet air shower array", M. Amenomori *et al.* (The Tibet ASγ Collaboration), Proceedings of the 30th International Cosmic Ray Conference, Merida, Mexico, 3-11 July 2007, vol.**4**, 99–102, (2008).

[15] "Sun's Shadow in the Solar Cycle 23 Observed with the Tibet Air Shower Array and Comparison with Simulation Studies", M. Amenomori *et al.* (The Tibet ASγ Collaboration), Proceedings of the 30th International Cosmic Ray Conference, Merida, Mexico, 3-11 July 2007, vol.**5**, 529–532, (2008).

[16] "Implication of the sidereal anisotropy of 5 TeV cosmic ray intensity observed with the Tibet III air shower array", M. Amenomori *et al.* (The Tibet ASγ Collaboration), Proceedings of the 30th International Cosmic Ray Conference, Merida, Mexico, 3-11 July 2007, vol.**5**, 593–596, (2008).

[17] "Study on TeV gamma Ray Emission from Cygnus Region Using the Tibet Air Shower", M. Amenomori *et al.* (The Tibet ASγ Collaboration), Proceedings of the 30th International Cosmic Ray Conference, Merida, Mexico, 3-11 July 2007, vol.**2**, 695–698, (2008).

[18] "Two-dimensional observation on TeV Cosmic-ray solar diurnal variation using the Tibet Air Shower Array", M. Amenomori *et al.* (The Tibet ASγ Collaboration), Proceedings of the 30th International Cosmic Ray Conference, Merida, Mexico, 3-11 July 2007, vol.**5**, 577–580, (2008).

[19] "The study of Periodic Variation of Cosmic Ray intensity with the Tibet III Air Shower Array", M. Amenomori *et al.* (The Tibet ASγ Collaboration), Proceedings of the 30th International Cosmic Ray Conference, Merida, Mexico, 3-11 July 2007, vol.**5**, 609–612, (2008).

[20] "A Monte Carlo study to measure the energy spectra of the primary heavy components at the knee using a new Tibet AS core detector array and a large underground muon detector array", J. Huang *et al.* (The Tibet ASγ Collaboration), Proceedings of the 30th International Cosmic Ray Conference, Merida, Mexico, 3-11 July 2007, vol.**2**, 329–312, (2008).

[21] "Tibet Air Shower Array: Results and Future Plan", M. Amenomori *et al.* (The Tibet ASγ Collaboration), Proceedings of TAUP2007, Sendai, Japan, Journal of Conference Series vol.**120**, 062024-1-3, (2008).

The Ashra Project

Overview

Ashra (*All-sky Survey High Resolution Air-shower detector*) [1, 2, 3] is a project to build an unconventional optical telescope complex that images very wide field of view, covering 77% of the sky, yet with the angle resolution of a few arcmin, sensitive to the blue to UV light with the use of image intensifier and CMOS technology. The project primarily aims to observe Cherenkov and fluorescence lights from the lateral and longitudinal developments of very-high-energy cosmic-ray air showers in the atmosphere. It can also be used to monitor optical transients in the wide field of sky. The observatory will firstly consist of one main station having 12 detector units and two sub-stations having 8 and 4 detector units. One detector unit has a few light collecting systems with segmented mirrors. The main station was constructed on Mauna Loa (3,300 m) on Hawaii Island in 2007.

We started observation of optical transients and pilot observation of Cherenkov tau neutrinos with some of the light collectors in 2008. By analyzing the accumulated data from these observations, we have already searched for optical and VHE-neutrino emissions, for example, in the field of GRB081203A around the Swift/BAT-triggered GRB time [4, 5, 6].

Project

The observatory will firstly consist of one main station having 12 detector units and two sub-stations having 8 and 4 detector units. One detector unit has a few light collecting systems with segmented mirrors. The features of the system were studied with a prototype detector unit located on Haleakala. The main station was constructed on Mauna Loa (3,300 m) in 2007.

The key technical feature of the Ashra detector rests on the use of electrostatic lenses to generate convergent beams rather than optical lens systems. This enables us to realize a high resolution over a wide field of view. This electron optics requires:

- *image pipeline;* the image transportation from imaging tube (image intensifier) to a trigger device and image sensors of fine pixels (CCD+CMOS), with high gain and resolution, and
- *parallel self-trigger:* the systems that trigger separately for atmospheric Cherenkov and fluorescence lights.

Observational Objectives

optical transients; Ashra will acquire optical image every 6 s after 4-s exposure. This enables us to explore optical transients, possibly associated with gamma ray bursts (GRBs), flares of soft gamma-ray repeaters (SGRs), supernovae explosion, and so on, in so far as they are brighter than $B \simeq 13$ mag, for which we expect 3-σ signals. The unique advantage is the on-time detection of the events without resorting to usual satellite alerts. 10$\sim$20 events per year are expected in coincidence with the Swift gamma-ray events. The field of view that is wider than satellite instruments allows to detect more optical transients, including an interesting possibility for an optical flash, not visible with gamma rays.

TeV gamma rays; Atmospheric Cherenkov radiation will be imaged by Ashra. Requiring the signal-to-noise ratio (SNR) $>$5, the system will allow to explore VHE gamma-ray sources with the energy threshold of several TeV at the limiting flux sensitivity of 5% Crab for 1-year observation.

EeV cosmic rays; For fluorescence lights from VHE cosmic rays the effective light gathering efficiency is comparable with that of the High Resolution Fly's Eye detector (HiRes). The arcmin pixel resolution of Ashra provides finer images of longitudinal development profiles of EeV cosmic ray (EeV-CR) air showers. The resolution of arrival direction with the stereo reconstruction is thus significantly improved and it is better than one arcmin for the primary energy of EeV and higher [7]. This is useful to investigate events clustered around the galactic and/or extragalactic sources. This in turn would give us information as to the strength and coherence properties of the magnetic field.

PeV-EeV neutrinos; Ashra may detect Cherenkov and/or fluorescence signals generated from tau-particle induced air-showers that is generated from interactions of tau neutrinos with the mountain and/or the earth. This is identified by peculiar geometry of the air-shower axis. The 1-year detection sensitivity with the full configuration of Ashra is 5 and 2 times larger than the Waxman-Bahcall limit for mountain-produced event (Cherenkov) and earth-skimming event (fluorescence), respectively. The most sensitive energy of around 100 PeV is suitable for the GZK neutrino detection.

The expected performance for each observational object is summarized in Table 1. An example of a 42-degree FOV image taken by the Ashra light collector is shown in Figure 1.

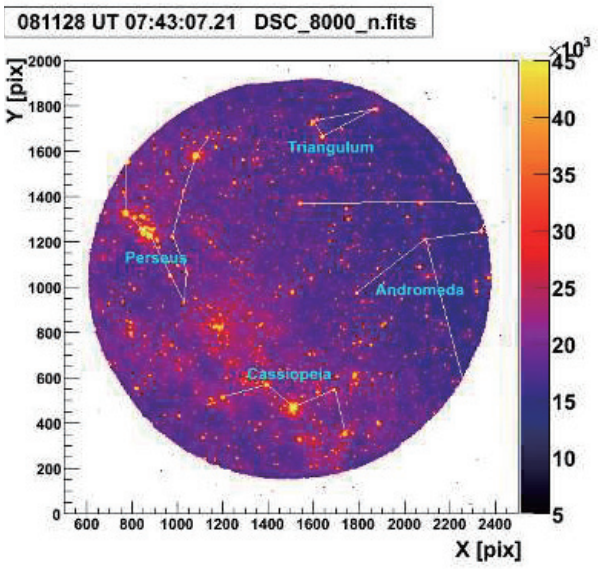

Fig. 1. Example of a 42-degree FOV image taken by the Ashra light collector. The solid lines are drawn to indicate constellations.

Site Preparation

After finishing the grading work for the area of 2,419 m^2 at the Mauna Loa site at the end of July 2005, installation of electrical power lines and transformers was performed until the beginning of September. We started the construction of the detector in October 2005 after receiving materials from Japan. By the middle of December 2005, the first shelters having motorized rolling doors, acrylic plate windows to maintain air-tightness, and heat-insulating walls and floors have been constructed and positioned on eight construction piers of concrete blocks at the Mauna Loa site. In the shelters, the optical elements of the light collectors have been already installed. The optical performance were checked and adjusted to be optimum with star light images from the pilot observation.

In December 2005, we evaluated the night sky background flux on Mauna Loa using the Ashra light collector

Opt. Transients	TeV-γ	Mountain-ν	Earth-skimming-ν	EeV-CR
B-UV	Cherenkov	Cherenkov	Fluorescence	Fluorescence
λ=300$\sim$420nm	several TeV	a few 100 TeV	a few 10 PeV	a few 100 PeV
15 mag./4s @3σ	5% Crab/1yr@5σ	5 WB-limit/1yr	2 WB-limit/1yr	1600/1yr $>$10 EeV
2 arcmin	6 arcmin	unknown	3 arcmin @ 100 PeV	1 arcmin @ 10 EeV

Table 1. Summary of performance with the full configuration (Ashra-2) of three Ashra sites. Detected light, energy threshold, sensitivity limit, and angular resolution are listed from top down for each objective. For EeV-CRs, trigger requirement is two or more stations. Waxman and Bahcall have calculated a neutrino flux upper limit from astrophysical transparent source, here referred to as the WB-limit. For the observation time for objectives other than optical transients, the realistic detection efficiency is taken into account.

installed and aligned in a shelter. The result is fairly consistent with the background in La Palma and Namibia by the HESS group From the star light observations, our understanding of the light correction efficiency to be accurate within 5% level.

The civil engineering construction of light collectors in shelters at the Mauna Loa site was completed in August 2007. Figure 2 shows a picture of the constructed Mauna Loa stations. In this Ashra-1 experiment, we are performing device installation and specific observation in a step-by-step way to enhance the scientific impacts.

Fig. 2. The Ashra main and sub stations at the Mauna Loa sites.

Observation

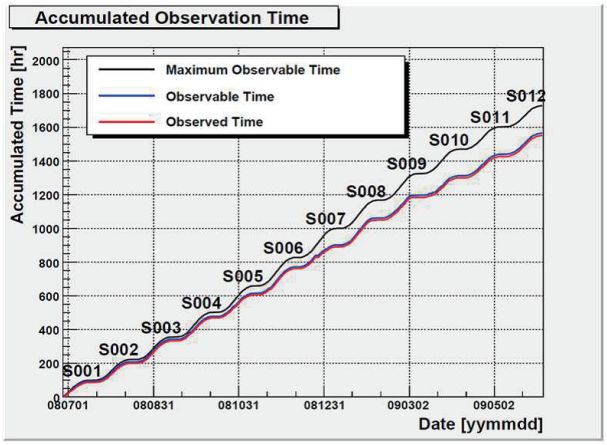

Fig. 3. Summary of Ashra optical transient observation time.

As a first step, we have started the observation of optical transients. During observation, Optical images were constantly collected every 6 s after 4-s exposure. Figure 3 summarizes our observation statistics up to now. Maximum observable time is defined by the following condition:

- *Sun condition;* the altitude of the sun must be lower than -18 degree.
- *Moon condition;* the altitude of the moon is lower than 0 degree, or the moon fraction is less than 0.2.

We have accumulated more than 1500 hours of observation time within one year of observation. Good weather rate of 90% shows the superiority of our site and operation efficiency of 99% demonstrates the stability of our operation, where good weather rate is defined by observable time divided by maximum observation time and operation efficiency is defined by observed time divided by observable time. Table2 summarizes coincidence events with satellite GRB triggers[8][9]. In those events, our wide field covers the GRB position at the GRB trigger time. Observed period shows the time period relative to GRB trigger time. In this time period, the GRB position is within our filed of view.

The next step is to start observation of Cherenkov air showers using the light collector towards Mauna Kea. It may detect Cherenkov signals originated from tau neutrinos which interacts with the mountain and/or the earth as described in the section below. We prepared the optical and photoelectric image pipeline system in that light collector. The installation of trigger and DAQ system was performed. Pilot observation to confirm the detection principle of tau neutrino has been carried out [6].

Search for early optical transients

We constructed a 2/3-scale prototype Ashra detector on Haleakala to verify the optical performances. From October 2004 to August 2005 at the observatory, We made good observations for 844 hours out of 1,526 hours of the moonless nighttime. The fine resolution (arc-minutes) in the ultra wide field of view (0.5 sr) has already been demonstrated using a 2/3-scale model. Our wide field observation covered the HETE-2 WXM error box at the time of GRB041211. 2,000 images were taken every 5 s with 4-s exposure from the time 1h7m before GRB041211 to 1h41m after GRB041211. We detected no objects showing time variation in the WXM error box. It indicates the 3-sigma limiting magnitudes of B$\sim$11.5 magnitude [10]. This is compared with other observations [11, 12]. We also successfully performed two more observations coincident with Swift: GRB050502b [13] and GRB050504 [14].

Satellite	Trigger Number	GRB Name	Trigger Time	Observed Period [sec]
Swift	322590	N/A	080828 UT 08:15:09.33	$-2.3\times10^3 - 1.1\times10^4$
Swift	324362	N/A	080910 UT 12:52:21.68	$-4.3\times10^3 - 7.7\times10^3$
Swift	336489	GRB081203A	081203 UT 13:57:11.57	$-1.2\times10^4 - 5.6\times10^3$
Fermi	262607680	GRB090428	090428 UT 10:34:38.46	$-8.1\times10^3 - 5.9\times10^3$
Fermi	262701807	GRB090429C	090429 UT 12:43:25.70	$-4.1\times10^3 - 7.1\times10^3$

Table 2. Summary of coincidence events with satellite GRB triggers[8][9]. Listed events are those which GRB trigger position are within our FOV at the GRB trigger time.

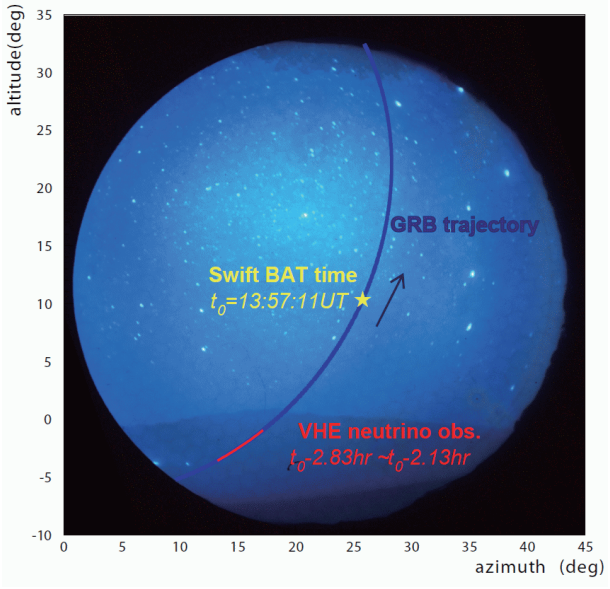

Fig. 4. Trajectory of the GRB081203A counter part in the field of view.

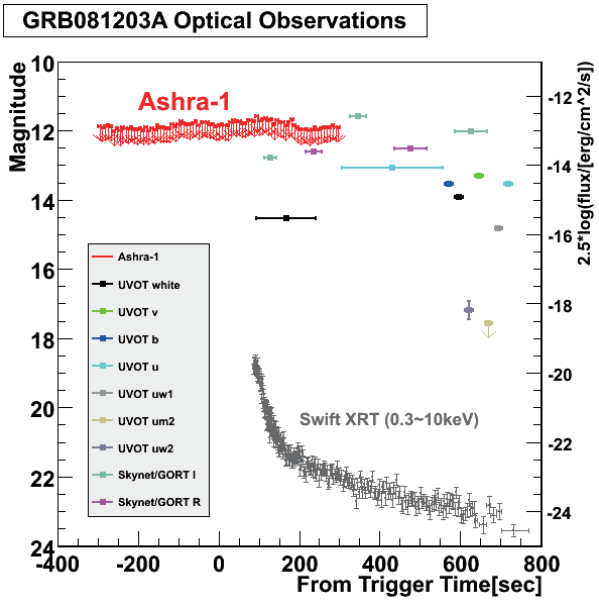

Fig. 5. Summarized lightcurve for GRB081203A around the trigger time. 3-sigma limiting magnitudes of our observation (labeled as Ashra-1) and other observations are compared as a function of time after GRB. The horizontal axis is in linear scale. The vertical axis in the right is only for the data by Swift XRT (gray data), where the scale is arbitrary.

The Ashra-1 light collector unit on Mauna Loa has the achieved resolution of a few arcmin, viewing 42 degree circle region of which center is located at Alt = 11.7 deg, Azi = 22.1 deg. The sensitive region of wavelength is similar with the B-band. Utilizing this light collector, we have searched for optical counterpart in the field of GRB081203A [15] around the Swift/BAT-triggered GRB time (T0). Figure 4 shows the trajectory of the GRB position in our field of view. We preliminary analyzed 83 images covering the field of GRB081203A every 7.2s with 6s exposure time respectively during the observation between T0-300s and T0+300s. We detected no new optical object within the PSF resolution around the GRB081203A determined by Swift-UVOT [16]. Around the Swift-BAT trigger time, we have obtained data in every 7.2 seconds with 6sec exposure. The examples of obtained preliminary S/N (signal to noise ratio) maps including the trigger time can be found at [1]. As a result of our preliminary analysis, the following 3-sigma limiting magnitudes are derived. The limiting magnitudes were estimated in comparison with stars in Tycho-2 Catalog to be distributed between 11.7 and 12.0. Figure 5 shows limiting optical magnitudes vs time comparing with the other measurements [4].

Search for Cherenkov tau neutrinos

We used a detection technique called 'the Earth-skimming neutrino'. This detection technique was originally proposed in 1990's [17] and already used by other observations. The essence of this technique is separation of target and detection. Small cross section of first interaction of neutrino favors dense material, while fine imaging of the interaction does not. If the first interaction is separated from the following interactions, we can evade from the above contradiction.

Reaching the Earth, a neutrino enters into the Earth's crust and mountains, interacts with materials via charged current interaction, and produces a lepton. The lepton propagates in the crust with loss of its energy. If it is a tau lepton, it decays after exit to the atmosphere, and generates detectable air shower. The length of the propagation of tau lepton in the rock makes a cluster around a few 10 km above 10^{17}eV due to the energy loss. Hence we can detect tau neutrinos of decades of energies with a fixed geological formation.

This detection technique has a maximum sensitivity around 100 PeV. Using this technique, we aim to connect PeV

to EeV by lowering the energy threshold of neutrino observation with air light. PeV is the energy range where ice and water Cherenkov experiments have their maximum sensitivities, while EeV is the energy range where experiments with air shower have. For that aim, we think that detection of Cherenkov radiation from air shower is important. In order to detect Cherenkov radiation emitted forward, shower front must be directed to the detector. Therefore, we chose a geometry widely viewing rock of over 10km thickness, that is, mountain. We designed an observation facing the mountain (Figure 6). In this observation, we used a light collector toward Mauna Kea.

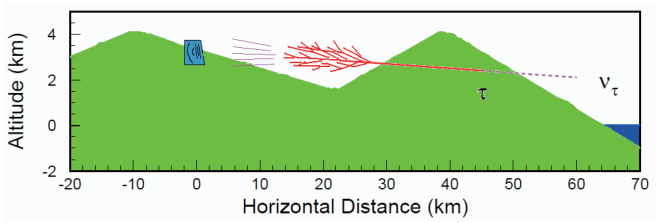

Fig. 6. Conceptual figure of this observation (the Earth-skimming neutrino detection technique). The right mountain is Mauna Kea and the left is Mauna Loa.

Cherenkov tau shower observation

We intended an observation in order to study neutrino emissions from transient objects. Also, performance check of our trigger system is another aim of this observation.

Before the observation, we simulated neutrino signals generated by tau leptons emerging from Mauna Kea (Figure 7). Then, we calibrated the detector with artificial sources, such as an LED and a radiant source. Furthermore, we verified the system's performance by an observations of cosmic rays (protons). Cosmic-ray observation was carried out with an FOV closer to the zenith than in the neutrino observation. Figure 8a shows an example of obtained image of Cherenkov radiation from air-showers, and Figure 8b shows a simulated event by CORSIKA. We can see that the obtained data resembles the simulated event. It demonstrates well the strength of the high angular resolution of our detector. As shown by the comparison of Figure 7 with the data (Figure 8a), our detector has an ability of detecting air showers from neutrinos.

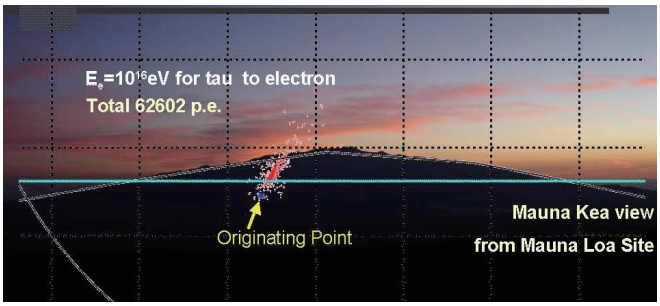

Fig. 7. Example of simulated neutrino event.

The observation for neutrino emission was executed in a duration from October to December in 2008 (Table 3). Fortunately we accomplished highly efficient observation. As a result we observed a GRB, GRB081203A, in a period before and after its occurrence, tens of GRBs after their occurrence, and tens of active galactic nuclei (AGN).

The obtained data were analyzed. In order to estimate the sensitivity we must take into account spurious events generated by background cosmic rays. In principle, the Earth-skimming neutrino detection technique is free from background events, thanks to the screening effect of the Earth's rock. Also, the FOV of this observation is nearly horizontal, hence thick atmosphere screens the normal cosmic-ray events. We studied the screening effects and confirmed the absence of background events from background sources. Then, the most frequent background was Cherenkov radiation from muons that interact with the detector itself. We simulated the radiation, and carefully removed them from the data.

Results of tau neutrino search

We did not discover any candidate of neutrino emission in the range from tens of PeV to EeV. We set preliminary upper limits to the fluence and flux of source models, related to the mechanism for the particle acceleration in transient objects. All the following limits are derived with 95% confidence level.

For GRB081203A precursor, we set a limit $E\phi(E) < 5.4 \times 10^{-8}$ [cm^{-2}], assuming a spectrum extended up to 5 EeV. For GRB081203A late prompt emission, the obtained limit is $E^2\phi(E) < 4.3$ [erg cm^{-2}]. Combination of the two observations for GRB081203A, the upper limit for neutrino emission [6] and the optical observation with our detector [5], leads to the conclusion that it is not contradictory to the normal particle acceleration. This discussion can be considered as a beginning of 'multi-particle astronomy'[18]. For GRB afterglow, the limit leads $E^2\phi(E) < 19$ [erg cm^{-2}]. Note that this limit is set by the source integrated analyses. Furthermore, neutrino emission from AGN was studied. The limit for diffuse flux is about 2nd order of magnitude larger than that by other experiments, but better than Auger experiment at 100 PeV. In addition to that, we set a meaningful upper limit, $E^{1.4}\phi(E) < 1.3 \times 10^{-12}$[cm^{-2}s^{-1}PeV$^{0.4}$], based on a source model assuming proton synchrotron emission. This limit corresponds to a diffuse flux rejected by experiments. However, it should be noted that our result is not affected by the source distribution in the universe because of a limit for point sources.

By means of Cherenkov tau shower observation, our detector is sensitive to neutrinos with energies of $1 \sim 100$ PeV. This energy range is just between the maximum sensitivities of ice experiments and other air-shower experiments. For future neutrino experiments, pointing accuracy in this region will become more important, in order to localize transient objects and investigate the mechanism of the particle acceleration in individual sources. The Ashra detector may be considered as a promising candidate to realize 'multi-particle astronomy'[18], which is necessary to understand particle acceleration in the universe.

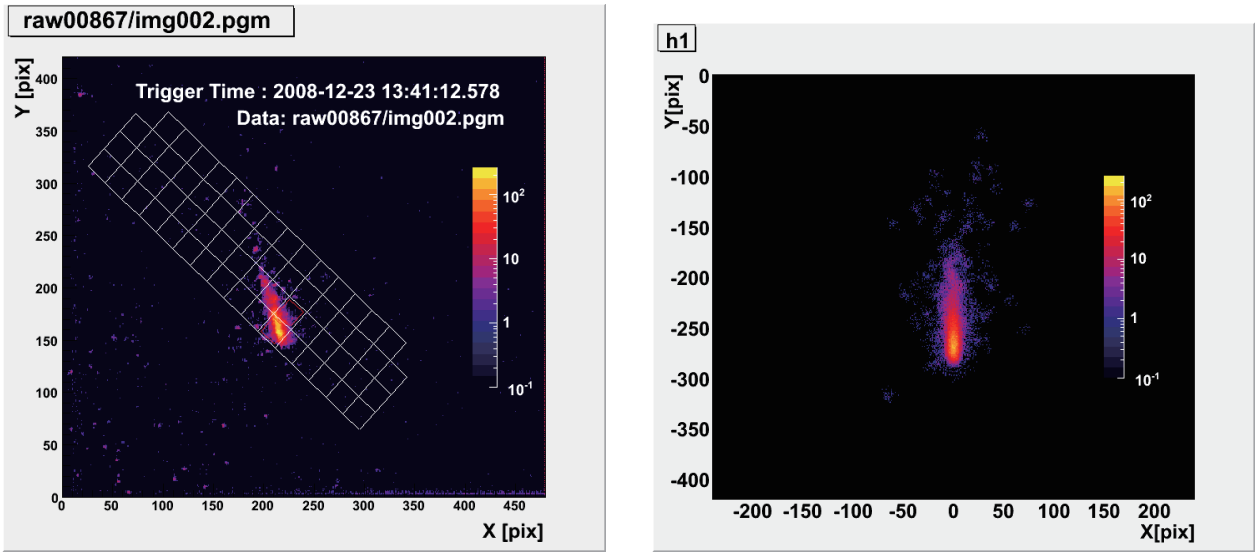

(a) data (b) simulated event

Fig. 8. Example of air-shower image from the cosmic-ray observation. The conditions for simulated event are as follows; proton, energy = 1EeV, core distance = 266m, angular resolution = 9 arcmin, and thinning = 10^{-6}. The color shows pixel value (max. is 255 counts).

Table 3. Observation time for Cherenkov tau neutrinos. Duty factor is defined by the observed time divided by the total time including daytime and full moon periods.

Period (UT)	Max. Observable Time [hr]	Observed Time [hr] (duty factor)
2008/10/28 – 11/11	95.5	75.3 (17%)
2008/11/15 – 12/10	164.6	140.5 (20%)

Bibliography

[1] http://www.icrr.u-tokyo.ac.jp/∼ashra

[2] Sasaki, M., 2003, "Very High Energy Particle Astronomy with All-sky Survey High Resolution Air-shower Detector (Ashra)", *Progress of Theoretical Physics Supplement,* vol. 151, pp. 192–200.

[3] Sasaki, M., et al., 2008, "The Ashra Project" Proc. 30th Intl. Cosmic Ray Conf. Merida 3, 1559.

[4] Aita, Y., et al., 2008, GCN Circ. 8632.

[5] Ogawa, S., et al., 2009, "Ashra Optical Transient Observation", 31th Intl. Cosmic Ray Conf. (Lodz), ID1410.

[6] Noda, K., et al., 2009, "VHE neutrino pilot observation with the Ashra detector", 31th Intl. Cosmic Ray Conf. (Lodz), ID313.

[7] Sasaki,M., et al., 2002, "Design of UHECR telescope with 1 arcmin resolution and 50° field of view", *Nucl. Instrum. Methods,* vol. A492, pp. 49–56.

[8] http://gcn.gsfc.nasa.gov/swift_grbs.html

[9] http://gcn.gsfc.nasa.gov/fermi_grbs.html

[10] Sasaki, M., et al., 2004. GCN Circ. 2846.

[11] Sasaki, M., et al., 2005. "Status of Ashra project," Proc. 29th Intl. Cosmic Ray Conf. Pune 8, 197–200.

[12] Sasaki, M., et al., 2005. "Observation of Optical transients with the Ashra Prototype," Proc. 29th Intl. Cosmic Ray Conf. Pune 5, 319–322.

[13] Sasaki, M., et al., 2005. GCN Circ. 3499.

[14] Sasaki, M., Manago, N., Noda, K., Asaoka, Y., 2005. "GRB050502b: Early Observation," GCN Circ. 3421.

[15] Parsons, A. M., et al., GCN Circ. 8595

[16] De Pasquale, M., et al.,GCN Circ. 8603.

[17] Fargion, D., 2002, ApJ **570** 909 (arXiv:astro-ph/9704205).

[18] Sasaki, M., 2000, in Proc. of ICRR workshop "ICRR2000 Satellite Symposium: Workshop of Comprehensive Study of the High Energy Universe".

ASTROPHYSICS and GRAVITY DIVISION

Overview

Astrophysics and Gravity Division consists of Gravitational Wave Group, The Sloan Digital Sky Survey Group and Theory Group. The Gravitational Wave Group conducts R&Ds for LCGT project jointly with researchers of gravitational wave experiment and theory in Japan. The main items of those R&Ds are TAMA project and CLIO project. The Sloan Digital Sky Survey Group continues accumulating data of images and spectroscopic observation of galaxies and publishing papers in collaboration with worldwide researchers. Theory Group conducts both theoretical study of the Universe and astroparticle physics.

Gravitational Wave Group

Status of TAMA Project

[Spokesperson : Kazuaki Kuroda]
ICRR, Univ. of Tokyo, Kashiwa, Chiba 277-8582

In collaboration with the members of: TAMA collaboration

NAOJ, Tokyo; KEK, Tsukuba; UEC, Tokyo; Osaka City Univ., Osaka; Kyoto Univ., Kyoto; Osaka Univ., Osaka; Niigata Univ., Niigata

Introduction

A gravitational wave is a physical entity in space-time predicted by Einstein's theory of general relativity. Its existence was proven by the observation of PSR1913+16 by Taylor and Hulse [9], who won the Nobel prize in 1993. However, nobody has succeeded to directly detect gravitational waves. The theory of gravitation can be tested by the detection of gravitational waves. A gravitational wave detector is the last eye of mankind to inspect the universe. In order to directly observe gravitational waves, we aim to construct the Large scale Cryogenic Gravitational wave Telescope (LCGT).

For the first step of constructing sensitive laser interferometer, we developed a 300 m baseline interferometric gravitational wave detector, TAMA, at the Mitaka campus of the National Astronomical Observatory of Japan (NAOJ) and several observations had been conducted. TAMA project started in April, 1995, as a five-year project and it was extended by two years after 1999. TAMA is organized by researchers belonging to universities and national laboratories. We achieved nine data-taking runs that span from two to eight weeks, which ended in 2004. About TAMA project, we had presented its development of Seismic Attenuation System (SAS) newly installed for four main mirrors and tried to achieve its design sensitivity. However, we finally found that the sensitivity at low frequencies were limited by so-called up-conversion noise possibly arising from the suspension and actuation system and cannot be improved anymore without a drastic change of the suspension system utilizing more sophisticated actuator.

*9 J. H. Taylor and J. M. Weisberg, Astrophysical J., **345** (1989) 434.

Achievement of TAMA

The achieved sensitivity of TAMA at the time of Data Taking Run 9 was reported in the previous Annual report (2005-2006).[1] Although there was a gap between the achieved sensitivity and the practically attainable one, at low frequencies, we could demonstrate that the basic techniques for the interferometer operation was acquired by the fulfillment of the target noise curve at frequencies more than 800 Hz, where the optical system properly worked and the control system was appropriate. The noise spectrum at frequencies lower than 30 Hz was disturbed by non-stationary ground motion and the spectrum in a frequency range from 30 Hz to 300 Hz was determined by the actuator noise to stabilize the mirror alignment mainly due to relatively larger seismic noise at Mitaka campus of NAOJ. In order to identify the noise source governing the spectrum in the frequency range from 30 Hz to 800 Hz, we had installed the Seismic Attenuation System (SAS) [2] for four main mirrors and improved the performance of antivibration at low frequencies. The sensitivity improvement is shown in Fig 1 under the SAS system.

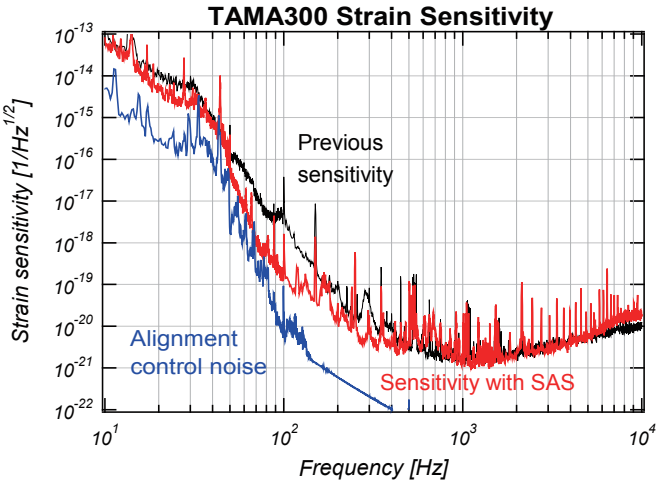

Fig. 1. After the installation of Seismic Attenuation System (SAS), the sensitivity has been improved by about one order at 100 Hz. The sensitivity was not limited by the alignment control noise as shown in the plot, but limited by another unidentified noise source, which turned out to be some up-conversion noise as reported as the following.

By this improvement at low frequencies, we had expected that we could overcome the actuator noise that governed the sensitivity at low frequencies less than 300 Hz. However, this expectation was negatively broken by the observed sensitivity, which showed the existence of some noise source at these frequencies. In order to inspect this noise source, we checked

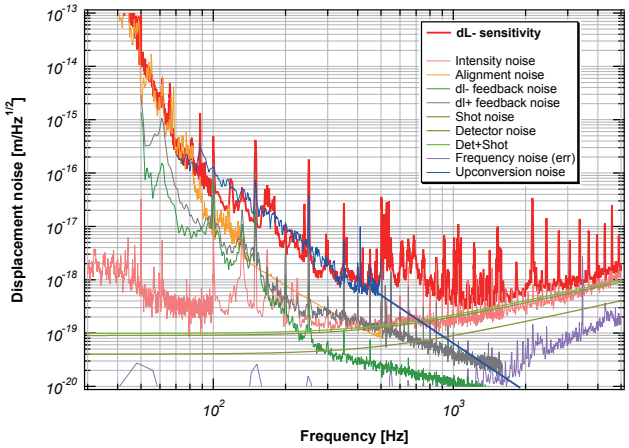

Fig. 2. Under the newly installed SAS, an up-conversion noise has been empirically observed, which limits the sensitivity at low frequencies less than 300 Hz.

the up-conversion noise that was found by LIGO project. This was arising from the Barkhousen effect in the bar magnets that were used for as part of actuation system for the control of the mirror. Actually, we applied a large excitation force at pendulum mode of the main mirror through the actuation magnet-coil system and observed the noise appeared at higher frequencies.

Figure 2 shows the noise spectrum taken by this method with changing the amplitude of the applied force. One can clearly perceive the effect of some up-conversion mechanism. The blue curve in the figure accords to the expected up-conversion noise under normal pendulum motion. This result empirically showed the existence of an up-conversion noise in the suspension system of TAMA. We can guess its physical reason of this phenomenon, such as magnetism, non-linearity of the pendulum, and so on. Note that this phenomenon has not been observed at CLIO interferometer placed at quieter site by two orders less in noise amplitude. We have not succeeded to identify its origin. We may need a drastic change of the suspension and actuation system (full manpower with money) to escape from this new noise. However, since the effect of this new noise reduces rapidly in more than quadric, the effect is not certainly dominant underground at Kamioka as indicated by the recent result of CLIO.

In regard with data analysis, we had made reports with LIGO project at the time when the sensitivity of TAMA300 had competitiveness [5, 6]. Without new observation, persistent activity on the development of data analysis was conducted using existing TAMA 300 observation data.[7, 8]

Bibliography

[1] H. Tagoshi it et al., Phys. Rev. D **63**(2001)062001-1-5.

[2] R. Takahashi *et al.*, Class. Quantum Grav. **25** (2007) 114036.

[3] D. Tatsumi *et al.*, "TAMA 300 interferometer development", TAUP 2007, September 11-15, 2007, Sendai.

[4] K. Arai*et al.*, "Recent Progress of TAMA 300", TAUP 2007, September 11-15, 2007, Sendai.

[5] B. Abbott *et al.*, Phys. Rev. D **72** (2005) 122004.

[6] B. Abbott *et al.*, gr-qc/0512078 (2005)

[7] H. Tagoshi *et al.*, "Results of Searches for inspiraling compact star binaries from TAMA 300fs observation in 2004-2004", TAUP 2007, September 11-15, 2007, Sendai.

[8] N. Kanda *et al.*,lq'Short gravitational wave signal searches in TAMA 300 data: stellar collapse and black hole", TAUP 2007, September 11-15, 2007, Sendai.

CLIO Project

[Spokesperson : Masatake Ohashi]

ICRR, Univ. of Tokyo, Kashiwa, Chiba 277-8582

In collaboration with members of: KEK, Tsukuba; Kyoto-U, Kyoto; ERI of UT, Tokyo

CLIO (Cryogenic Laser Interferometer Observatory) is a 100 m-baseline underground cryogenic interferometer at the Kamioka Mine. CLIO forms a bridge connecting the CLIK (7 m prototype cryogenic interferometer at Kashiwa campus) and the planed LCGT (3 km cryogenic interferometer at Kamioka). The site of CLIO, near the Super-Kamiokande neutrino detector, is shown in Fig. 3. The tunnel was dug in 2002, and a strain meter for geophysics was installed in 2003 [1]. The construction of CLIO began in late 2003, and installation of the mode cleaner vacuum system was reported in the annual report (2003–2004). Four sets of cryostats and whole vacuum system were installed (annual report 2004–2005). We started the operation of CLIO in 2006 (annual report 2006).

One of the aims of CLIO is to demonstrate the thermal noise suppression by cooling the mirrors. The main mirrors are cooled at 20 K by refrigerators. The lowest noise level of CLIO is designed to be $10^{-19}\mathrm{m}/\sqrt{\mathrm{Hz}}$ around 100 Hz, which would be $10^{-18}\mathrm{m}/\sqrt{\mathrm{Hz}}$ if cryogenics is not applied [2]. The current best sensitivity at the room temperature was obtained in the end of 2006. The displacement sensitivity around 300Hz reached at $6 \times 10^{-19}\mathrm{m}/\sqrt{\mathrm{Hz}}$. Of special note is its high strain sensitivity below 20Hz. It is comparable with LIGO sensitivity in spite of much shorter baseline. Now we are reducing the excess noise to realize the thermal noise limited sensitivity. And we have checked the cooling of mirrors not to harm the sensitivity in 2007.

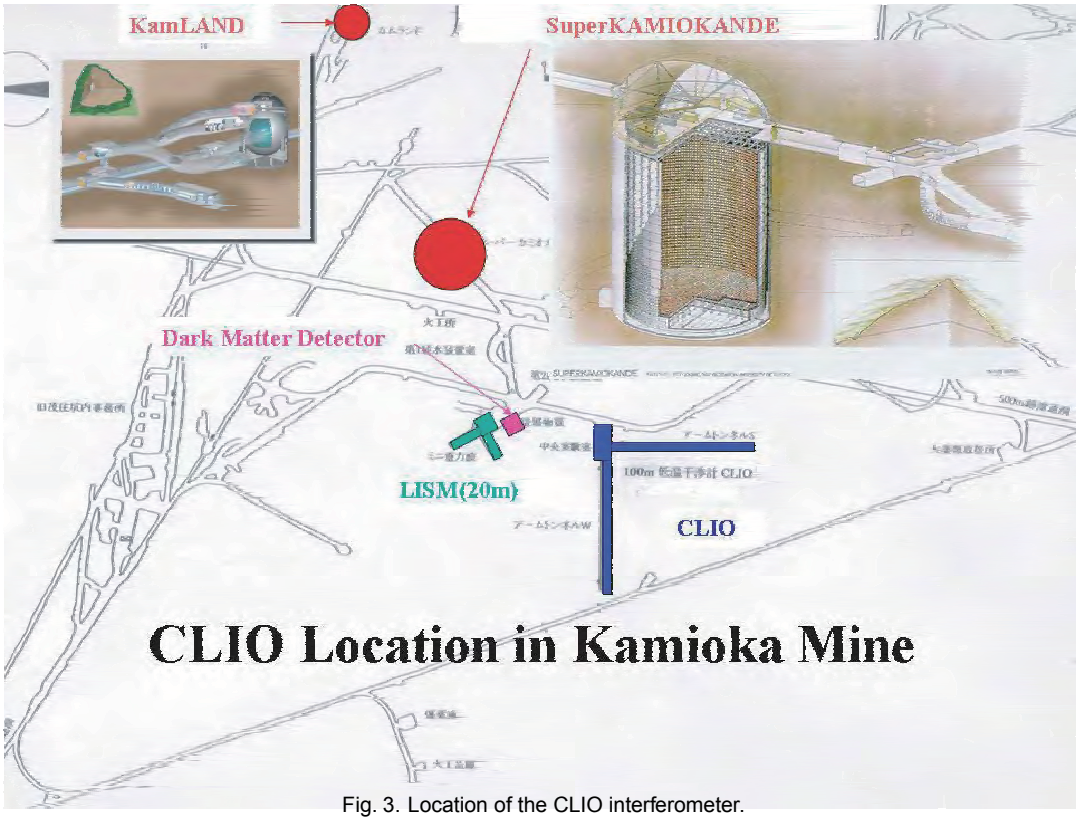

Fig. 3. Location of the CLIO interferometer.

Fig. 4. Overview of the CLIO interferometer.

Fig. 5. a sapphire mirror and cryogenic suspension system.

Once the objective is attained, the CLIO interferometer is used to observe gravitational wave events in parallel with the TAMA interferometer until completion of the construction of LCGT. The merits of the underground site are lower seismic noise and temperature stability. The former characteristic makes interferometer locking easily controlled, and the latter assures long-term stable operation (LISM) [3].

The 57-hours observation data were taken at February 2007 and analyzed for continuous gravitational wave from the pulsar J0835-4510 (Vela pulsar) at twice its rotation frequency (22.38 Hz). We use an analysis method based on a matched filtering with a correction of pulsar spin down, a Doppler effect caused by the relative motion between the pulsar and the Earth, and so on. We obtained an upper limit of $h_{0(\mathrm{U.L.})} = 5.3 \times 10^{-20}$ at 99.4 % confidence level. This value corresponds to the upper limit on the ellipticity of the neutron star, $\varepsilon = 29$ [4].

We have achieved the target sensitivity for the room temperature on November 5th (Fig. 6) 2008 which is limited by the fundamental noise sources, seismic noise in the low frequency, pendulum thermal noise and mirror thermal noise between 20 Hz and 100 Hz and shot noise in the high frequency. We emphasis that what the sensitivity is limited by two kind of thermal noises in the room temperature means that CLIO is qualified to observe thermal noise reductions by cooling the

mirrors in the next step.

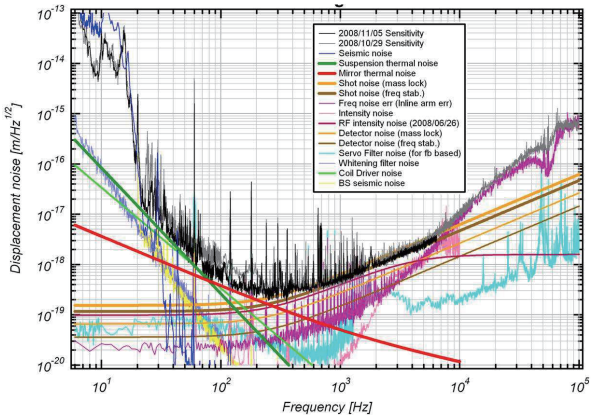

Fig. 6. CLIO displacement noise spectrum: The black curve is the current best sensitivity at room temperature. This spectrum is represented by the thermal noises of pendulum and mirror.

Actually we cooled down one of the four mirrors as the first step of full process of cooling all mirrors and showed that the cooling did not contaminate the noise floor obtained at the room temperature. An effect of cooling will be seen drastically as a mirror thermal noise reduction when the second mirror is cooled down since the two front mirrors are dominant to determine the floor level of the mirror thermal noise. We have already started cooling down the second mirror in July and we are currently making efforts to hunt other technical noises caused by this second cooling process such as mirror contaminations or shrinking wires.

Bibliography

[1] S. Takemoto, *et al.*, Journal of Geodynamics **41** (2006) 23.

[2] M. Ohashi, *et al.*, Class. Quantum Grav. **20** (2003) S599.

[3] S. Sato, *et al.*, Phys. Rev. **D 69** (2004) 102005.

[4] T. Akutsu, *et al.*, Class. Quantum Grav. **25** (2008) 184013.

LCGT Project

[Spokesperson : Kazuaki Kuroda]
ICRR, Univ. of Tokyo, Kashiwa, Chiba 277-8582

In collaboration with the members of:
National Astronomical Observatory (Japan), KEK, Physics Department (University of Tokyo, UT), Department of Advanced Material Science (UT), Earthquake Research Institute (UT), Department of Earth Science and Astronomy (UT), Institute for Laser Science (University of Electro-Communications), Department of Physics (Osaka City University), Department of Physics (Osaka University), Physics Department (Kyoto University), Yukawa Institute (Kyoto University), Advanced Research Institute for Sciences and Humanities (Nihon University), System Engineering (Hosei University), Ochanomizu University, Agency of Industrial Science and Technology, National Institute of Information and Communications Technology, Hirosaki University, Tohoku University, Niigata University, Rikkyo University, Waseda University, Nagaoka University of Technology, Hiroshima University, Ryukyu University, Department of Astronomy (Beijing Normal University), Center for Astrophysics (University of Science and Technology, China), Institute for High Energy Physics (Chinese Academy of Science), Purple Mountain Observatory (China), Industrial Technology Research Institute (Taiwan), Inter University Centre for Astronomy & Astrophysics (IUCAA), Physics Department of Physics (University of Western Australia), Laboratory of Laser Interferometry (Sternberg State Astronomical Institute, Moscow Univ.), Louisiana State University, MPI-AEI, California Institute of Technology, Rochester Institute of Technology, Columbia University, Birmingham University, Glasgow University, Maryland University.

Introduction

The organization of LCGT was augmented by creating a position of the project manager since October, 2008. We reformed the working groups that share tasks of LCGT construction and revised documents that describe the design of LCGT. Five coordinators were newly introduced to be positioned above the working groups of LCGT and they chair related working groups as follows;

- Facility
  - tunnel construction
  - crust strain meter
- Vacuum&Suspension
  - vacuum system
  - anti-vibration&suspension system
  - cryostat system
  - refrigerator system
- Interferometer
  - interferometer support system
  - interferometer control system
  - digital control system
- Laser
  - laser source system
  - input&output optical system
  - mirror design&fabrication
- data analysis
  - data analysis
  - data collecting system
  - computer facility

Under the MOU among three Institute (ICRR) and organizations (NAOJ and KEK) which is an extension of the previous MOU among three directors since 1994, we prepared to form an executive panel of LCGT consisting of members of those three directors with three representatives of research. The panel is effect since 1st, April, 2009.

We promote LCGT project for the first priority of future project in ICRR supported by all gravitational wave physicists in Japan and oversea collaborators.

Objective of LCGT

After the discovery of the highly relativistic binary neutron star system [10], a new young binary pulsar was detected [11]. The former discovery increased the coalescence rate from 10^{-6} to 10^{-5} a year in a galaxy as big as our Galaxy [12] and the latter pushed up by another factor of six. Although it was good news for the detection of gravitational waves, we still needed to wait for long time to detect by the presently existing detectors. This was the reason why we planed LCGT (Large-scale Cryogenic Gravitational wave Telescope). The objective of LCGT is to detect at least one gravitational wave event in a year. There are many other possible gravitational wave sources in the universe other than the coalescence of binary neutron stars. However, the coalescence of binary neutron stars differs completely from other sources in the sense that its wave form is precisely predicted, and its existence has certainly been confirmed.

Status of LCGT Project

The target sensitivity of LCGT is to observe binary neutron star coalescence events occurring at 230 Mpc with S/N=8 [13] in its optimum configuration. This is ten-times more sensitive than that of the LIGO (I), and by two orders more than that of TAMA at their most sensitive frequencies.[2] This will be attained by an interferometers located underground (as in Fig. 7), using a three-kilometer length baseline, cooling mirrors at cryogenic temperature, and a high-power laser source employing 150 W output. The optical configuration is a power recycled Fabry-Perot-Michelson interferometer with the resonant-sideband-extraction (RSE) scheme (in Fig. 8). The detailed design of the control system was tested for the resonant sideband extraction scheme.[3] Table 1 lists the important parameters of LCGT, which were revised three times from the original design.[4] Ultimate sensitivity of a laser interferometer is determined by seismic noise at low frequencies (10-30 Hz) (which is reduced by improving the vibration isolation system), and it is limited by photon shot noise at higher frequencies (more than 300 Hz), which can be improved only by increasing the light power in the main cavities. The sensitivity of middle frequencies (30-300 Hz) is limited by the photon recoil force noise. This requires that thermal noise is reduced both by decreasing the temperature and by decreasing the internal mechanical loss (*i.e.*, increasing the mechanical Q of vibration modes). The source of thermal noise comes from both mirror internal vibration, mechanical loss of the optical coating and swing noise of the pendulum suspending the mirror. The reduction of thermal noise is attained by cooling both the mirror and the suspension system that suspends the mirror.

Table 1. LCGT design parameters to detect binary neutron-star coalescence events in 230 Mpc.

Item	Parameter
Baseline Length	3 km
Interferometer	One set
	Power recycled Fabry-Perot
	-Michelson with RSE
Optical Power	Laser:150 W; Finesse:1550
	Input power at BS: 825 W
	Cavity power 800 kW
Beam radius at End	3 cm
Main Mirror	Sapphire 30 kg, 20 K
	Diameter 25 cm
	Mechanical Q:10^8
Suspension	Frequency: 1 Hz; Q:1×10^8
pendulum	10 K
Vacuum	$\leq 10^{-7}$ Pa

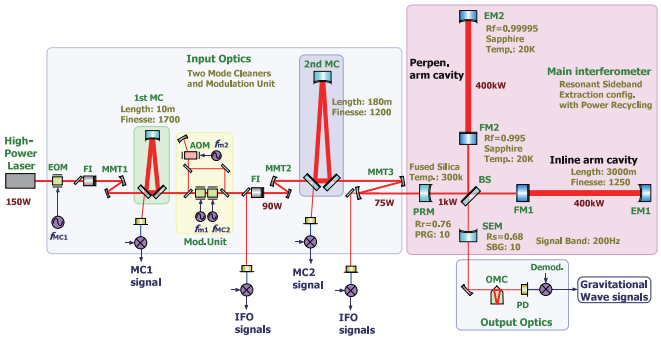

Fig. 8. Optical design of LCGT. The optical configuration is a power recycled Fabry-Perot-Michelson interferometer with the resonant-sideband-extraction (RSE) scheme.

The laser system is designed by the experience of TAMA laser that is an injection locking master-slave laser pumped laser diodes. The output of the master laser (2 W) is injected into a slave laser of 100 W under a scheme of injection-locking. The output of the slave is amplified to 150 W by an optical amplifier (Fig. 9).

Figure 10 compares the sensitivity curve of LCGT with those of TAMA, CLIO (a 100 m prototype cryogenic interferometer placed underground of Kmioka mine), GEO, Virgo and LIGO (initial LIGO, Adv. LIGO). The sensitivity at low frequencies of LCGT is attained by SAS, which will be proven by the current SAS in TAMA. That of higher frequencies is attained by higher laser power, which has been basically shown by TAMA. The mid-frequency region is improved by cryogenic mirror and suspension system, which will be proven by

*10 M. Burgay, *et al.*, Nature, **426** (2003) 531.
*11 D.R. Lorimer, *et al.*, Astrophysical J. **640**(2006) 428.
*12 C. Kim, V. Kalogera and D. R. Lorimer, Astrophysical J. **584** (2003) 985.
*13 The signal-to-noise-ratio so far was 10 considering high rate of non-stationary noise that dominated in TAMA. However, recent improvement of handling noise assures us to adopt widely accepted number, 8

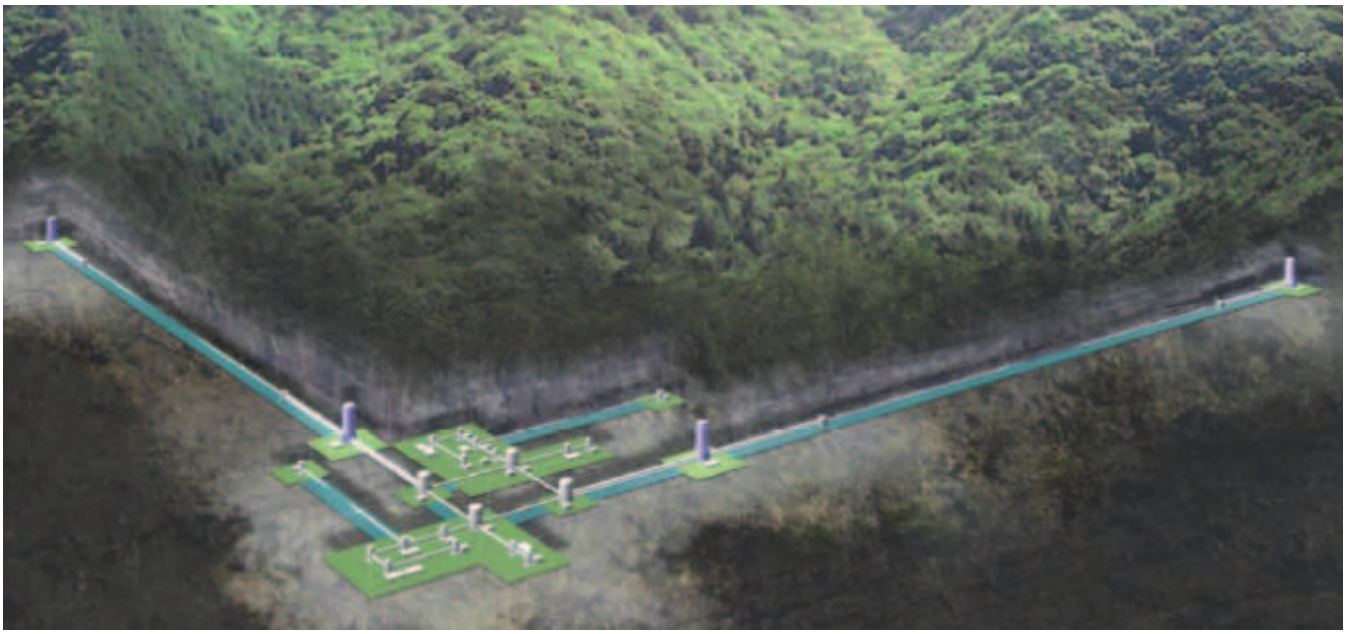

Fig. 7. The interferomter of LCGT is placed underground at Kamioka mine for fairly quiet seismic motion.

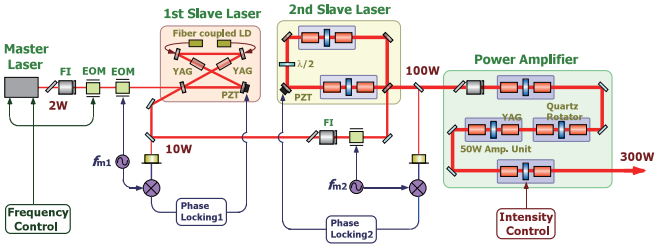

Fig. 9. A laser source system for LCGT. The output of the master laser (2 W) is injected into a slave laser of 100 W under a scheme of injection-locking.

the on-going project of CLIO. Although the improvement, especially two orders of magnitude at low frequencies, is adventurous, it is not impossible until the construction period of LCGT that needs four years after the beginning of the construction.

The main effort on the research and development for LCGT has been placed on cryogenic mirrors for the past years. The implementation of cryogenic mirrors is one of the most straight-forward solutions to improve the sensitivity.

The design of the cryogenic mirror system is shown in Fig. 11. The mirror is suspended by two loops of sapphire fibers connected to an auxiliary mirror that is a part of suspension point interferometer. This mirror is also suspended from an alignment control platform that is suspended with an insulator rod connected through the center holes of the radiation shields to an isolation table suspended by a low-frequency vibration isolator, which is placed at room temperature. The auxiliary mirror has a heat link to the platform and another heat link connects the platform and a heat anchor point (4 K) inside the vacuum located just above the platform.

Both the cryogenic system and the vibration isolator are

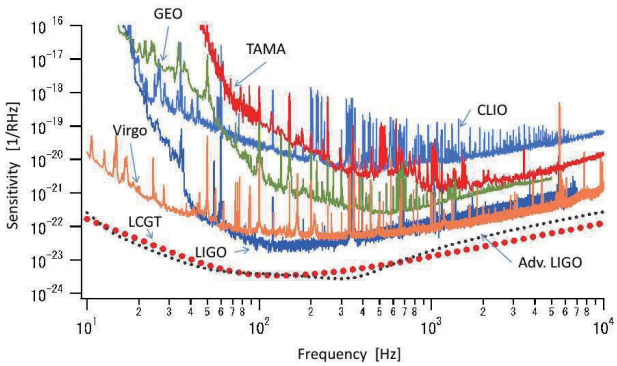

Fig. 10. LCGT sensitivity (dotted red curve) compared with those of TAMA (red one), CLIO (a 100m prototype cryogenic interferometer placed underground of Kmioka mine, light blue one), GEO (green one), LIGO (initial LIGO, blue one, Adv. LIGO, dotted black one) and Virgo (orange one). The horizontal axis is frequency [Hz] and the vertical axis represents sensitivity spectrum for gravitational waves [1/$\sqrt{}$Hz].

put inside a common high-vacuum chamber.

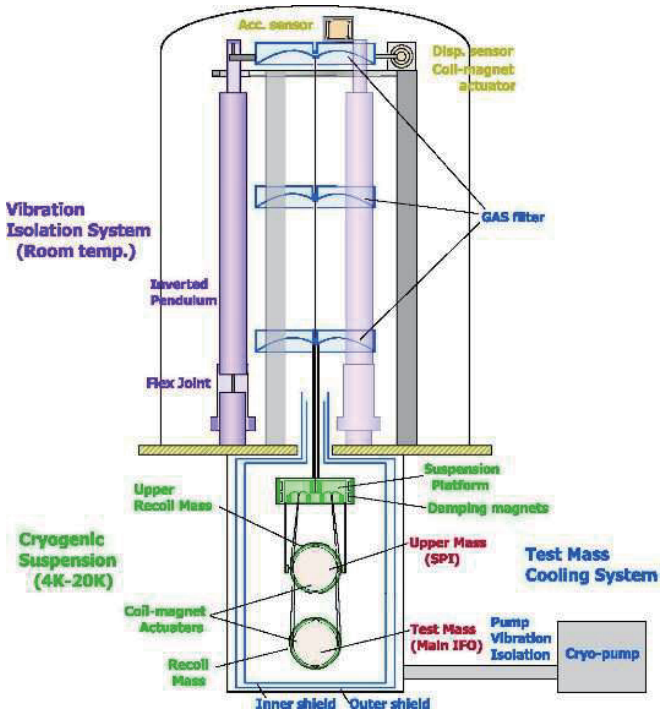

Fig. 11. Schematic design of the cryogenic suspension system. The mirror is suspended by sapphire fibers connected to an auxiliary mirror, which is suspended by metal wires from a platform that has a heat link to a 4 K heat anchor inside the vacuum. The platform is also suspended with an insulator rod connected through the holes of radiation shields to an isolation table suspended by a seismic attenuation system placed at room temperature in the common high vacuum.

R&D

Basic Research for cryo-mirror system

To realize the cryo-mirror concept, the following research subjects were conducted and reported:

1. Removal of heat produced by high-power laser illumination (annual report 1997-1998 and also in references [5])
2. Holding the high Qs of the mirror internal modes and suspension pendulum [6]
3. Reducing the contamination of mirror surfaces (annual report 2000?2001 and also in [7]).
4. Estimating heat production by optical loss in the mirror [8].
5. Alignment control of mirrors in a cryogenic environment [9]
6. Low mechanical loss of the optical coating (annual report 2003-2004 and also in reference [10])

As for item 5, we confirmed that a superconducting film could be used for the receptor of the magnetic force in place of permanent bar magnets that are normally used in the existing detectors. The film can be easily sputtered on the mirror surface without harmfully degrading the mechanical Q of the mirror. With respect to the last item, we reported on a measurement of the bulk substrate of the mirror at cryogenic temperature in the annual report (2003–2004). We could correctly estimate the thermal vibration noise of the optical coating while considering the inhomogeneous loss that had been neglected at an early stage of interferometer development. The substrate of the cryogenic mirror was sapphire, which has a large thermo-elastic thermal noise at room temperature. However, since the thermal-expansion ratio of sapphire at cryogenic temperature goes down to nearly 0 and the heat conductivity becomes greater, the thermo-elastic noise drastically reduces at the cryogenic temperature. Thermal noise estimated from the Q of the coating was well below the design sensitivity of LCGT, which means that this coating noise does not limit the sensitivity, whereas, the sensitivity of a room-temperature mirror is limited by this effect. This is the significant merit of the cryogenic mirror system.

For a practical cryogenic detector, more practical R&Ds will be needed for the installation of cryogenic mirrors. One of the earliest R&D activities along this line was the Kashiwa cryogenic interferometer system reported in the annual report (2000–2001; 2002–2003; 2003–2004). By this Kashiwa cryogenic interferometer, we learned the necessity of several practical R&D items and began to construct the CLIO interferometer in Kamioka to establish techniques for the cryogenic interferometer (2005?2006 annual reports).

Parametric instability of high power cavities

The most serious problem was pointed by Braginskii. [14] Large power density of Fabry-Perot cavity may cause so-called parametric instability, which is produced by the coupling between optical cavity modes with elastic vibration modes of the mirror substrate. Since the sapphire has larger elastic wave velocity, the number density of elastic modes is fewer than that of synthesized silica mirror, which is the case of advanced LIGO. And also the coupling constant between optics and mechanics is smaller in LCGT than in advanced LIGO due to the smaller beam size of LCGT. This merit comes from the adoption of cryogenics of LCGT[11]. Recent publication shows the effective suppression of the increase of the instability by adopting a negative feedback directly applied to the mirror.[12]

Substrate selection device

LCGT adopts cryogenic mirrors to reduce thermal noise in place of expanding laser beam radius that is planed both in the Advanced LIGO and the Advanced Virgo. Al_2O_3 monocrystal is selected as the cryogenic mirror substrate because it has excellent mechanical and thermal properties. However, there were some optical problems to be solved. High optical absorption and in-homogeneity of refractivity are concerned with the reproducibility of large ingots exceeding 20 cm. While some small-sized Al_2O_3 crystal substrates had good absorption quality and better homogeneity enough to satisfy the

*[14] Braginskii, *et al.*, Physics Lett. A **305** (2002)111.

LCGT requirement, larger samples (10cm in diameter, 6cm in length) had less quality [13]. Moreover, we know that the fabrication technology of Al_2O_3 crystal to date is not mature enough to consistently produce large substrates of adequate quality. In order to inspect optical homogeneity of large pieces of Al_2O_3 crystal for the production of better quality, we developed a scanning technique of birefringence measurement with high sensitivity and reported the determination of the optical axis of the uni-axial crystal and the measurement of the fluctuation of birefringence. We established a tool to distinguish the quality required to pass the specification of LCGT by this R&D in the annual report (2006–2007).

Other R&Ds

Apart from the above R&D issues, a high power laser system that produces more than 100 W is continually being developed by a group in Advanced Material Science, School of New Frontier Science, University of Tokyo. Also, researchers at KEK tested the mechanical strength of suspension fiber of sapphire crystal [15] and the result of heat radiation leaking from room temperature tube to the cryogenic chamber was quantitatively measured as reported in the section of CLIO.[16] We steadily advance towards the realization of LCGT by these R&D activities.

Summary and Scope of LCGT

We have restructured the organization and added minor changes to the design of LCGT. Persistent R&Ds have been successfully conducted and we are ready to construct the interferometer of LCGT at any time.

Bibliography

[1] M. Ohashi *et al.* "Status of LCGT and CLIO", TAUP 2007, September 11-15, 2007, Sendai.

[2] K. Kuroda *et.al.*, "Current status of LCGT", Seventh Edoardo Amaldi conference on gravitational waves, Sydney, July 8-14, 2007.

[3] F. Kawazoe *et al.*, presented at Amaldi 7 meeting, Sydney, July 8-14, 2007.

[4] K. Kuroda *et.al.*, Int. J. Mod. Phys. **D 8** (1999) 557; K. Kuroda,*et al.*, Class. Quantum Grav. **19** (2002) 1237; T. Uchiyama, *et al.*, Class. Quantum Grav. **21** (2004) S1161.

[5] T. Uchiyama, *et.al.*, Phys. Lett. **A 242** (1998) 211.

[6] T. Uchiyama, *et.al.*, Phys. Lett. **A 261** (1999) 5;*ibid* **A273**(2000)310.

[7] S. Miyoki, *et al.*, Cryogenics **40** (2000) 61: *ibid* **41** (2001) 415.

[8] T. Tomaru, *et al.*, Phys. Lett. **A 283** (2001) 80.

[9] N. Sato, *et al.*, Cryogenics **43** (2003) 425.

[10] K. Yamamoto, *et al.*, Class. Quantum Grav. **21** (2004) S1075.

[11] Parametric Instability in the LCGT arm cavity, K. Yamamoto, *et al.*, J. Phys. Conference series 122, 012015, 2008.

[12] Mathew Evans, GWADW09, May 11-15, 2009, Fortlauderdale, Florida.

[13] M. Tokunari et al., J. Phys.: Conference Series 32 (2006) 432.

[14] Z. Yan, *et al.*, Applied Optics **40**(2006) 1.

[15] T. Suzuki, *et al.*, Seventh Edoardo Amaldi conference on gravitational waves, Sydney, July 8-14, 2007.

[16] T. Tomaru, *et al.*, J. Phys. Conference series 122, 012009, 2008.

Sloan Digital Sky Survey

[Spokesperson : Masataka Fukugita]

ICRR, University of Tokyo, Kashiwa, Chiba 277-8582

In collaboration with the members of:
University of Tokyo, 7-3-1 Hongo, Bunkyo-ku, Tokyo 113-0033, Japan; Nagoya University, Chikusa, Nagoya 464-8602, Japan; National Astronomical Observatory of Japan, 2-21-1 Osawa, Mitaka, Tokyo 181-8588, Japan; Tohoku University, Aramaki, Aoba, Sendai 980-8578, Japan; Japan Women's University, 2-8-1, Mejirodai, Bunkyo-ku, Tokyo, 112-8681, Japan; The University of Chicago, 5640, South Ellis Ave., Chicago, IL 60637, USA; Fermi National Accelerator Laboratory, P.O. Box 500, Batavia, IL 60510, USA; Institute for Advanced Study, Einstein Drive, Princeton, NJ 08540, USA; Johns Hopkins University, Baltimore, MD 21218, USA; Los Alamos National Laboratory, Los Alamos, NM 87545, USA; Max-Planck-Institute for Astronomy, Königstuhl 17, D-69117 Heidelberg, Germany; Max-Planck-Institute for Astrophysics, Karl Schwarzschildstrasse 1, D-85748 Garching, Germany; New Mexico State University, P.O. Box 30001, Dept 4500, Las Cruces, NM 88003, USA; University of Pittsburgh, 3941 O'Hara St., Pittsburgh, PA 15260, USA; Princeton University, Princeton, NJ 08544, USA; United States Naval Observatory, P.O. Box 1149, Flagstaff, AZ 86002-1149; University of Washington, Box 351580, Seattle, WA 98195, USA

The SDSS completed its originally planned phase of operations — SDSS-I — on 30 June 2005 after five years of operation. The goal initially set was to cover 10,000 square degrees

of sky, but at the time the production survey began, the Five Year Baseline was developed to provide a more realistic metric against which the progress was evaluated. This decreased the target area to 8,387 square degrees (7,642 square degrees in the northern sky and 745 square degrees in the southern sky). The imaging carried out over 5 years has sustained the planned pace. At the end of the survey 97% of the baseline area were observed for the northern-sky baseline and 99% of southern-sky baseline were completed. Spectroscopic surveys, however, are somewhat behind the schedule. Only 74% of the baseline area were observed for the north (100% for the south). This is due to unusually poor weather conditions in the spring of 2003 and in the winter of 2004. The time consuming spectroscopic runs were severely affected. Otherwise, all the operations have been working smoothly (98% is the mean uptime fraction), producing the data as expected. Software has undergone extensive fine tunings and all the data were re-reduced for a number of times, which are now made public as *The Data Release of the Sloan Digital Sky Survey I* to *VII* (DR1-DR7), the last one comprising 8,423 square degrees of imaging and 8,032 square degrees of spectroscopic surveys done to 14 July 2008. This database contains 230 million objects including 1,374,080 objects with spectroscopic information. These numbers include 928,567 galaxies and 118,664 quasars obtained with the uniform selection criteria.

The SDSS has entered a new phase, SDSS-II, continuing through July, 2008. SDSS-II have carried out three distinct surveys — the Sloan Legacy Survey, SEGUE (The Sloan Extension for Galactic Understanding and Exploration), and the Sloan Supernova Survey — to address fundamental questions about the nature of the Universe, the origin of galaxies and quasars, and the formation and evolution of our own Galaxy, the Milky Way.

The Sloan Legacy Survey is the continuation of SDSS-I to complete spectroscopic survey to fill the gap in the Northern Galactic Cap which was not observed during SDSS-I due to poor weather conditions. Constructing the largest possible single contiguous survey volume will improve the following three main results: the determination of the power spectrum, the photometric calibration, and the legacy which SDSS will supply to the astronomical world. The goal is contiguous region of 7,808 square degrees in both imaging and spectroscopy.

SEGUE is mining the stellar content of the Milky Way in order to create a detailed 3-dimensional map of the Galaxy. SEGUE will image 3,320 square degrees mostly at $|b| < 30^\circ$ and obtain spectra of 240,000 stars in the disk and spheroid, revealing the age, composition and phase space distribution of stars within the various Galactic components. These stellar excavations will provide essential clues to the structure, formation, and evolution of our Galaxy. SEGUE has finished with imaging of 3240 square degrees and 237,388 stellar spectra.

The Sloan Supernova Survey is a time-domain survey involving repeat imaging of the same region of the sky (the SDSS Southern equatorial stripe; about 2.5 degree wide by $\sim$120 degree long) every other nights over the course of three 3-month campaigns (Sep-Nov). A primary scientific motivation is to detect and measure multi-band light-curves for $\sim$200 Type Ia supernovae in the redshift range $z = 0.1 - 0.3$. This sample, with excellent photometric calibration, should provide insights into systematics of SNe Ia as calibrated standard candles. The survey of the three years (2005-2007) have been finished successfully and found 494 spectroscopically confirmed SNe Ia in the redshift range between 0.05 and 0.40. About 85% of SNe Ia are discovered before maximum light. Follow-up spectra were taken at various telescopes through collaboration including MDM(2.4m), NOT(2.6m), APO(3.5m), NTT(3.6m), KPNO(4m), WHT(4.2m), Subaru(8.2m), HET(9.2m), Keck(10m), and SALT(10m).

The prime scientific goals of the SDSS are focused on extragalactic themes, such as the large-scale structure of galaxies over a very large volume of the Universe, and detailed characterisations of the galaxy properties and those of quasars.

The clustering of galaxies observed in the SDSS, when mapped in three dimensional space, looks very similar to that expected in the model of the Universe dominated by cold dark matter (CDM) with density fluctuations starting from nearly scale-invariant adiabatic perturbations, as predicted in the model of inflation. As a quantitative measure this density field is characterised by the statistic called the power spectrum, the squared amplitude of the Fourier modes of fluctuations, which is written,

$$P(k) = |\delta_k|^2 = \int d^3r \xi(r) e^{-ik\cdot r} \qquad (1)$$

where $\xi(r)$ is the two-point correlation function of galaxies. The important result is an accurate derivation of this power spectrum from galaxy clustering over the scale from 10 to 200 Mpc, and the demonstration that it joins smoothly the spectrum derived from the temperature field imprinted on the cosmic microwave background measured by *Wilkinson Microwave Anisotropy Probe* (WMAP) (see Fig. 1). Combined with WMAP that explores the Universe at $z \approx 1000$, this lends the most convincing support to the standard model of structure formation in the Universe based on the ΛCDM model. Moreover, the large-scale structure data of SDSS reduced the parameter degeneracies that exist within the CMB analyses; the combined data of WMAP and SDSS yield the cosmological parameters $\Omega_m = 0.29 \pm 0.04$, $\Omega_\Lambda = 0.71 \pm 0.04$ and $H_0 = 71 \pm 4$ km s^{-1}Mpc^{-1} at the year of 2004. Two years later, 3-year WMAP data was released. It includes the new measurement of the low-l polarization power spectrum, which detects the reionization signature and determines the corresponding optical depth. This measurement breaks the severe degeneracy in the 1-year WMAP data and causes the dramatic tightening of the constraints on various important cosmological parameters. Now the value added by other datasets is clearly reduced. However, the information from large scale structure of galaxies give substantial improvements by cutting error bars.

SDSS has applied another selection of galaxies — the selection of luminous red galaxies (LRG). Approximately 10% of SDSS galaxies belong to this category. The advantage of this selection is to allow us to explore much deep sky. The sight increases from $600h^{-1}$ Mpc ($z = 0.2$) to $1200h^{-1}$ Mpc ($z = 0.4$), quadrupling the survey volume compared with the main galaxy sample. The constraints on cosmological

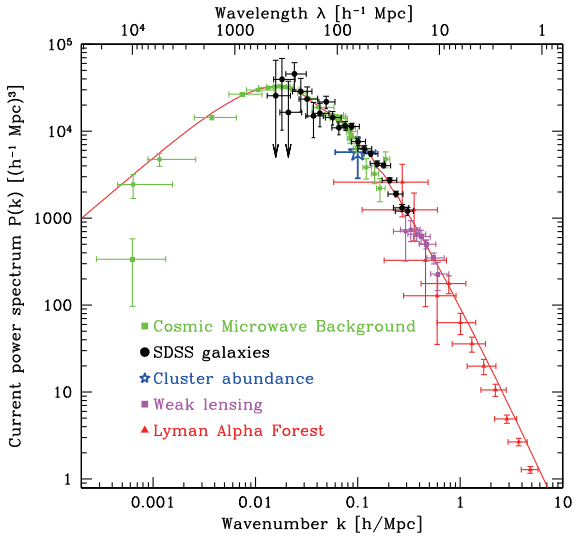

Fig. 1. The power spectrum of galaxy clustering scaled to the present epoch (SDSS galaxies) plotted with four other independent measures, extending four decades on spatial resolution, and demonstrating remarkable consistency. These data provide fundamental constraints on cosmological models. Figure is taken from Tegmark et al. Astrophys. J. **606**, 702 (2004).

parameters obtained by combining 3-year WMAP data and SDSS LRG measurements are $\Omega_m = 0.239 \pm 0.018$, $\Omega_\Lambda = 0.761 \pm 0.018$ and $H_0 = 73 \pm 2$ km s^{-1}Mpc^{-1}. This set is taken as an authoritative in the astronomy community.

Baryonic acoustic oscillations (BAO) is a reminiscence of the sound wave oscillation in the pre-recombination era, which is most dramatically seen in CMB multipoles. In real space this leads to a peak in the two-point correlation function $\xi(r)$ at about $r_s = 100h^{-1}$ Mpc. In Fourier space this process leads to oscillations in the power spectrum. The wavelength of these oscillations will be $k_s = 2\pi/r_s = 0.06h$ Mpc^{-1}. Eisenstein et al. (2005) has detected this acoustic peak in correlation function of SDSS LRG and determine the curvature of the Universe to 1% accuracy, $\Omega_\Lambda + \Omega_m = 1.01 \pm 0.01$, which is comparable to the latest WMAP3+SDSS LRG analysis. The analysis of the main galaxies and LRGs in the SDSS DR5 sample determines $\Omega_m = 0.256 \pm 0.029$ using the dependence of r_s on the matter density Ω_m (Fig. 2). This value of the matter density is derived from the locations of BAO in the galaxy power spectrum and in the CMB. This is an extremely clean geometrical cosmological measurement, as the physics of the BAO production is well understood. With larger samples and a wider redshift range, the BAO "standard ruler" can be used to constrain the cosmology at high precision through the comoving distance-redshift relation. Forthcoming surveys will be designed to exploit this effect.

Although CDM models seem to be very successful on large scales, one of the most serious challenges facing CDM models is the so-called "missing satellite" problem. CDM models predicts at least 1-2 orders of magnitude more low-mass sub-halos at the present epoch compared to the observed abundance of dwarf galaxies surrounding the Milky Way and M31. All-sky photographic surveys cover most of the sky, but are limited to surface brightnesses of ~ 25.5 mag arcsec^{-2}.

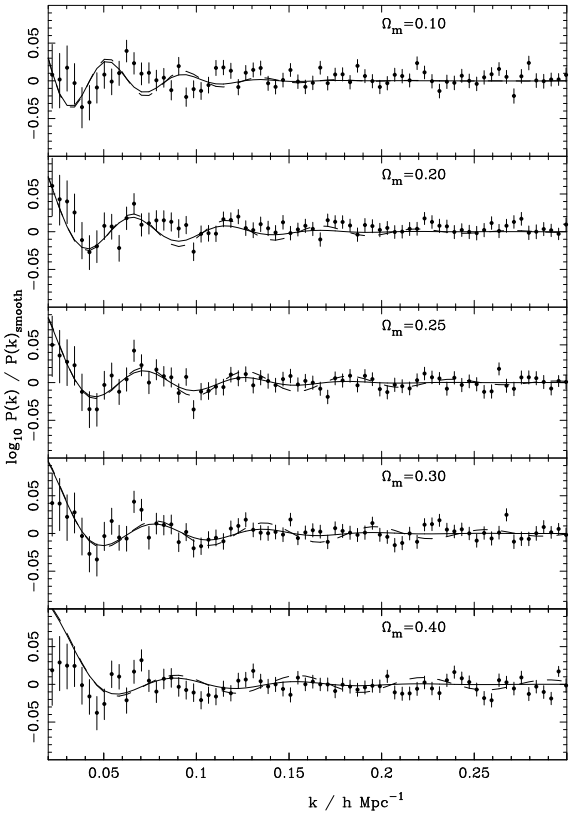

Fig. 2. Ratio of the power spectra calculated from the SDSS to the overall shape of the measured power spectra (filled circles with 1σ errors). Solid lines represents the BAO predicted by a CDM model with matter densities given in each panel and h = 0.73, and a 17% baryon fraction. As can be seen, the observed oscillations approximately match those predicted for $0.2 \leq \Omega_m \leq 0.3$. Figure is taken from Percival et al. Astrophys. J. **657**, 51 (2007).

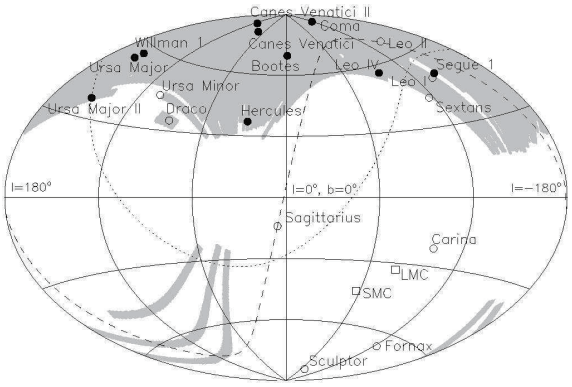

Fig. 3. Locations of Milky Way satellites in Galactic coordinates. Filled circles are satellites discovered by SDSS, and open circles are previously known Milky Way dSphs. Figure is taken from Belokurov et al. Astrophys. J. **654**, 897 (2007).

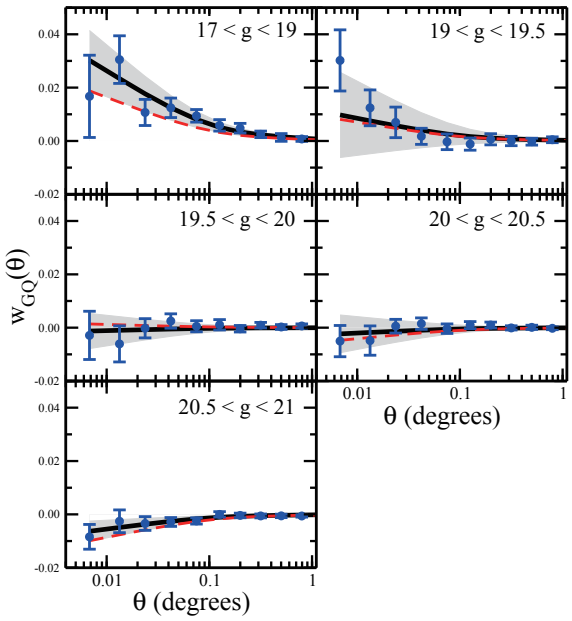

Fig. 4. Measurement of $w_{GQ}(\theta)$, cross-correlation between foreground galaxies and distant quasars, as a function of quasar g-band magnitude. The dark solid curve is the fitting model. Figure is taken from Scranton et al. Astrophys., J. **633**, 589 (2005).

The selection effects are also difficult to model with accuracy. The SDSS makes it possible to carry out a systematic survey for satellite galaxies, which are detectable through overdensity of stars in position-color-magnitude space. A total of 10 new Milky Way satellites with effective surface brightness $\mu_V \geq 28$ mag arcsec^{-2} have been discovered in SDSS data (Fig. 3) in addition to the previously known 9 Milky Way dwarf spheroidals. Some preliminary studies of these indicate that they may be dark matter dominated. We need more investigation to see if these are the "missing satellites".

Gravitational lensing is also a subject to which the SDSS is making a significant contribution in a number of ways. The SDSS is one of the first few that observed a weak effect of gravitational lensing of galaxy images by foreground galaxies. The lensing effect appears as distorted images of galaxies due to the gravitational shear field, but it is only on the order of a few percent, compared with the order of unity effect of randomly oriented galaxies that have intrinsically different shapes. Millions of galaxies are needed to extract this small signal from noise of the order of unity. With the SDSS galaxy sample, this distortion was unambiguously detected, showing that the mass concentration around galaxies behaves as $r^{-0.8}$ as a function of distance r, consistently with the famous $r^{-1.8}$ law of the galaxy-galaxy correlation. Another effect of gravitational lensing by foreground galaxies is a magnification of distant sources, *cosmic magnification*. Gravitational magnification has two effects. First, the flux received from distant sources is increased, resulting in a relatively deeper apparent magnitude limited survey. Second, the solid angle is stretched, diluting the surface density of source images on the sky. The net result of these competing effects is an induced cross-correlation between physically separated populations that depends on how the loss of sources due to dilution is balanced by the gain of sources due to flux magnification. Using $\sim 200,000$ quasars and 13 million galaxies, cosmic magnification has been detected for the first time at 8σ level (Fig. 4).

The large quasar sample of the SDSS also provides an excellent platform to search for classical strong gravitational lenses of quasar images, i.e., splitting of images. 16 lenses are found from 46000 quasar images. Among the novel cases that deserve special scientific discussion, we quote the large-separation lensed quasar, SDSS J1004+4112 of four images with their maximum separation being 14.6 arcsec and SDSS J1029+2623 with two images with their separation of 22.5 arcsec (Figure5). These are the case where split lensed images are further enhanced by a cluster of galaxies. A statistical analysis to infer cosmological and mean galaxy parameters from the lens sample yielded $\Omega_m = 0.26 \pm 0.08$, $\Omega_\Lambda = 0.74 \pm 0.17$, consistent with the values derived from WMAP and SDSS power spectrum analysis.

As it became apparent already at imaging first light, the SDSS project has made unrivalled contributions to our understanding of high redshift quasars from its commissioning phase. By now the project has found 19 quasars with redshift higher than 5.7 (*i*- dropout quasars) from ∼6,600 square degrees — Among them 8 are with $z > 6$: there are no $z > 6$ quasars reported from other projects. The highest redshift is 6.42, which means that the light was emitted only 0.84 Gyr after the Big Bang. These high-z quasars, together with a sample for lower-z, show the abundance of luminous quasars declining exponentially with redshift from $z \approx 3$ towards early epochs. This is a significant constraint on the model of quasar formation at high redshifts.

Also important aspect with high redshift quasars is that they allowed us to observe a change of the ionisation state of the intergalactic medium (IGM) in a high redshift universe. We know that a free electron and a proton recombine to form a neutral hydrogen atom at $z \approx 1000 - 1500$. We also know that IGM was again highly reionised before $z \approx 3$. When and how the reionisation took place is a matter of significant interest

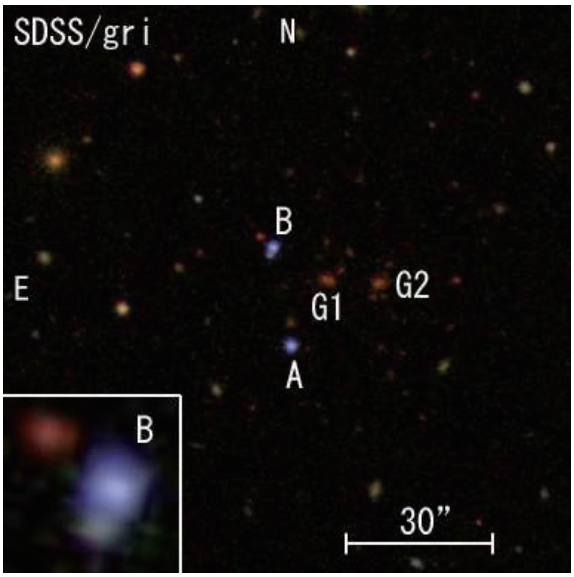

Fig. 5. *gri* composite SDSS image of SDSS J1029+2623. The quasar images (blue stellar objects) are indicated by A and B. G1 and G2 (red extended objects) are likely to be member galaxies of a lensing cluster at $z \sim 0.55$. Figure is taken from Inada et al. Astrophys. J. (Letters) **653**, L97 (2006).

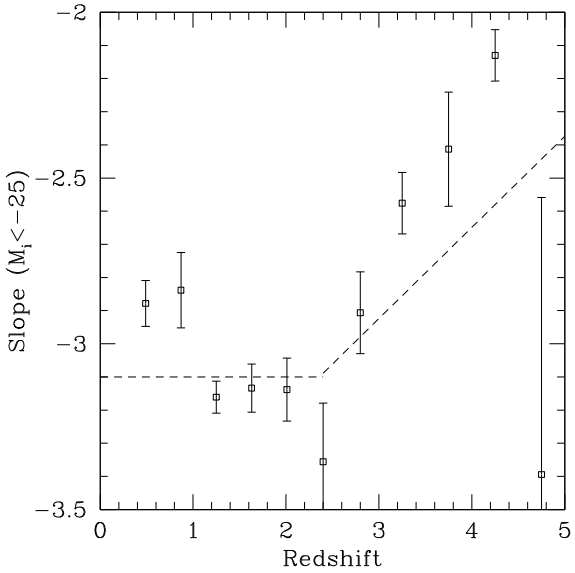

Fig. 7. Bright-end slope of the Quasar Luminosity Function as a function of redshift determined from a linear least-squares fit to the $M_i(z=2) < -25$. The slope of the luminosity function significantly flattens with redshift $z > 3$. Figure is taken from Richards et al. Astron. J. **131**, 2766 (2006).

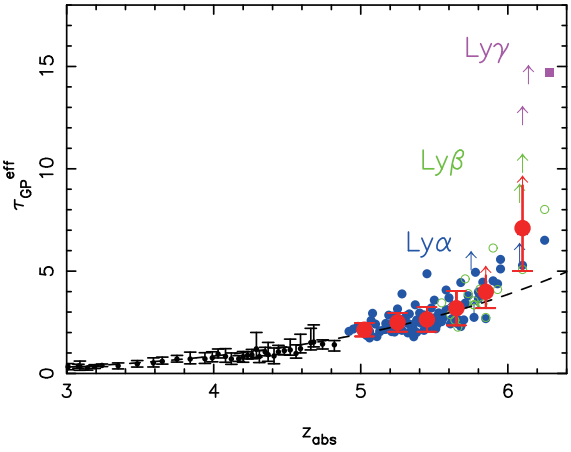

Fig. 6. Evolution of optical depth combined with the Lyα, Lyβ, and Lyγ results. At $z > 5.5$, the best-fit evolution has $\tau_{GP}^{eff} \approx (1+z)^{>10.9}$, indicating an accelerated evolution. Figure is taken from Fan et al. Astron. J. **132**, 117 (2006).

from the point of view of galaxy formation. The SDSS quasar spectra show the flux shortwards the Lyman α line rapidly vanishing at $z \geq 6$ (called the Gunn-Peterson trough), indicating the change of state of the IGM at this redshift (Figure 6). Cosmic reionisation is also evident from the WMAP 3-year data and its epoch $z_r = 8 \pm 2$ is consistent with SDSS result if we consider the error of optical depth determined from WMAP data. A problem newly created is the question whether the star formation activity, as inferred from faint galaxy observations, is sufficient to ionise the entire IGM at $z \approx 6$.

Besides high redshift quasars, a large number of quasars are collected and their properties are being studied. We have released four catalogues of quasars, the fourth one containing 77,429 quasars in 5,740 square degrees. The long-awaited quasar luminosity function (the work requires proper understanding of the selection function) was determined for well-defined and homogeneous sample consisting of 15,343 quasars within an effective area of 1622 square degrees. Derived luminosity function has a flatter bright-end slope at high redshift than at low redshift (Fig. 7). This slope change must be accounted for in models of the evolution of accretion onto supermassive black holes.

Theory Group

Neutrino mass, Dark Matter and Baryon Asymmetry via TeV-Scale Physics without Fine-Tuning

[Spokesperson : M. Aoki]

ICRR, Univ. of Tokyo, Kashiwa, Chiba 277-8582

In collaboration with the members of Toyama U. and Universidad Autónoma de Madrid.

We propose an extended version of the standard model, in which neutrino oscillation, dark matter, and baryon asymmetry of the Universe can be simultaneously explained by the TeV-scale physics without assuming unnatural hierarchy among the mass scales. Tiny neutrino masses are generated at the three loop level due to the exact Z_2 symmetry, by which stability of the dark matter candidate is guaranteed. The extra Higgs doublet is required not only for the tiny neutrino masses but also for successful electroweak baryogenesis. The model provides discriminative predictions especially in Higgs phenomenology, so that it is testable at current and future collider experiments.

Bibliography

[1] M. Aoki, S. Kanemura, and O. Seto, Phys. Rev. Lett. **102** (2009) 051805, [arXiv:0807.0361 [hep-ph]].

Light Higgs boson scenario in the SUSY seesaw model

[Spokesperson : M. Asano]

ICRR, Univ. of Tokyo, Kashiwa, Chiba 277-8582

In collaboration with the members of ICRR, Sokendai, Univ. of Toyama and Kyoto Univ..

In the light Higgs boson scenario in which the lightest Higgs boson mass is lighter than 114 GeV, we discuss consistency with see-saw mechanism. Using lepton flavor violating charged lepton decays, we investigate the mass bound for the right-handed neutrino. We show that this scenario would be testable in future experiments. We also discuss the effect of the modification of renormalization group equations by the right-handed neutrinos on the $b \to s\gamma$ process and the relic abundance of dark matter in the light Higgs boson scenario.

Bibliography

[1] M. Asano, T. Kubo, S. Matsumoto and M. Senami, arXiv:0807.4922 [hep-ph].

D-term assisted Anomaly Mediation in E6 motivated models

[Spokesperson : M. Asano]

ICRR, Univ. of Tokyo, Kashiwa, Chiba 277-8582

In collaboration with the members of ICRR, KEK, Tohoku Univ. and Nagoya Univ..

In E6 GUTs model, we investigate effects of D-term contributions which can tachyonic slepton problem in anomaly mediated supersymmetry breaking scenario. We show mass spectrum at several sample points. There would be a distinct signature of this scenario at the LHC. We also discuss some characteristic features of the neutralino dark matter in this model.

Bibliography

[1] M. Asano, T. Kikuchi and S. G. Kim, arXiv:0807.5084 [hep-ph].

Precision Measurements of Little Higgs Parameters at the International Linear Collider

[Spokesperson : M. Asano]

ICRR, Univ. of Tokyo, Kashiwa, Chiba 277-8582

In collaboration with the members of ICRR, Meiji Gakuin Univ., KEK, Tohoku Univ. and Univ. of Toyama.

In the Littlest Higgs model with T-parity, we study production processes of new gauge bosons at the international linear collider. Through Monte Carlo simulations of the production processes, we show that the heavy gauge boson masses can be deter- mined very accurately at the ILC for a representative parameter point of the model. ¿From the simulation result, we also discuss the determination of other model parameters and its impact on the future measurement of the thermal abundance of the dark matter relics in our universe.

Bibliography

[1] E. Asakawa, M. Asano, K. Fujii, T. Kusano, S. Matsumoto, R. Sasaki, Y. Takubo and H. Yamamoto, arXiv:0901.1081 [hep-ph], to be published in Phys. Rev. D.

Non-linear evolution of matter power spectrum in modified theories of gravity

[Spokesperson : T. Hiramatsu]

ICRR, Univ. of Tokyo, Kashiwa, Chiba 277-8582

In collaboration with the members of Univ. of Tokyo and Univ. of Portsmouth.

Recently considerable efforts have been made to study the possibility of a large distance modification of General Relativity, which may account for the late-time acceleration of the Universe. We focus on the non-linear behaviour of the matter power spectrum in some viable theoretical models of modified gravity, $f(R)$ gravity models and the DGP brane-world model. The present work is based on an improved cosmological perturbation theory developed in our previous paper, called closure theory. We developed a numerical algorithm to solve a set of the integral-differential equations derived from the closure theory [1]. Using this scheme, we predicted the matter power spectrum in a $f(R)$ gravity model proposed by Hu and Sawicky and the DGP model at the 1-loop level[2]. We found that, in all cases, the resultant power spectra tend to converge to the prediction in GR on small scales, which is realised by the Vainstein effect (DGP) or the Chameleon effect ($f(R)$). In addition, we checked that the Parametrized-Post-Friedmann formalism by Hu and Sawicky can be also used in these modified theories of gravity if small modifications of the model parameters are allowed.

Bibliography

[1] T. Hiramatsu, A. Taruys, Phys. Rev. **D79** (2009) 103526, [arXiv:0902.3772 [astro-ph.CO]].

[2] K. Koyama, A. Taruya and T. Hiramatsu, Phys. Rev. **D79** (2009) 123512, [arXiv:0902.0618 [astro-ph.CO]].

Flavor physics in supersymmetric theories

[Spokesperson : J. Hisano]

ICRR, Univ. of Tokyo, Kashiwa, Chiba 277-8582

In collaboration with the members of Univ. of Tokyo, Munich Tech. Univ., and Tohoku Univ..

In the supersymmetric (SUSY) extension of the standard model (SM), CP- and/or flavor-violating SUSY-breaking terms are introduced, and they lead to rare processes, such as EDMs and charged-lepton flavor violating processes. These observables are known to be sensitive to source of the SUSY

breaking and also physics beyond the SUSY SM. In [1], we systematically evaluated the predictions for the EDMs at the beyond-leading-order (BLO) within supersymmetric frameworks with flavor-violating soft terms. We found that the BLO contributions to the EDMs dominate over the leading-order (LO) effects in large regions of the supersymmetric parameter space. Next, in [2] we reevaluated the charged-lepton flavor violating processes in the SUSY seesaw model and discussed correlation of the $Br(\mu \to e\gamma)$ and other observables within the prospect of the MEG experiment sensitivity.

Bibliography

[1] J. Hisano, M. Nagai and P. Paradisi, arXiv:0812.4283 [hep-ph].

[2] J. Hisano, M. Nagai, P. Paradisi and Y. Shimizu, arXiv:0904.2080 [hep-ph].

Probing reheating temperature of the universe with gravitational wave background

[Spokesperson : K. Nakayama]

ICRR, Univ. of Tokyo, Kashiwa, Chiba 277-8582

In collaboration with the members of ICRR, Univ. of Tokyo and RESCEU.

Thermal history of the universe after big-bang nucleosynthesis (BBN) is well understood both theoretically and observationally, and recent cosmological observations also begin to reveal the inflationary dynamics. However, the epoch between inflation and BBN is scarcely known. In this paper we show that the detection of the stochastic gravitational wave background around 1Hz provides useful information about thermal history well before BBN. In particular, the reheating temperature of the universe may be determined by future space-based laser interferometer experiments such as DECIGO and/or BBO if it is around 10^{6-9} GeV, depending on the tensor-to-scalar ratio.

Bibliography

[1] K. Nakayama, S. Saito, Y. Suwa and J. Yokoyama, JCAP **0806** (2008) 020 [arXiv:0804.1827 [astro-ph]].

Direct/indirect detection signatures of non-thermally produced dark matter

[Spokesperson : K. Nakayama]

ICRR, Univ. of Tokyo, Kashiwa, Chiba 277-8582

In collaboration with the members of ICRR.

We study direct and indirect detection possibilities of neutralino dark matter produced non-thermally by e.g. the decay of long-lived particles, as is easily implemented in the case of anomaly or mirage mediation models. In this scenario, large self-annihilation cross sections are required to account for the present dark matter abundance, and it leads to significant enhancement of the gamma-ray signature from the Galactic Center and the positron flux from the dark matter annihilation. It is found that GLAST and PAMELA will find the signal or give tight constraints on such nonthermal production scenarios of neutralino dark matter.

Bibliography

[1] M. Nagai and K. Nakayama, Phys. Rev. D **78** (2008) 063540 [arXiv:0807.1634 [hep-ph]].

Non-Gaussianity from isocurvature perturbations

[Spokesperson : K. Nakayama]

ICRR, Univ. of Tokyo, Kashiwa, Chiba 277-8582

In collaboration with the members of ICRR and IPMU.

We develop a formalism to study non-Gaussianity in both curvature and isocurvature perturbations. It is shown that non-Gaussianity in the isocurvature perturbation between dark matter and photons leaves distinct signatures in the CMB temperature fluctuations, which may be confirmed in future experiments, or possibly, even in the currently available observational data. As an explicit example, we consider the QCD axion and show that it can actually induce sizable non-Gaussianity for the inflationary scale, $H_{\rm inf} = O(10^9 - 10^{11})$ GeV. We also study a scenario that large non-Gaussianity arises from the baryon asymmetry of the Universe. There are baryogenesis scenarios containing a light scalar field, which may result in baryonic isocurvature perturbations with some amount of non-Gaussianity. As an example we consider the Affleck-Dine mechanism and show that a flat direction of the supersymmeteric standard model can generate large non-Gaussianity in the curvature perturbations.

Bibliography

[1] M. Kawasaki, K. Nakayama, T. Sekiguchi, T. Suyama and F. Takahashi, JCAP **0811** (2008) 019 [arXiv:0808.0009 [astro-ph]].

[2] M. Kawasaki, K. Nakayama and F. Takahashi, JCAP **0901** (2009) 002 [arXiv:0809.2242 [hep-ph]].

[3] M. Kawasaki, K. Nakayama, T. Sekiguchi, T. Suyama and F. Takahashi, JCAP **0901** (2009) 042 [arXiv:0810.0208 [astro-ph]].

Hilltop Non-Gaussianity

[Spokesperson : K. Nakayama]

ICRR, Univ. of Tokyo, Kashiwa, Chiba 277-8582

In collaboration with the members of ICRR and IPMU.

We study non-Gaussianity induced by a pseudo Nambu-Goldstone boson with a cosine-type scalar potential. We focus on how the non-Gaussianity is affected when the pseudo Nambu-Goldstone boson rolls down from near the top of the scalar potential where the deviation from a quadratic potential is large. We find that the resultant non-Gaussianity is similar to that obtained in the quadratic potential, if the pseudo Nambu-Goldstone boson accounts for the curvature perturbation; the non-Gaussianity is enhanced, otherwise.

Bibliography

[1] M. Kawasaki, K. Nakayama and F. Takahashi, JCAP **0901** (2009) 026 [arXiv:0810.1585 [hep-ph]].

Cosmic Rays from Dark Matter Annihilation and Big-Bang Nucleosynthesis

[Spokesperson : K. Nakayama]

ICRR, Univ. of Tokyo, Kashiwa, Chiba 277-8582

In collaboration with the members of ICRR, Lancaster Univ., and Tohoku Univ..

Recent measurements of cosmic-ray electron and positron fluxes by PAMELA and ATIC experiments may indicate the existence of annihilating dark matter with large annihilation cross section. We show that the dark matter annihilation in the big-bang nucleosynthesis epoch affects the light element abundances, and it gives stringent constraints on such annihilating dark matter scenarios for the case of hadronic annihilation. Constraints on leptonically annihilating dark matter models are less severer. We also show that the dark matter annihilation scenarios to explain the positron excess may also be compatible with the discrepancy of the cosmic lithium abundances between theory and observations. The wino-like neutralino in the supersymmetric standard model is a good example for it.

Bibliography

[1] J. Hisano, M. Kawasaki, K. Kohri and K. Nakayama, Phys. Rev. D **79** (2009) 063514 [arXiv:0810.1892 [hep-ph]].

[2] J. Hisano, M. Kawasaki, K. Kohri, T. Moroi and K. Nakayama, Phys. Rev. D **79** (2009) 083522 [arXiv:0901.3582 [hep-ph]].

Cosmological Moduli Problem from Thermal Effects

[Spokesperson : K. Nakayama]

ICRR, Univ. of Tokyo, Kashiwa, Chiba 277-8582

In collaboration with the members of ICRR and IPMU.

We estimate the cosmological abundance of a modulus field that has dilatonic couplings to gauge fields, paying particular attention to thermal corrections on the modulus potential. We find that a certain amount of the modulus coherent oscillations is necessarily induced by a linear thermal effect. We argue that such an estimate provides the smallest possible modulus abundance for a given thermal history of the Universe. As an example we apply our results to a saxion, a bosonic supersymmetric partner of an axion, and derive a tight bound on the reheating temperature. We emphasize that the problem cannot be avoided by fine-tuning the initial deviation of the modulus field, since the minimal amount of the modulus is induced by the dynamics of the scalar potential.

Bibliography

[1] K. Nakayama and F. Takahashi, Phys. Lett. B **670** (2009) 434 [arXiv:0811.0444 [hep-ph]].

Neutrino Signals from Annihilating/Decaying Dark Matter in the Light of Recent Measurements of Cosmic Ray Electron/Positron Fluxes

[Spokesperson : K. Nakayama]

ICRR, Univ. of Tokyo, Kashiwa, Chiba 277-8582

In collaboration with the members of ICRR and Lancaster Univ..

The excess of cosmic-ray electron and positron fluxes measured by the PAMELA satellite and ATIC balloon experiments may be interpreted as the signals of the dark matter annihilation or decay into leptons. In this letter we show that the dark matter annihilation/decay which reproduces the electron/positron excess may yield a significant amount of high-energy neutrinos from the Galactic center. In the case, future kilometer-square size experiments may confirm such a scenario, or even the Super-Kamiokande results already put constraints on some dark matter models.

Bibliography

[1] J. Hisano, M. Kawasaki, K. Kohri and K. Nakayama, Phys. Rev. D **79** (2009) 043516 [arXiv:0812.0219 [hep-ph]].

Upperbound on Squark Masses in Gauge-Mediation Model with Light Gravitino

[Spokesperson : S. Sugiyama]

ICRR, Univ. of Tokyo, Kashiwa, Chiba 277-8582

In collaboration with the members of ICRR, KEK, and Univ. of Tokyo.

We examine stabilities of our supersymmetry-breaking false vacuum in a low-energy direct gauge mediation model of SUSY breaking. The stability required in the high-temperature early universe leads to upperbounds on masses of squarks and gluino as $m_{\tilde{q}} \lesssim 1$ TeV and $m_{\tilde{g}} \lesssim 1$ TeV for the light gravitino of mass $m_{3/2} \lesssim 16$ eV.

Bibliography

[1] J. Hisano, M. Nagai, S. Sugiyama, T. T. Yanagida, arXiv:0804.2957 [hep-ph].

A Realistic Extension of Gauge-Mediated SUSY-Breaking Model with Superconformal Hidden Sector

[Spokesperson : S. Sugiyama]

ICRR, Univ. of Tokyo, Kashiwa, Chiba 277-8582

In collaboration with the members of ICRR.

The sequestering of supersymmetry (SUSY) breaking parameters, which is induced by superconformal hidden sector, is one of the solutions for the μ/B_μ problem in gauge-mediated SUSY-breaking scenario. However, it is found that the minimal messenger model does not derive the correct electroweak symmetry breaking. In this paper we present a model

which has the coupling of the messengers with the SO(10) GUT-symmetry breaking Higgs fields. The model is one of the realistic extensions of the gauge mediation model with superconformal hidden sector. It is shown that the extension is applicable for a broad range of conformality breaking scale.

Bibliography

[1] M. Asano, J. Hisano, T. Okada, S. Sugiyama, arXiv:0810.4606 [hep-ph].

Non-Gaussianity from Symmetry

[Spokesperson : T. Suyama]

ICRR, Univ. of Tokyo, Kashiwa, Chiba 277-8582

In collaboration with a member of IPMU

We pointed out that a light scalar field fluctuating around a symmetry-enhanced point can generate large non-Gaussianity in density fluctuations. We named such a particle as an "ungaussiton", a scalar field dominantly produced by the quantum fluctuations,generating sizable non-Gaussianity in the density fluctuations. We derived a consistency relation between the bispectrum and the trispectrum, $\tau_{\rm NL} = 10^3 f_{\rm NL}^{4/3}$, which can be extended to arbitrary high order correlation functions. If such a relation is confirmed by future observations, it will strongly support this mechanism.

Bibliography

[1] T. Suyama and F. Takahashi, JCAP **0809** (2008) 007 [arXiv:0804.0425 [astro-ph]].

Primordial Curvature Fluctuation and Its Non-Gaussianity in Models with Modulated Reheating

[Spokesperson : T. Suyama]

ICRR, Univ. of Tokyo, Kashiwa, Chiba 277-8582

In collaboration with members of ICRR, Saga Univ. and Aoyama-Gakuin Univ.

We investigated non-Gaussianity in the modulated reheating scenario where fluctuations of the decay rate of the inflation generate adiabatic perturbations, paying particular attention to the non-linearity parameters $f_{\rm NL}, \tau_{\rm NL}$ and $g_{\rm NL}$ as well as the scalar spectral index and tensor-to-scalar ratio which characterize the nature of the primordial power spectrum. We found that the non-linearity between the decay rate and the modulus field which determines the decay rate can generate much greater non-Gaussianity. We also discussed a consistency relation among non-linearity parameters which holds in the scenario and find that the modulated reheating yields a different one from that of the curvaton model.

Bibliography

[1] K. Ichikawa, T. Suyama, T. Takahashi and M. Yamaguchi, Phys. Rev. D **78** (2008) 063545 [arXiv:0807.3988 [astro-ph]].

Exact gravitational lensing by cosmic strings with junctions

[Spokesperson : T. Suyama]

ICRR, Univ. of Tokyo, Kashiwa, Chiba 277-8582

We pointed out that the results by Brandenberger et al. in Phys.Rev.D77:083502(2008) that the geometry around the straight cosmic strings with stationary junctions is flat to linear order in the string tension can be immediately extended to any order.

Bibliography

[1] T. Suyama, Phys. Rev. D **78** (2008) 043532 [arXiv:0807.4355 [astro-ph]].

OBSERVATORIES and A RESEARCH CENTER

Location of the Institute and the Observatories in Japan

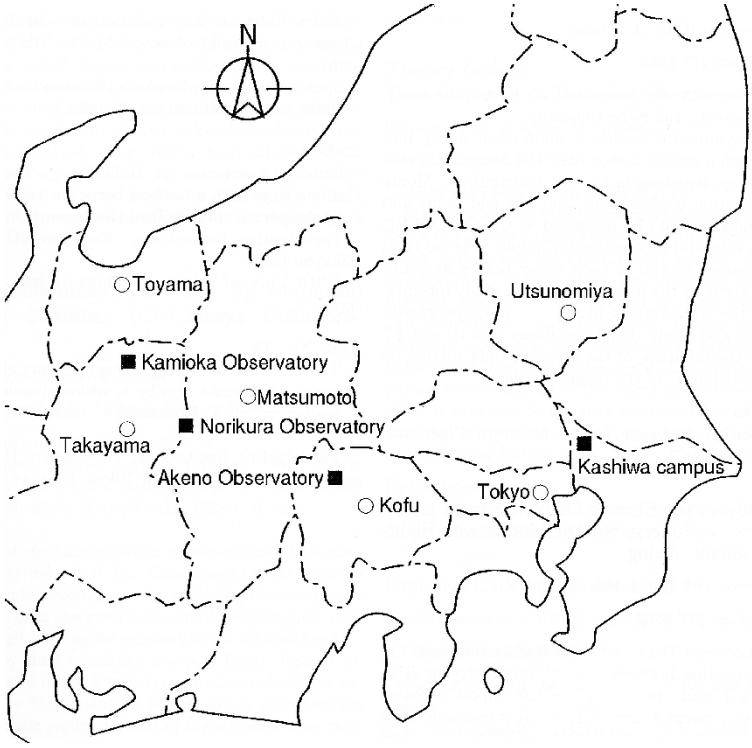

Norikura Observatory

Location:	Iwaitani, Nyukawa-cho, Takayama-shi, Gifu Prefecture 506-2254 N 36°06′, E 137°33′, 2770 m a.s.l.
Telephone (Fax):	+263-33-7456
Telephone (satellite):	090-7721-5674
Telephone (car):	090-7408-6224

Akeno Observatory

Location:	5259 Asao, Akeno-machi, Hokuto-shi, Yamanashi Prefecture 407-0201 N 35°47′, E 138°30′, 900 m a.s.l.
Telephone / Fax:	+551-25-2301 / +551-25-2303

Kamioka Observatory

Location:	456 Higashi-mozumi, Kamioka-cho, Hida-shi, Gifu Prefecture 506-1205 N 36°25′26″, E 137°19′11″, 357.5 m a.s.l.
Telephone / Fax:	+578-85-2116 / +578-85-2121

Research Center for Cosmic Neutrinos

Location:	5-1-5 Kashiwanoha, Kashiwa, Chiba Prefecture 277-8582
Telephone / Fax:	+4-7136-3138 / +4-7136-3115

NORIKURA OBSERVATORY

1. Introduction

Norikura Observatory (36.10°N and 137.55°E) was founded in 1953 and attached to ICRR in 1976. It is located at 2770 m above sea level, and is the highest altitude manned laboratory in Japan. Experimental facilities of the laboratory are made available to all the qualified scientists in the field of cosmic ray research and associated subjects. The AC electric power is generated by the dynamo and supplied throughout the observatory. In 1996, two dynamos of 70 KVA each were replaced with the new ones. The observatory can be accessed easily by car and public bus in summer (July-September). The 50th anniversary of Norikura Observatory was celebrated in 2003.

The feasibility of the automatic operation of Norikura Observatory during winter period has been tested since winter 2004 in order to study the possibilities to reduce maintenance and labor costs without seriously damaging to the use of researches. A long-distance (∼40km) wireless LAN system (11M bps) was set up in 2003. Two new easy-to-handle and easy-to-maintain dynamos of 115 KVA each were installed in 2004 as well. The unmanned operation of Norikura Observatory was successful in the first winter, during which the battery backed-up solar panels and/or wind power generators kept supplying the electricity to the wireless LAN and ongoing cosmic-ray experiments.

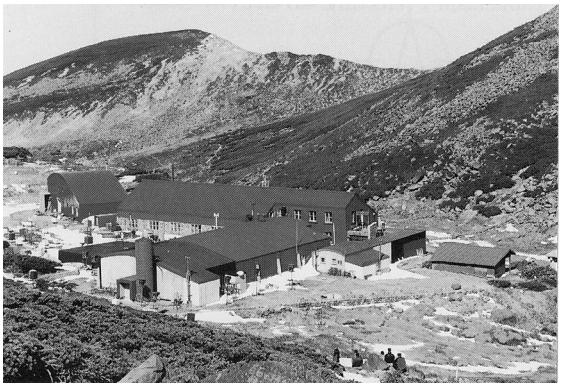

Fig. 1. Norikura Observatory.

Present major scientific interests of the laboratory is focused on the modulation of high energy cosmic rays in the interplanetary space associated with the solar activity and the generation of energetic particles by the solar flares, both of which require long-term monitoring. This research has been carried out by the group of universities, where ICRR provides them with laboratory facility. A part of the facility has been open for the environmental study at high altitude such as the aerosol removal mechanism in the atmosphere or for the botanical study of the high altitude environment.

2. Cosmic Ray Physics

For the modulation study[2], two small experiments have been operated continuously for a long time. One is a neutron monitor operated to study the correlation of solar activity and the cosmic ray flux. The other is a high counting muon telescope consisting of 36 m^2 scintillation counters to study the time variation of cosmic rays with energies of 10–100 TeV over 20 years. The neutron monitor data are open to researchers worldwide as a world observation network point (WDC). The 5 years from 2000 corresponded to the solar maximum (2000) to a declining phase in the solar cycle 23. The sun spot number in 2004 is approximately one fourth of the those at maximum. Nonetheless, there occurred active cosmic-ray phenomena associated with Coronal Mass Ejection (CME). As regards solar cosmic rays, although many ground level enhancement (GLE) phenomena took place every year, such GLEs were observed only by neutron monitors in Japan, as the maximum cosmic-ray energy was several GeV in the GLEs and the magnetic rigidity cutoff in Japan is approximately 10 GeV for charged particles initiating secondary muons. The sunspot numbers in the solar cycle 23 was smaller than those in the previous cycle 22, indicating less solar activities of cycle 23. Although the GLEs above 10 GeV were not observed in cycle 23, the total number of GLEs were greater in cycle 23 than in cycle 22. This suggests that the charged particle acceleration associated with CME was less frequent in the cycle 23 than in the cycle 23. On the other hand, Forbush decreases in galactic cosmic rays caused by CME in the Sun were observed frequently in cycle 23, though the solar activities have been in a declining phase since 2000. The worldwide observation of Forbush decreases may contribute significantly to space weather study.

In addition, space weather observation is actively made by a 25 m^2 muon hodoscope at Norikura Observatory[1], [2],[3],[4],[5], [6],[7],[8]. A loss cone anisotropy is observed by a ground-based muon hodoscope in operation at Norikura Observatory in Japan for 7 hours preceding the arrival of an interplanetary shock at Earth on October 28, 2003. Best fitting a model to the observed anisotropy suggests that the loss cone in this event has a rather broad pitch-angle distribution with a half-width about 50° from the interplanetary magnetic field (IMF). According to numerical simulations of high-energy particle transport across the shock, this implies that the shock is a ”quasi-parallel” shock in which the angle between the magnetic field and the shock normal is only 6°. It is also suggested that the leadtime of this precursor is almost independent of the rigidity and about 4 hour at both 30 GV for muon detectors and 10 GV for neutron monitors (see paper [7]).

The Sun is the nearest site to the Earth capable of accelerating particles up to high energies. When the Sun becomes active, flares are frequently observed on its surface. The flare

accelerates the proton and ion to high energy and they are detected on the Earth soon after the flare. Among the particles generated by the flare, high energy neutrons provide the most direct information about the acceleration mechanism as they come straight from the flare position to the Earth without deflected by the magnetic field.

In 1990, Nagoya group constructed a solar neutron telescope consisting of scintillators and lead plates, which measures the kinetic energy of incoming neutrons up to several hundred MeV. This telescope observed high energy neutrons associated with a large flare occurred on the 4th of June, 1991. The same event was simultaneously detected by the neutron monitor and the high counting muon telescope of Norikura Observatory. This is the most clear observation of solar neutrons at the ground level in almost ten years since the first observation at Jungfraujoch in 1982.

A new type of the large solar neutron telescope (64 m^2 sensitive area) was constructed by Nagoya group in 1996. It consists of scintillators, proportional counters and wood absorbers piled up alternately. This takes a pivotal role among a worldwide network of ground based solar neutron telescopes of the same type in Yangbajing in Tibet, Aragatz in Armenia, Gornergrat in Switzerland, Chacaltaya in Bolivia and Mauna Kea in Hawaii. The Sun is being watched for 24 hours using this network.

Fig. 2. New Solar-Neutron Telescope of Nagoya Group.

The Sun reached the maximum activity in 2000 and the active phase continued for the next few years. All the telescopes in Norikura Observatory, neutron telescope, neutron monitor, muon telescope and muon hodoscope, have been operated almost continuously through the solar cycle 23 in order to obtain comprehensive information on the solar flare phenomena. Important hints for understanding the mechanism of cosmic-ray acceleration near the solar surface will be obtained by these measurements, especially by energy spectra measured by the timing information of arriving neutrons and muons.

Furthermore, the relation between the electric fields induced by thunderclouds is studied recently[10]. The electric fields with thunderclouds change the intensity of secondary cosmic rays observed on the ground. This effect has been investigated using several detectors located at Norikura Observatory where excesses of 1 % and more of the average counting rate are observed when the observatory is covered with thunderclouds. A frequency analysis of the time series of days with such excesses for the period 26 October 1990 to 15 January shows the expected summer maximum in the rate of occurrence and, surprisingly, a 26-day variation. An electric field mill was installed to help determine the relationship between the intensity variations and the strength and direction of the field near the detector system: the excess is usually observed when a negative electric field (accelerating negative charges downward) greater than 10 kV/m is present in the atmosphere above the observatory. Based on Monte Carlo simulations, it is predicted that excess counting rates measured without charge discrimination will be expected as a consequence of the excess of positive muons among the secondary cosmic rays.

In addition to the long-term cosmic-ray observations mentioned above, various kinds of short-dated experiments are carried out every year taking an advantage of the high altitude of the observatory. A few examples include a search for super heavy particles with plastic plates, a precise measurement of atmospheric gamma rays and muons, collection of cosmic dusts contained in the snow and the performance study of the balloon borne cosmic ray experiments.

3. Environmental Study

One of the interesting topics is atmospheric environment especially relating with atmospheric aerosol particles and water soluble gases. Because of its height, AC power supply, accommodation facility, and accessibility of cargos, the cosmic ray observatory at Mt. Norikura provides a very unique opportunity for atmospheric observation, especially for free-tropospheric conditions. (The atmosphere lower than a few kilometer is highly affected by the ground. This height level is named as 'atmospheric boundary layer'. The height of the boundary layer is about 4 km in daytime and about 2 km in nighttime around Norikura area. The atmosphere higher than this atmospheric boundary layer is called 'free troposphere'.) Originally, atmospheric observation at the cosmic ray observatory was initiated to study cosmogenic radionuclides with Prof. Suzuki at Shizuoka University. During early stage of the research at Mt. Norikura, a local effect of air contamination was recognized. To reduce air contamination from diesel exhausts and other activities around the observatory, an atmospheric observation hut (6 m^2) was installed at the west end (windward) of the observatory in September 1999. From year 2000, continuous monitoring (mostly mid-May to mid-October) of meteorology was started, number-size distribution of aerosols, dew point, aerosol chemical composition, ozone and radon concentrations, and column amount of aerosols from sky radiometer and ceilometer. Monitoring of ozone and radon concentrations was extended during 2 winters from 2001 to 2003. During summer season, also collected were rain, fog, water-condensed aerosol samples. These samples combined with other parameters were used in several thesis (master) works and provided useful information about future seeds of hygroscopic study of aerosols. During the past 5 years, the following results[11],[12],[13] were obtained at Mt.

Norikura.

(1) Polluted air pumping effects over central Japanese Alps in summer

Under the clear sky conditions in summer, polluted air from mountain valley area is lifted up about 4km of altitude (1km above the mountain top) over Mt. Norikura. The height of observatory is within the atmospheric boundary layer in the daytime, and is out of (higher than) the atmospheric boundary layer in nighttime. The ratio of aerosol volume concentration for daytime (polluted valley wind) to nighttime (clean free-tropospheric) conditions was about 10. The air pumping effects over central Japanese Alps carry about 10 time higher concentration of aerosols to the free-troposphere over Japan in summer. Under the high-pressure system centered over the northwest Pacific in typical summer condition, backward air trajectories were originated from the northwest Pacific to Mt. Norikura and forward trajectories returned to the north Pacific with some deviations to east Russia and the Kurile Islands. The air pumping effects over mountain area provide a strong pollution source mechanism to the free-troposphere over the western Pacific region including East Asia.

(2) Seasonal variation of aerosol chemistry in free troposphere

An automated aerosol sampler was installed at the site in September 2000 to obtain seasonal aerosol samples. The sampler collected aerosols from mid-May to mid-October in 2001 and 2002. Results of its analysis showed seasonal changes in major and minor constituents of aerosols associating with changes of dominant air mass type over Japan.

(3) Vertical profiles of aerosols and clouds near the top of the atmospheric boundary layer

Ceilometer (lidar with small output energy) was installed in summer 2002, and was operated in 4 summer seasons. The aerosol and cloud profiles near the top of the atmospheric boundary layer have been observed. Some events of Asian dust, and of smoke from Siberian forest fire at lower free troposphere have been detected.

4. Botanical Study

It is predicted that ecosystems in high-latitudes and alpine regions are sensitive to global climatic warming. The significant increasing trends in air temperature are found in the Hida Mountains, where Mt. Norikura is located. Thus, effects of climatic change caused by global warming on alpine ecosystems must be urgently studied in the alpine region of central Japan. The Hida Mountains, strongly influenced by cold-air masses from Siberia in winter, receive some of the heaviest snowfall in the world. Due to heavy snowfall, dynamics of alpine ecosystems may be peculiar to the Hida Mountains. However, few studies have been made because of difficulty in approach to the alpine study site. The inter-university research program of ICRR, gave an opportunity to make an intensive study all year around in the alpine region on Mt. Norikura[14],[15].

(1) Tree line dynamics

The tree form of evergreen sub-alpine fir (Abies mariesii) is studied at the upper distribution limit (2500m above sea level) on Mt. Norikura. Leader stems degenerate above the maximum snowpack line (3-4m high) , whereas branches below the snowpack line grow densely. In winter, leaves above snowpack line were severely damaged by environmental stresses, such as abrasion by wind-blown snow particles, desiccation, photoinhibition. Longevity of leaves was shortened to 4-5 years due to high mortality rate in winter. In contrast, leaves below snowpack line were protected from environmental stresses and their longevity was 11 years. As a result, biomass below the snowpack line takes more than 80with climate change should have unfavorable effects on tree line Abies mariesii.

(2) Alpine region

Pinus pumila, an alpine prostrated pine, is dominant in the alpine regions (2500～3000m above sea level). At wind-protected sites, Pinus pumila grows vigorously with the tree height of 1-2m. They were beried in snowpack throughout the winter. At the wind-exposed ridge, growth is suppressed with the tree height of 0.2-0.5m. Throughout the winter, the surface of the pine community was exposed due to strong wind at the ridge. Leeward leaves were sound, because pine stems with high elasticity were prostrated and buried in snow. Thus, alpine pine can catch and accumulate snow to protect itself. This feature may be advantageous to alpine trees in comparison with sub-alpine trees (Abies mariesii). On the other hand, at the windward side (western), cuticular layer covering epidermal cells of leaf was abraded probably due to wind-blown snow and ice particles. By spring, abraded leaves at the windward side were dead caused by desiccation and photoinhibition. Even Pinus pumila community could reduce its habitat in small snowfall condition caused by global warming.

Impact of global warming due to so-called greenhouse gases like CO2, CH4 and others on vegetation ecology is among the most serious environmental issues. To investigate how plants response to global warming, an experiment of greenhouse effect on vegetation has been continued at a high mountain, Mt. Norikura (3,025 m a.s.l.), central Japan, since 1997. Five open-top chambers which are small greenhouses with a size of maximum open-top diameter, the maximum basal diameter and the height of the chamber were 47 cm, 85 cm and 30 cm, respectively, were set over alpine plant communities consisting of small woody plants and herbaceous vegetation. At places inside and outside of the chambers, seasonal changes in vegetation growth and phenology were observed every month. Using automatic data-recorders, some climate elements such as air and ground temperatures, humidity and rainfall have been observed every hour. Some results through the experiment were quite remarkable. Due to the temperature enhancement of about 0.8○C for air temperature and about 0.3○C for ground temperature, plant growth

rates and phenological changes showed notable differences between inside and outside of the chambers. The responses to warming, however, were different by different plant species. The results suggest[16],[17] that dominant species in plant community should be replaced by the species with a high physiological response to warming and with a growing form extending tree crown.

Bibliography

[1] "Precursors of geomagnetic storms observed by the muon detector network", K. Munakata, J. W. Bieber, S. Yasue, C. Kato, M. Koyama, S. Akahane, K. Fujimoto, Z. Fujii, J. E. Humble, and M. L. Duldig, *J. Geophys. Res.*, Vol. 105, No.A12, pp. 27,457-27,468 (2000).

[2] "Solar cycle variations of modulation parameters of galactic cosmic- rays in the heliosphere", K. Munakata, H. Miyasaka, I. Sakurai, S. Yasue, C. Kato, S. Akahane, M. Koyama, D. L. Hall, Z. Fujii, K. Fujimoto, S. Sakakibara, J. E. Humble, and M. L. Duldig, *Adv. Space Res.*, Vol.29, No.10, pp.1527-1532 (2002).

[3] "A 1.7 year quasi-periodicity in cosmic ray intensity variation observed in the outer heliosphere", C. Kato, K. Munakata, S. Yasue, K. Inoue, and F. B. McDonald, *J. Geophys. Res.*, Vol.18, No.A10, p.1367, doi:10.1029/2003JA009897 (2003).

[4] "Exploration of the heliosphere by cosmic rays", K. Munakata, published as the chapter 2 of *Advances in Solar-Terrestrial Physics*, pp.101-116, edited by H. Oya, published by TERRAPUB, Tokyo (2004).

[5] "Cosmic-ray modulation in the heliosphere: global and near-earth measurements and modeling", K. Munakata, Rapporteur paper in 28th *International Cosmic Ray Conference*, Vol.8, edited by T. Kajita et al., pp.251-276, Univ. Acad. Press, Tokyo (2004).

[6] "Geometry of an interplanetary CME on October 29, 2003 deduced from cosmic rays", T. Kuwabara, K. Munakata, S. Yasue, C. Kato, S. Akahane, M. Koyama, J. W. Bieber, P. Evenson, R. Pyle, Z. Fujii, M. Tokumaru, M. Kojima, K. Marubashi, M. L. Duldig, J. E. Humble, M. Silva, N. Trivedi, W. Gonzalez and N. J. Schuch, *Geophys. Res. Lett.*, Vol.31, L19803, doi:10.1029/2004GL020803 (2004).

[7] "A "loss-cone" precursor of an approaching shock observed by a cosmic-ray muon hodoscope on October 28, 2003", K. Munakata, T. Kuwabara, S. Yasue, C. Kato, S. Akahane, M. Koyama, Y. Ohashi, A. Okada, T. Aoki, H. Kojima and J. W. Bieber, *Geophys. Res. Lett.*, Vol.32, L03S04, doi:10.1029/2004GL021469, 2005.

[8] "CME-geometry and cosmic-ray anisotropy observed by a prototype muon detector network", K. Munakata, T. Kuwabara, J. W. Bieber, P. Evenson, R. Pyle, S. Yasue, C. Kato, Z. Fujii, M. L. Duldig, J. E. Humble, M. R. Silva, N. B. Trivedi, W. D. Gonzalez and N. J. Schuch, *Adv. Space Res.*, doi:10.1016/j.asr.2003.05.064, 2005, in press.

[9] "Acceleration below Thunder Clouds at Mount Norikura", by the Tibet hybrid experiment", Y. Muraki *et al.*, Proceedings in the 28th International Cosmic Ray Conference, (31 July - 7 August 2003, Tsukuba, Japan), Vol.7, pp 4177-4180.

[10] "Effects of atmospheric electric fields on cosmic rays", Y. Muraki *et al.*, Phys. Rev. D, **69**, 123010–1-13 (2004).

[11] K. Osada, M. Kido, C. Nishita, K. Matsunaga, Y. Iwasaka, M. Nagatani, H. Nakada, Changes in ionic constituents of free tropospheric aerosol particles obtained at Mt. Norikura (2770 m a. s. l.), central Japan, during the Shurin period in 2000, Atmos. Environ., 36, 5469-5477, 2002.

[12] "Atmospheric diffusion process based on time change of ^{222}Rn vertical profile", K. Yoshioka, Journal of Aerosol Research, Japan, 17, 267-275, 2002 (in Japanese).

[13] "Free-tropospheric aerosols based on airplane and mountain observations", K. Osada, Journal of Aerosol Research, Japan, 15, 335-342, 2000 (in Japanese).

[14] "Diurnal changes in needle gas exchange in alpine Pinus pumila during snow-melting and summer seasons", A. Ishida, T. Nakano, S. Sekikawa, E. Maruta, T. Masuzawa, Ecological Research 16, 107-116 (2001).

[15] "Effects of high light and low temperature during harsh winter on needle photodamage of Abies Mariesii growing at the forest limit on Mt. Norikura in Central Japan", J. Yamazaki, A. Ohashi, Y. Hashimoto, E. Negishi, S. Kumagai, T. Kubo, T. Oikawa, E. Maruta, Plant Science 165, 257-264, (2003).

[16] "Chemistry of surface water at a volcanic summit area, Norikura, central Japan: Multivariate statistical approach", K. Anazawa and H. Ohmori, Chemosphere, 45, 807-816, (2001).

[17] "Experimental research on vegetation response to artificial warming on a mid-latitude high mountain, central Japan", H. Ohmori, J.H. Iguchi, T. Ohta, A. Terazono and K. Hikita, Geogr. Rev. Japan, 77, 301-320, (2004).

AKENO OBSERVATORY

The Observatory is in Akeno town of Hokuto-city situated 20 km west of Kofu and 130 km west of metropolitan Tokyo. The location is at the longitude of 138.5°E and the latitude of 35.5°N. The altitude is ∼900 m above sea level (Fig.1).

The Observatory was established in 1977 as a research center for air shower studies in the very high energy region. It has been administered by the ICRR as a facility of joint-university-use.

The Akeno Air Shower Experiment started in 1979 with an array covering 1 km^2 area (1 km^2 array). The array was enlarged to 20 km^2 in 1985 and was gradually expanded to Akeno Giant Air Shower Array (AGASA) of approximately 100 km^2 area by 1990.

Fig. 1. Aerial View of Akeno Observatory and 1 km^2 array area

One of the distinctive features of Akeno experiments is that the measurement was made over five decades of energies well covering 10^{15} eV - 10^{20} eV by using both the surface detector (for electromagnetic component) and the shielded detector (for muon component). The wide energy coverage was accomplished by the arrays of scintillation detectors of various inter-detector spacings from 3 m to 1 km and with different triggering conditions.

The AGASA was an air shower array composed of 111 scintillation detectors and 27 muon detectors. Each component was placed by about 1 km separation and covered the ground area of 100 km^2 in the neighboring villages of the observatory. All detectors were interconnected by optical fibers for the precise timing determination and the data transmission (Fig.2). The AGASA was the largest air shower array in the world. Its operation was ceased in January of 2004 after the construction of Telescope Array (TA) had been funded in 2003.

The AGASA observed a total of 11 events with energies exceeding 10^{20}eV in 13 years of operation, and heralded rich physics of ultra-high energy cosmic rays now being explored by the Pierre Auger Observatory in Argentina and the TA in Utah, USA.

The observatory is now used as a support base for the operation of TA. It also supports two related experiments and

Fig. 2. AGASA scintillation detector and data acquisition system.

various R & D works for the development of detectors used for the observation high energy cosmic rays.

KAMIOKA OBSERVATORY

Kamioka observatory is located at 1000m underground (2700 m water equivalent) in the Kamioka Mine, Gifu prefecture, about 200 km west of Tokyo. The observatory was established in 1995 in order to operate Super-Kamiokande. The underground laboratories are located under Mt.Ikeno-yama and accessible to the experimental site through a 1.7 km horizontal tunnel. The observatory also has surface research buildings and a dormitory located at the distance of 15 minutes drive from the entrance of the mine. The Super-Kamiokande experiment had discovered neutrino oscillations through the observations of atmospheric and solar neutrinos (see the section for Neutrino and Astroparticle Division). The atmospheric neutrino oscillation was confirmed by the K2K accelerator neutrino experiment, which was conducted between 1999 and 2004. A new long baseline neutrino oscillation experiment (the T2K experiment) using a high intensity beam, 50 times of the K2K neutrino beam, by the J-PARC proton accelerator, will inject first neutrino beam to the Super-Kamiokande detector in April, 2009.

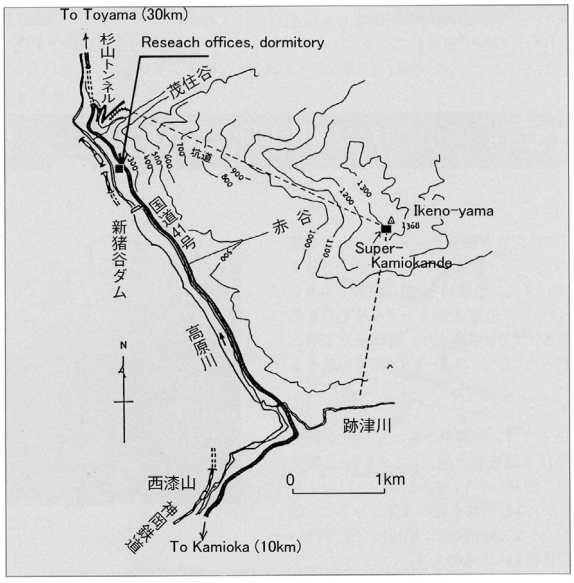

Fig. 1. Map of Kamioka observatory.

The low cosmic ray flux and low seismic noise environment in the underground site enables us to conduct various researches. There is a 100 m long laser interferometer, which is a proto-type of the planned 3 km gravitational wave antenna called LCGT, aiming to detect gravitational waves from extraterrestrial sources (see section of Astrophysics Gravity Division). Using the low radioactive background environment in the Kamioka Mine, A dark matter experiment, called XMASS is being prepared. The XMASS group has performed R&D study using a small proto-type detector and subsequently, the construction of the 800kg liquid xenon detector was started in 2007 and will be ready for data taking by the autumn in 2009. The R&D study of a tracking type detector for dark matter search by the Kyoto University group (the NEWAGE experiment) has also been performed in an underground laboratory. A double beta decay experiment, the CANDLE experiment (Osaka Univ.), is planned to be located in the Kamioka Underground Observatory. In order to support those experiments and also related R&D works, the Observatory is equipped with low background Germanium detector, ICP-MS and so on to measure extremely low radioactive backgrounds.

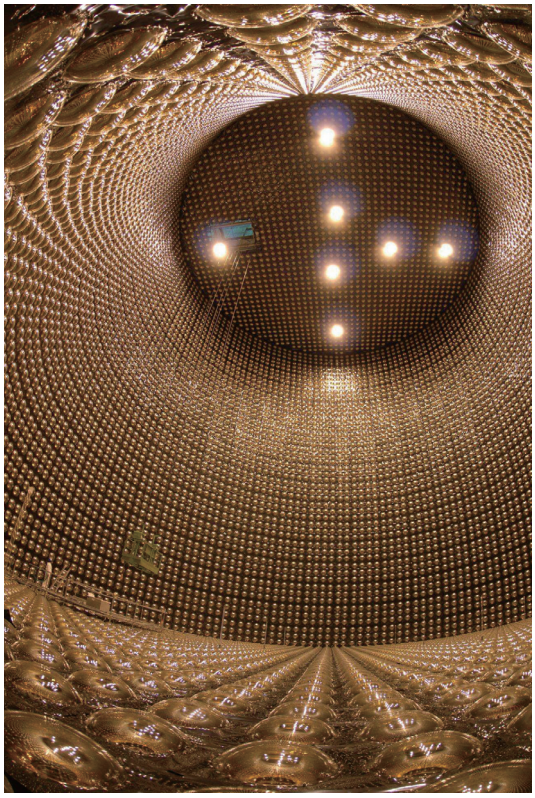

Fig. 2. Super-Kamiokande detector.

Fig. 3. 100 m baseline laser interferometers for gravitational wave and geophysics in Kamioka mine.

RESEARCH CENTER FOR COSMIC NEUTRINOS

The Research Center for Cosmic Neutrinos was established in April, 1999. The main objective of this Center is to study neutrinos based on data from various observations and experiments. In order to promote studies of neutrino physics, it is important to provide the occasion to discuss theoretical ideas and experimental results on neutrino physics. Therefore, one of the most important practical jobs of this Center is the organization of neutrino-related meetings. On Jun. 27th, 2008, we hosted one domestic neutrino workshop on "Current status of neutrino physics". About 41 physicists participated in this meeting.

Members of this Center have been involved in the Super-Kamiokande, K2K and T2K experiments, carrying out researches in neutrino physics. Atmospheric neutrino data from Super-Kamiokande give one of the most precise pieces of information on neutrino oscillations. With increased data, it is more important to have better predictions of the neutrino flux. Therefore, in addition to data analysis of the above experiments, we work on predicting the atmospheric neutrino flux. In order to accurately predict this flux, it is important to know details of the data based on measurements of primary and secondary cosmic-ray fluxes. For this reason, we have a close collaboration with researchers working on cosmic-ray flux measurements.

It is important that the general public knows about the achievements in the present science. For this reason, we have a public lecture every year. In FY2008, we held the public lecture on April 12 (Sat) at Kashiwa. Two active scientists working on the neutrino physics lectured on the latest research findings of the neutrino physics. About 86 people heard the lectures.

Fig. 1. Public lecture held in Kashiwa in April 12, 2008.

This Center, together with the computer committee of ICRR, is in charge of operating the central computer system in ICRR. The computer system was upgraded in Jan. 2008 by about a factor of 5 to 10 in the performance relative to the previous one, and it had been highly utilized for the analysis and simulation of the various cosmic-ray physics. This Center also supported the users of the computer system, including the physicists working outside ICRR.

Since 2004, this Center has been acting as the body for accepting the ICRR inter-university programs related to the low-background underground facility in the Kashiwa campus. The facility is currently equipped with 4 Ge detectors mainly for the measurements of cosmic radioactive isotopes. The scientific activities that are related to this facility is described elsewhere.

Fig. 2. Computer facility operated since Jan. 2008.

APPENDICES

A. ICRR Workshops and Ceremonies

Inauguration Ceremony and Symposium of Telescope Array

Date: August 25th, 2008
Place: Media Hall of Kashiwa Library, University of Tokyo, Kashiwa, Japan

Outline: The construction of the Telescope Array (TA) experiment was completed in Utah, USA and it started an observation of ultra-high energy cosmic rays in March, 2008. The Collaborators of TA are from USA, Korea, Russia and Japan. An inauguration ceremony of TA was held on August 25th, 2008 inviting Prof. K. Hirao, Vice President of University of Tokyo for Research, Prof. Tom Parks, Vice President for Research, University of Utah and Prof. Jim Whitmore, Program Director, National Science Foundation. The TA collaborators, researchers in the field and representatives of the industry assembled together to celebrate the start of TA. After the ceremony, a mini-symposium was held. Prof. K. Sato of physics department presented the study of the propagation of ultra-high energy cosmic rays and his expectation to TA's observation. Prof. M. Fukushima of ICRR's TA group gave a report of the construction and stated a prospect of physics.

Participants: 101 from Japan, 6 from USA and 1 from Korea.

B. ICRR Seminars

1. Apr 10, 2008: Masaki Asano (ICRR, University of Tokyo), "Neutralino Dark Matter in Light Higgs Boson Scenario"
2. Apr 17, 2008: Takashi Hiramatsu (ICRR, University of Tokyo), "Evolution of cosmological perturbations in a brane world scenario"
3. Apr 25, 2008: Yuki Shimizu (ICRR, University of Tokyo), "CALET: high energy cosmic ray experiment on the ISS/JEM"
4. May 9, 2008: Hirohisa Sakurai (Yamagata University), "Time variations of cosmogenic nuclide and solar activities"
5. May 30, 2008: Kentaro Terada (Hiroshima University), "In-situ isotope analysis of extraterrestrial materials by Ion microprobe"
6. Jun 17, 2008: Venya Berezinsky (INFN, Laboratori Nazionali del Gran Sasso), "Ultra High Energy Cosmic Rays: from Galactic to Extragalactic Cosmic Rays"
7. Jun 24, 2008: Mohammad S. Athar (Aligarh Muslim University, India), "Neutrino Nucleus Cross Sections"
8. Jul 9, 2008: Hiroaki Yamamoto (LIGO, Caltech), "Current status of Advanced LIGO"
9. Jul 9, 2008: Takashi Uchiyama (ICRR, University of Tokyo), "Toward Large-scale Gravitational Wave Detector in Japan (CLIO to LCGT)"
10. Jul 11, 2008: Gary Varner (University of Hawaii), "Microwave Radio Detection of UHE Air Showers"
11. Sep 26, 2008: Kumiko Kotera (Institute of Astrophysics of Paris), "The Optical Depth of the Universe Seen through Ultrahigh Energy Cosmic Ray Spectacles"
12. Oct 27, 2008: Hiroyuki Nakanishi (Kagoshima University), "Square Kilometer Array Project"
13. Nov 7, 2008: Hiroko Miyahara (ICRR, University of Tokyo), "Variations of solar activity and the galactic cosmic rays during the last 1200 years deduced from cosmogenic nuclides"
14. Dec 1, 2008: Shoji Torii (Waseda University), "Cosmic Ray Electron (+Positron) Spectrum Observed by Antarctica Balloon Flights and Its Interpretations"
15. Dec 2, 2008: Gerasimos Rigopoulos (University of Helsinki), "On the Infrared divergences of Inflationary Perturbations"

16. Dec 12, 2008: Hiroshi Miyakawa (ICRR, University of Tokyo), "Development of the next generation gravitational wave detector"
17. Dec 16, 2008: Hiro Tajima (SLAC National Accelerator Laboratory), "Gamma-ray Universe revealed by Fermi Gamma-ray Space Telescope"
18. Dec 24, 2008: Toshio Terasawa (Tokyo Institute of Technology), "Particle Acceleration and Propagation: Plasma Physics and Cosmic Rays"
19. Jan 9, 2009: Carsten Rott (Ohio State University), "Neutrino Oscillation Measurements at the South Pole"
20. Feb 27, 2009: Federico Urban (University of British Columbia), "The cosmological constant as a manifestation of the conformal anomaly"
21. Mar 17, 2009: German Hermann (Max-Planck-Institut fuer Kernphysik), "Ground-based gamma-ray astrophysics: today and tomorrow"
22. Mar 24, 2009: Marco Casolino (INFN and Physics Department of University of Rome), "Pamela Experiment"

C. List of Publications — Fiscal Year 2008

(a) Papers Published in Journals

1. "Supernova detection", M. Nakahata, J.Phys.Conf.Ser.136:022042, 2008.
2. "Search for Proton Decay via $p \to e^+\pi^0$ and $p \to \mu^+\pi^0$ in a Large Water Cherenkov Detector", Super-Kamiokande Collaboration (H. Nishino et al.), Phys.Rev.Lett.102:141801, 2009.
3. "Kinematic reconstruction of atmospheric neutrino events in a large water Cherenkov detector with proton identification", Super-Kamiokande Collaboration (M. Fechner et al.), Phys.Rev.D79:112010, 2009.
4. "First Study of Neutron Tagging with a Water Cherenkov Detector", Super-Kamiokande Collaboration (H. Watanabe et al.), Astroparticle Physics 31, 320-328, 2009.
5. "Future of neutrino experiments", T. Kajita, Pramana 72:109-117, 2009.
6. "Working group report: Neutrino physics", Sandhya Choubey et al, Pramana 72:269-275, 2009.
7. "Future neutrino oscillation experiment with 2 detectors at Kamioka and Korea", T. Kajita, J.Phys.Conf.Ser.120:052045, 2008.
8. "Atmospheric neutrinos and the implications to cosmic ray interactions", T. Kajita, Nucl.Phys.Proc.Suppl.175:301-306, 2008.
9. "Distillation of Liquid Xenon to Remove Krypton", XMASS Collaboration (K. Abe et al.), Astroparticle Physics 31, 290-296, 2009.
10. "Measurement of single charged pion production in the charged-current interactions of neutrinos in a 1.3-GeV wide band beam", K2K Collaboration (A. Rodriguez et al.), Phys.Rev.D78:032003, 2008.
11. "Probing nonstandard neutrino physics by two identical detectors with different baselines", N. C. Ribeiro et al., Phys. Rev. D 77, 073007, 2008.
12. "CANGAROO-III Observations of the 2006 Outburst of PKS 2155-304", Y. Sakamoto et al., Astrophys. J. 676, 113, 2008.
13. "Observation of an Extended Very High Energy Gamma-Ray Emission from MSH 15-52 with CANGAROO-III", T. Nakamori et al., Astrophys. J. 677, 297, 2008.
14. "CANGAROO-III Search for Gamma Rays from Kepler's Supernova Remnant", R. Enomoto et al., Astrophys. J. 683, 383, 2008.

15. ”Observation of Very High Energy Gamma Rays from HESS J1804-216 with CANGAROO-III Telescopes”, Y. Higashi et al., Astrophys. J. 683, 957, 2008.

16. ”Very high energy gamma-ray observations of the Galactic Plane with the CANGAROO-III telescopes”, M. Ohishi et al., Astropart. Phys. 30, 47, 2008.

17. ”CANGAROO-III Search for TeV Gamma-Rays from Two Clusters of Galaxies”, R. Kiuchi et al., Astrophys. J. in press, 2009, arXiv:0908.3301 [astro-ph.HE].

18. ”Search for VHE Gamma Rays from SS433/W50 with the CANGAROO-II Telescope”, Sei. Hayashi et al., Astropart. Phys. in press, 2009, arXiv:0909.0133 [astro-ph.HE].

19. ”Reanalysis of Data Taken by the CANGAROO 3.8 Meter Imaging Atmospheric Cherenkov Telescope: PSR B1706-44, SN 1006, and Vela”, T. Yoshikoshi et al., Astrophys. J. 702, 631, 2009.

20. ”End-to-end absolute Energy calibration of atmospheric fluorescence telescopes by an electron linear accelerator”, T. Shibata et al., Nucl. Instr. and Methods A597, 61-66, 2008.

21. ”Multi-TeV Gamma-Ray Observation from the Crab Nebula Using the Tibet-III Air Shower Array Finely Tuned by the Cosmic-Ray Moon’s Shadow”, M. Amenomori et al., The Astrophysical Journal, 692, 61-72, 2009.

22. ”The energy spectrum of all-particle cosmic rays around the knee region observed with the Tibet-III air-shower array”, M. Amenomori et al., Advances in Space Research, 42, 467-472, 2008.

23. ”The all-particle spectrum of primary cosmic rays in the wide energy range from 10^{14} eV to 10^{17} eV observed with the Tibet-III air-shower array”, M. Amenomori et al., The Astrophysical Journal, 678, 1165-1179, 2008.

24. ”Conduction Effect of Thermal Radiation in a Metal Shield Pipe in a Cryostat for a Cryogenic Interferometric Gravitational Wave Detector”, T. Tomaru et al., Jpn. J. Appl. Phys. 47, 3, 1771-1774, 2008.

25. ”Effect of energy deposited by cosmic-ray particles on interferometric gravitational wave detectors”, K. Yamamoto, et al., Phys. Rev. D78, 022004, 2008.

26. ”Search for continuous gravitational waves from PSR J0835-4510 using CLIO data”, T. Akutsu, et al., Class. Quantum Grav. 25 184013, 2008.

27. ”Status of LCGT and CLIO”, M. Ohashi, Journal of Physics: Conference Series, 120, 032008, 2008.

28. ”The Sixth Data Release of the Sloan Digital Sky Survey ”, Adelman-McCarthy, J. K. et al., ApJS, 175, 297-313, 2008.

29. ”Implications for Galaxy Evolution from Cosmic Evolution of the Supernova Rate Density”, T. Oda, et al., PASJ, 60, 169, 2008

30. ”First-Year Spectroscopy for the Sloan Digital Sky Survey-II Supernova Survey”, C. Zheng, et al., AJ, 135, 1766-1784, 2008.

31. ”The Subaru/XMM-Newton Deep Survey (SXDS). II. Optical Imaging and Photometric Catalogs”, H. Furusawa, et al., ApJS, 176, 1-18, 2008.

32. ”A Measurement of the Rate of Type Ia Supernova at Redshift $z \sim 0.1$ from the First Season of the SDSS-II Supernova Survey ”, B. Dilday, et al., ApJ, 682, 262-282, 2008.

33. ”Luminosity Function Constraints on the Evolution of Massive Red Galaxies since $z \sim 0.9$”, R. Cool, et al., ApJ, 682, 919-936, 2008.

34. ”The Milky Way Tomography with SDSS. II. Stellar Metallicity”, Ivezić, Ž., et al., ApJ, 684, 287-325, 2008.

35. ”Light-curve studies of nearby Type Ia supernova with a Multiband Stretch method”, N. Takanashi, et al., MNRAS, 389, 1577-1592, 2008.

36. ”The Sloan Digital Sky Survey-II: Photometry and Supernova Ia Light Curves from the 2005 Data”, J. A. Holtzman, et al., AJ, 136, 2306-2320, 2008.

37. ”Delay Time Distribution Measurement of Type Ia Supernova by the Subaru/XMM-Newton Deep Survey and Implications for the Progenitor”, T. Totani, et al., PASJ, 60, 1327, 2008.

38. ”Discovery of an Unusual Optical Transient with the Hubble Space Telescope”, K. Barbary, et al., ApJ, 690, 1358-1362, 2009.

39. ”Neutrino mass, Dark Matter and Baryon Asymmetry via TeV-Scale Physics without Fine-Tuning”, M. Aoki, et al., Phys. Rev. Lett. 102, 051805, 2009.

40. ”Precision Measurements of Little Higgs Parameters at the International Linear Collider”, E. Asakawa, et al., arXiv:0901.1081 [hep-ph], to be published in Phys. Rev. D.

41. ”Chasing the non-linear evolution of matter power spectrum with numerical resummation method: solution of closure equations”, T. Hiramatsu, et al., Phys. Rev. D79, 103526, 2009.

42. ”Non-linear Evolution of Matter Power Spectrum in Modified Theory of Gravity”, K. Koyama, A. Taruya and T. Hiramatsu, Phys. Rev. D79, 123512, 2009.

43. ”CP Violation in B_s Mixing in the SUSY SU(5) GUT with Right-handed Neutrinos”, J. Hisano, et al., Phys. Lett. B669, 301, 2008.

44. ”Discriminating Electroweak-ino Parameter Ordering at the LHC and Its Impact on LFV Studies”, J. Hisano, et al., JHEP 0906, 044, 2009.

45. ”Formation of intermediate-mass black holes as primordial black holes in the inflationary cosmology with running spectral index”, T. Kawaguchi, et al., MNRAS 388, 1426, 2008.

46. ”Big-Bang Nucleosynthesis and Gravitino”, M. Kawasaki, et al., Phys. Rev. D78, 065011, 2008.

47. ”Electron and Photon Energy Deposition in Universe”, T. Kanzaki, et al., Phys. Rev. D78, 103004, 2008.

48. ”Isocurvature fluctuations in Affleck-Dine mechanism and constraints on inflation models”, S. Kasuya, et al., JCAP 0810, 017, 2008.

49. ”Probing reheating temperature of the universe with gravitational wave background”, K. Nakayama, et al., JCAP 0806, 020, 2008. [arXiv:0804.1827 [astro-ph]].

50. ”Direct/indirect detection signatures of non-thermally produced dark matter”, M. Nagai, et al., Phys. Rev. D78, 063540, 2008. [arXiv:0807.1634 [hep-ph]].

51. ”Non-Gaussianity from isocurvature perturbations”, M. Kawasaki, et al., JCAP 0811, 019, 2008. [arXiv:0808.0009 [astro-ph]].

52. ”Non-Gaussianity from Baryon Asymmetry”, M. Kawasaki, et al., JCAP 0901, 002, 2009. [arXiv:0809.2242 [hep-ph]].

53. ”A General Analysis of Non-Gaussianity from Isocurvature Perturbations”, M. Kawasaki, et al., JCAP 0901, 042, 2009. [arXiv:0810.0208 [astro-ph]].

54. ”Hilltop Non-Gaussianity”, M. Kawasaki, et al., JCAP 0901, 026, 2009. [arXiv:0810.1585 [hep-ph]].

55. ”Positron/Gamma-Ray Signatures of Dark Matter Annihilation and Big-Bang Nucleosynthesis”, J. Hisano, et al., Phys. Rev. D79, 063514, 2009. [arXiv:0810.1892 [hep-ph]].

56. ”Cosmological Moduli Problem from Thermal Effects”, K. Nakayama, et al., Phys. Lett. B670, 434, 2009. [arXiv:0811.0444 [hep-ph]].

57. ”Neutrino Signals from Annihilating/Decaying Dark Matter in the Light of Recent Measurements of Cosmic Ray Electron/Positron Fluxes”, J. Hisano, et al., Phys. Rev. D79, 043516, 2009. [arXiv:0812.0219 [hep-ph]].

58. ”Cosmic Rays from Dark Matter Annihilation and Big-Bang Nucleosynthesis”, J. Hisano, et al., Phys. Rev. D79, 083522, 2009. [arXiv:0901.3582 [hep-ph]].

59. ”Primordial Helium Abundance from CMB: a constraint from recent observations and a forecast”, K. Ichikawa, et al., Phys. Rev. D78, 043509, 2008.

60. ”Probing the Effective Number of Neutrino Species with Cosmic Microwave Background”, K. Ichikawa, et al., Phys. Rev. D78, 083526, 2008.

61. ”Cosmological Constraints on Isocurvature and Tensor Perturbations”, M. Kawasaki, et al., Prog. Theor. Phys. 120, 995, 2008.

62. ”Upperbound on Squark Masses in Gauge-Mediation Model with Light Gravitino”, J. Hisano, et al., Phys. Lett. B665, 237, 2008. [arXiv:0804.2957 [hep-ph]].
63. ”A Realistic Extension of Gauge-Mediated SUSY-Breaking Model with Superconformal Hidden Sector”, M. Asano, et al., Phys. Lett. B673, 146, 2009. [arXiv:0810.4606 [hep-ph]].
64. ”Non-Gaussianity from Symmetry”, T. Suyama, et al., JCAP 0809, 007, 2008.
65. ”Primordial Curvature Fluctuation and Its Non-Gaussianity in Models with Modulated Reheating”, K. Ichikawa, et al., Phys. Rev. D78, 063545, 2008.
66. ”Exact gravitational lensing by cosmic strings with junctions”, T. Suyama, Phys. Rev. D78, 043532, 2008.
67. ”Hidden particle production at the ILC”, K. Fujii, et al., Phys. Rev. D78, 015008, 2008.

(b) Conference Papers

1. ”Kamiokande and Super-Kamiokande results on Neutrino Astrophysics”, M. Nakahata, Proceedings of XIII International Workshop on ”Neutrino Telescopes”, Venice, Italy, March 2009.
2. ”Development of a large area gas photomultiplier with GEM/μPIC”, H. Sekiya, Proceedings of the 34th International Conference on High Energy Physics(ICHEP2008) Jul 29 - Aug 5, 2008 - Philadelphia, PA, arXiv:0809.3319
3. ”Search for Nucleon Decay in Super-Kamiokande”, M. Miura, LXIVth Recontres de Moriond, Electroweak interactions and Unified Theories 7-14th March 2009.
4. ”Future possibilities with the J-PARC neutrino beam” T. Kajita, Proceedings of the 23rd International Conference on Neutrino Physics and Astrophysics (Neutrino 2008), Christchurch, New Zealand, 26-31 May 2008. J. Phys. Conf. Ser. 136:022020, 2008.
5. ”Summary of the 3rd International Workshop on a Far Detector in Korea for the J-PARC Beam” T. Kajita, et al., Proceedings of 3rd International Workshop on a Far Detector in Korea for the J-PARC Neutrino Beam, Tokyo, Japan, 30, p151-160, Sep-1 Oct 2007.
6. ”Reach of Future Accelerator and Reactor Neutrino Efforts” T2K Collaboration (Y. Obayashi for the collaboration), Presented at Flavor Physics and CP Violation (FPCP 2008), Taipei, Taiwan, 5-9 May 2008. e-Print: arXiv:0807.4012 [hep-ex].
7. ”T2KK sensitivity with more systematic error terms” K. Okumura, Far Detector in Korea for the J-PARC Neutrino Beam, p57-60.
8. ”Future possibilities with the J-PARC neutrino beam” T. Kajita, Proc. Of the XXIII International Conference on Neutrino Physics and Astrophysics, J. of Physics. Conference Series Vol.136, 022020, 2008.
9. ”Highlights in the T2KK workshops in 2005 and 2006” T. Kajita, et al., Proc. of the 3rd International Workshop on a Far Detector in Korea for the J-PARC Neutrino Beam, pp3-14, 2008.
10. ”Summary of the 3rd International Workshop on a Far Detector in Korea for the J-PARC Beam” T. Kajita, et al., Proc. of the 3rd International Workshop on a Far Detector in Korea for the J-PARC Neutrino Beam, pp151-160, 2008.
11. ”Future of neutrino experiments” T. Kajita, Proc. of the 10th Workshop on High Energy Physics Phenomenology, Pramana 72, pp109-117, 2009.
12. ”Status and prospects for solar and atmospheric neutrinos” T. Kajita, Proc. of the 10th International Workshop on Neutrino Factories, Superbeams, and Betabeams (NuFact08), Proceedings of Science (NuFact08), p006, 2008.
13. ”The implications from CANGAROO-III observations of TeV blazar PKS 2155-304”, K. Nishijima, et al., HIGH ENERGY GAMMA-RAY ASTRONOMY: Proceedings of the 4th International Meeting on High Energy Gamma-Ray Astronomy, AIP Conf. Proc. 1085, 486-489, 2008.
14. ”CANGAROO-III observation of gamma rays from the Galactic Center”, T. Mizukami, et al., HIGH ENERGY GAMMA-RAY ASTRONOMY: Proceedings of the 4th International Meeting on High Energy Gamma-Ray Astronomy, AIP Conf. Proc. 1085, 364-367, 2008.
15. ”Status of CANGAROO-III”, R. Enomoto et al., HIGH ENERGY GAMMA-RAY ASTRONOMY: Proceedings of the 4th International Meeting on High Energy Gamma-Ray Astronomy, AIP Conf. Proc. 1085, 661-663, 2008.

16. ”Proceedings of the 5th Fluorescence Workshop”, El Escorial - Madrid, Spain, 16-20 September 2007

17. ”GRB081203A: Ashra-1 observation of early optical and VHE-neutrino emission”, The Ashra-1 collaboration(Y. Aita, et al.), GCN GRB OBSERVATION REPORT, 8632, 2008.

18. ”MONITORING OF AEROSOLS AND CLOUDS USING AN IMAGING LIDAR BASED ON A HIGH-RESOLUTION, WIDE FIELD-OF-VIEW TELESCOPE”, H. Kuze, et al., The 2008 International Laser Radar Conference (ILRC24), S05P11, Boulder, Colorado, USA, June 23-27, 2008.

19. ”Analysis of primary cosmic ray proton and helium components at the knee energy region with the Tibet hybrid experiment”, The Tibet ASγ Collaboration (M. Amenomori et al.), Proceedings of the 30th International Cosmic Ray Conference, Merida, Mexico, 3-11 July 2007, vol.2, 117-120, 2008.

20. ”Chemical composition of cosmic rays at the knee measured by the Tibet air-shower-core detector”, The Tibet ASγ Collaboration(M. Amenomori et al.), Proceedings of the 30th International Cosmic Ray Conference, Merida, Mexico, 3-11 July 2007, vol.2, 121-124, 2008.

21. ”Future plan for observation of cosmic gamma rays in the 100 TeV energy region with the Tibet air shower array : physics goal and overview”, The Tibet ASγ Collaboration (M. Amenomori et al.), Proceedings of the 30th International Cosmic Ray Conference, Merida, Mexico, 3-11 July 2007, vol.2, 353-356, 2008.

22. ”Future plan for observation of cosmic gamma rays in the 100 TeV energy region with the Tibet air shower array : simulation and sensitivity”, The Tibet ASγ Collaboration (M. Amenomori et al.), Proceedings of the 30th International Cosmic Ray Conference, Merida, Mexico, 3-11 July 2007, vol.2, 357-360, 2008

23. ”A search for 100 TeV celestial gamma rays with the Tibet air shower array and a future prospect”, The Tibet ASγ Collaboration (M. Amenomori et al.), Proceedings of the 30th International Cosmic Ray Conference, Merida, Mexico, 3-11 July 2007, vol.2, 575-578, 2008.

24. ”Seven-year observation of multi-TeV gamma rays from the Crab Nebula with the Tibet air shower array”, The Tibet ASγ Collaboration (M. Amenomori et al.), Proceedings of the 30th International Cosmic Ray Conference, Merida, Mexico, 3-11 July 2007, vol.2, 799-802, 2008.

25. ”Search for pulsed multi-TeV gamma rays from the Crab pulsar with the Tibet III air shower array”, The Tibet ASγ Collaboration (M. Amenomori et al.), Proceedings of the 30th International Cosmic Ray Conference, Merida, Mexico, 3-11 July 2007, vol.2, 783-786, 2008.

26. ”Gamma-hadron separation of parent particles of air showers above several 10 TeV energies using Tibet-III air-shower array”, The Tibet ASγ Collaboration (M. Amenomori et al.), Proceedings of the 30th International Cosmic Ray Conference, Merida, Mexico, 3-11 July 2007, vol.2, 583-583, 2008.

27. ”Study of discrimination between cosmic gamma rays and protons at multi-TeV energies with the Tibet air shower array”, The Tibet ASγ Collaboration (M. Amenomori et al.), Proceedings of the 30th International Cosmic Ray Conference, Merida, Mexico, 3-11 July 2007, vol.3, 1493-1493, 2008.

28. ”The cosmic ray all-particle spectrum in the wide energy range from 10^{14} eV to 10^{17} eV observed with the Tibet-III air shower array”, The Tibet ASγ Collaboration (M. Amenomori et al.), Proceedings of the 30th International Cosmic Ray Conference, Merida, Mexico, 3-11 July 2007, vol.4, 103-106, 2008.

29. ”Zenith angle dependence of the size spectrum of air showers around the knee observed with the Tibet air shower array”, Tibet ASγ Collaboration (M. Amenomori et al.), Proceedings of the 30th International Cosmic Ray Conference, Merida, Mexico, 3-11 July 2007, vol.4, 99-102, 2008.

30. ”Sun’s Shadow in the Solar Cycle 23 Observed with the Tibet Air Shower Array and Comparison with Simulation Studies”, Tibet ASγ Collaboration (M. Amenomori et al.), Proceedings of the 30th International Cosmic Ray Conference, Merida, Mexico, 3-11 July 2007, vol.5, 529-532, 2008.

31. ”Implication of the sidereal anisotropy of 5 TeV cosmic ray intensity observed with the Tibet III air shower array”, Tibet ASγ Collaboration (M. Amenomori et al.), Proceedings of the 30th International Cosmic Ray Conference, Merida, Mexico, 3-11 July 2007, vol.5, 593-596, 2008.

32. ”Study on TeV gamma Ray Emission from Cygnus Region Using the Tibet Air Shower”, Tibet ASγ Collaboration (M. Amenomori et al.), Proceedings of the 30th International Cosmic Ray Conference, Merida, Mexico, 3-11 July 2007, vol.2, 695-698, 2008.

33. ”Two-dimensional observation on TeV Cosmic-ray solar diurnal variation using the Tibet Air Shower Array”, Tibet ASγ Collaboration (M. Amenomori et al.), Proceedings of the 30th International Cosmic Ray Conference, Merida, Mexico, 3-11 July 2007, vol.5, 577-580, 2008.

34. ”The study of Periodic Variation of Cosmic Ray intensity with the Tibet III Air Shower Array”, Tibet ASγ Collaboration (M. Amenomori et al.), Proceedings of the 30th International Cosmic Ray Conference, Merida, Mexico, 3-11 July 2007, vol.5, 609-612, 2008.

35. ”A Monte Carlo study to measure the energy spectra of the primary heavy components at the knee using a new Tibet AS core detector array and a large underground muon detector array”, J. Huang et al., Proceedings of the 30th International Cosmic Ray Conference, Merida, Mexico, 3-11 July 2007, vol.2, 329-332, 2008.

36. ”Tibet Air Shower Array: Results and Future Plan”, Tibet ASγ Collaboration (M. Amenomori et al.), Proceedings of TAUP2007, Sendai, Japan, Journal of Conference Series 120, 062024-1-3, 2008

37. ”Neutralino dark matter in light Higgs boson scenario”, M. Asano, et al., 16th International Conference on Supersymmetry and the Unification of Fundamental Interactions (SUSY08), (16-21 Jun 2008, Seoul, Korea), AIP Conf. Proc. 1078, 566, 2009.

38. ”Measurements of the model parameter in the littlest Higgs model with T-parity”, M. Asano, et al., International Linear Collider Workshop (LCWS08 and ILC08), (16-20 Nov 2008, Chicago, Illinois), arXiv:0901.4863 [hep-ph].

39. ”Charged Lepton-Flavor Violation in Beyond-Standard Models”, J. Hisano, Flavor Physics and CP Violation (FPCP 2008), (Taipei, Taiwan, 5-9 May 2008), arXiv:0807.0149 [hep-ph].

40. ”Supersymmetry and cosmology: Inflation, gravitino and axion”, M. Kawasaki, GRAND UNIFIED THEORIES: CURRENT STATUS AND FUTURE PROSPECTS AIP Conf. Proc. 1015, 226, 2008.

41. ”Inflationary cosmology of axion models in supergravity”, K. Nakayama, AIP Conf. Proc. 1040, 61, 2008.

42. ”Gravitational wave background as a probe of reheating temperature of the universe”, K. Nakayama, et al., AIP Conf. Proc. 1078, 515, 2009.

43. ”Transition of the 11-year solar cycle and its effect on climate change”, H. Miyahara, Proceedings of the symposium on ”Historical Records and Modern Science”, 2008.

44. ”Study on cosmic ray variations using beryllium-10 in Dome Fuji Shallow Ice core”, H. Miyahara, et al., Malt Annual Report, 2008.

45. ”Variation of the solar cycle length during the grand solar minimum in the 4th century B.C. deduced from 14C contents in Japanese camphor tree rings”, K. Nagaya, et al., Summaries of Researches Using AMS at Nagoya University(XX), 2008.

(c) ICRR Reports

1. ICRR-Report-526-2008-1
   ”Search for TeV Gamma-ray Emission from Clusters of Galaxies with CANGAROO-III Imaging Atmospheric Cherenkov Telescopes”
   Ryuta Kiuchi

2. ICRR-Report-527-2008-2 (October 31, 2008)
   ”Non-Gaussianity from isocurvature perturbations”
   Masahiro Kawasaki, Kazunori Nakayama, Toyokazu Sekiguchi, Teruaki Suyama and Fuminobu Takahashi

3. ICRR-Report-528-2008-3 (September 16, 2008)
   ”Non-Gaussianity from Baryon Asymmetry”
   Masahiro Kawasaki, Kazunori Nakayama and Fuminobu Takahashi

4. ICRR-Report-529-2008-4 (October 1, 2008)
   ”A General Analysis of Non-Gaussianity from Isocurvature Perturbations”
   Masahiro Kawasaki, Kazunori Nakayama, Toyokazu Sekiguchi, Teruaki Suyama and Fuminobu Takahashi

5. ICRR-Report-530-2008-5 (October 9, 2008)
   ”Hilltop Non-Gaussianity”
   Masahiro Kawasaki, Kazunori Nakayama and Fuminobu Takahashi

6. ICRR-Report-531-2008-6 (October 10, 2008)
   ”Positron/Gamma-Ray Signatures of Dark Matter Annihilation and Big-Bang Nucleosynthesis”
   Junji Hisano, Masahiro Kawasaki, Kazunori Kohri and kazunori Nakayama

7. ICRR-Report-532-2008-7 (February 6, 2009)
   ”A Realistic Extension of Gauge-Mediated SUSY Breaking Model with Superconformal Hidden Sector”
   Masaki Asano, Junji Hisano, Takashi Okada, and Shohei Sugiyama

8. ICRR-Report-533-2008-8 (November 4, 2008)
   ”Cosmological Moduli Problem from Thermal Effects”
   Kazunori Nakayama and Fuminobu Takahashi

9. ICRR-Report-534-2008-9 (January 21, 2009)
   ”Precision Measurements of Little Higgs Parameters at the International Linear Collider”
   Eri Asakawa, Masaki Asano, Keisuke Fujii, Tomonori Kusano, Shigeki Matsumoto, Rei Sasaki, Yosuke Takubo and Hitoshi Yamamoto

10. ICRR-Report-535-2008-10 (December 17, 2008)
    ”Neutrino Signals from Annihilating/Decaying Dark Matter in the Light of Recent Measurements of Cosmic Ray Electron/Positron Fluxes”
    Junji Hisano, Masahiro Kawasaki, Kazunori Kohri and Kazunori Nakayama

11. ICRR-Report-536-2008-11 (January 23, 2009)
    ”Cosmic Rays from Dark Matter Annihilation and Big-Bang Nucleosynthesis”
    Junji Hisano, Masahiro Kawasaki, Kazunori Kohri, Takeo Moroi and Kazunori Nakayama

12. ICRR-Report-537-2008-12 (February, 2009)
    ”Search for Nucleon Decay into Charged Antilepton plus Meson in Super-Kamiokande”
    Haruki Nishino

13. ICRR-Report-538-2008-13 (February 9, 2009)
    ”Study of Non-Standard Neutrino Interactions with Atmospheric Neutrino Data in Super-Kamiokande”
    Mitsuka Gaku

D. Doctoral Theses

1. ”Study of Non-Standard Neutrino Interactions with Atmospheric Neutrino Data in Super-Kamiokande”,
   G. Mitsuka,
   Ph.D Thesis, Mar. 2009.

2. ”Search for Nucleon Decay into Charged Antilepton plus Meson in Super-Kamiokande”,
   H. Nishino,
   Ph.D Thesis, Mar. 2009.

3. ”Search for TeV Gamma-Ray Emission from the Supernova Remnant W44 with the CANGAROO-III Telescopes”,
   Yohei Yukawa,
   Ph.D. Thesis, Mar. 2009.

E. Public Relations

(a) ICRR News

ICRR News is a newspaper published quarterly in Japanese to inform the Institute's activities. This year's editors were H.Sagawa. It includes :

1. reports on investigations by the staff of the Institute or made at the facilities of the Institute,
2. reports of international conferences on topics relevant to the Institute's research activities,
3. topics discussed at the Institute Committees,
4. list of publications published by the Institute [ICRR-Report, ICRR-Houkoku (in Japanese)],
5. list of seminars held at the Institute,
6. announcements,
7. and other items of relevance.

The main topics in the issues in 2008 fiscal year were:

No.66 (Jun 6, 2008)

- Address from new director of ICRR, Takaaki Kajita.
- Address from ex-director of ICRR, Yoichiro Suzuki.

No.67 (Nov 30, 2008)

- XMASS experiment, Yoichiro Suzuki.
- Detection for eigenfrequency of the Earth, Yoshiaki Tamura.
- Commemoration about ex-director of ICRR, Yoji Totsuka, Takaaki Kajita.
- Commemoration about Yoji Totsuka, Masayuki Nakahata.
- Report on ICRR open campus 2008, Hideo Itoh.
- Announcements.
- Self-introduction/Staff reassignment.
- ICRR-Seminar/Report.

(b) Public Lectures

- "Science Cafe for Novel Prize of Physics 2008"
  Mar 1 2009, Kashiwa, Chiba,
  Hideo Itoh(ICRR, University of Tokyo)
- "Neutrino on Elementary Particles"
  Jan 12 2009, Saga,
  Hideo Itoh(ICRR, University of Tokyo)
- "Concern between elementary particles and the universe"
  Dec 12 2008, Mitaka, Tokyo,
  Hideo Itoh(ICRR, University of Tokyo)
- "Pioneer of Elementary Particle Physics and Advanced Study of the one"
  Jan 25 2009, Daiba, Tokyo,
  Hideo Itoh(ICRR, University of Tokyo)

- ”Modern Picture of the Universe”
  Mar 15 2009, Higashi-Nakano, Tokyo,
  Hideo Itoh(ICRR, University of Tokyo)
- ”About Novel Prize of Physics 2008”
  Mar 15 2009, Higashi-Nakano, Tokyo,
  Hideo Itoh(ICRR, University of Tokyo)
- ”What’s symmetry? -About Novel Prize 2008”
  Nov 15 2008, Matsue, Shimane,
  Hideo Itoh(ICRR, University of Tokyo)
- ”Concern between elementary particles and the universe”
  Mar 14 2009, Matsue, Shimane,
  Hideo Itoh(ICRR, University of Tokyo)
- ”Searching the universe using small small particles”
  Apr 18 2008, Kashiwa, Chiba,
  Hideo Itoh(ICRR, University of Tokyo)
- ”Message from the universe”
  Oct 18 2008, Katsushika, Tokyo,
  Hideo Itoh(ICRR, University of Tokyo)
- ”How to search the cosmic ray”
  Jan 15 2009, Yubari, Hokkaido,
  Hideo Itoh(ICRR, University of Tokyo)
- ”Picture of the universe using elementary particles and cosmic ray”
  Apr 18 2008, Kashiwa, Chiba,
  Hideo Itoh(ICRR, University of Tokyo)
- ”Picture of the universe using elementary particles and cosmic ray”
  Jul 18 2008, Atsugi, Kanagawa,
  Hideo Itoh(ICRR, University of Tokyo)
- ”Public Lecture on Neutrino”,
  April 12 2008, Kashiwa, Chiba,
  ”Studying mysteries of neutrino using neutrino beam”, Tsuyoshi Nakaya (Kyoto University).
  ”Neutrino is dominating the universe -Role of neutrino in cosmology-”, Naoshi Sugiyama (ICRR, University of Tokyo).

(c) Visitors

KASHIWA Campus (Total: 3 groups, 31 people)

- Chiba Advanced Technology Experience Program
- MEXT Science Partnership Project (SPP): total 2 schools

KAMIOKA Observatory (Total: 136 groups, 2981 people)

- Yumeno Tamago Jyuku (Hida Academy for High School Students)
- MEXT Super Science High School (SSH) project: total 4 schools
- Schools and Universities: total 34 groups
- Others: 97 groups

F. Inter-University Researches

Numbers of Researchers

	Number of Applications	Number of Adoptions	Number of Researchers
Facility Usage			
Kamioka Observatory	39	39	554
Norikura Observatory	10	10	73
Akeno Observatory	4	4	96
Emulsion and Air Shower Facilities in Kashiwa	2	2	19
Low-level Radio-isotope Measurement Facilities in Kashiwa	6	6	35
Gravitational Wave Facilities in Kashiwa	4	4	94
Over Sea Facilities	16	16	153
Other	18	18	241
Collaborative Researches			
Cosmic Neutrino Researches	35	35	502
High Energy Cosmic Ray Researches	45	45	516
Theoretical Researches or Rudimental Researches	9	9	167
Research Center for Cosmic neutrinos	10	10	80
Others			
Conferences	3	3	55
Special Activity on Abroad	0	0	0

Research Titles

1. Energy calibration for Super-Kamiokande
2. Study of solar neutrino energy spectrum
3. Study of simulation for atmospheric neutrino
4. Study of nucleon decay $p \rightarrow \nu K$
5. Study of the low energy solar neutrinos
6. Study of solar neutrino energy spectrum
7. Precise measurement of Day/Night effect for B8 solar neutrinos
8. Sidereal daily variation of 10TeV galactic cosmic-ray intensity observed by the Super-Kamiokande
9. Study for Supernova monitor
10. Development of the new online DAQ system for Super-Kamiokande
11. Study of flavor identification of atmospheric neutrinos
12. Study for the electron neutrino appearance search in the T2K experiment
13. Study in upward-going muons and high energy neutrinos
14. Study of Supernova Relic Neutrinos
15. Search for Nucleon Decay
16. Development of neutrino-nucleus interactions for the precise neutrino oscillation experiment

17. Search for proton decay via $e^+\pi^0$ mode
18. R&D of a 1Mton water Cherenkov Hyper-Kamiokande
19. Study of atmospheric neutrinos and neutrino oscillations
20. Neutrino interaction study using accelerator data
21. R&D of J-PARC-Kamioka Long Baseline Experiment T2K
22. Study for lowering backgrounds of radioisotopes in large volume detectors
23. Direction-sensitive dark matter search experiment
24. Study of purification system for liquid xenon
25. Development of InP detector for measurement of solar ν
26. Design of detector for dark matter search by using simulation
27. Study on absorption and scattering of vacuum ultraviolet light in liquid xenon
28. A study on emission spectrum of liquid xenon
29. Study of ambient gamma-ray and neutron flux at Kamioka Observatory
30. Development of low concentration radon detection system
31. R&D for the Astroparticle Detector by using Liquid Xenon
32. 3-flavor Oscillation study in atmospheric neutrinos
33. Scintillation efficiency for the liquid xenon detector
34. Direct dark matter search with liquid xenon detector
35. Study for double beta decay of 48Ca
36. Study of the formation and the evolution of the Universe with prompt observations of gamma-ray bursts
37. Observation of Galactic Cosmic ray by the Large Area Muon Telescope
38. Observation of the highest energy Solar Cosmic Rays
39. Observation of solar neutrons in solar cycle 24
40. Ecophysiological studies of alpine plants
41. A Study of the Radiation Damage to Polyimide film
42. Space weather observation using muon hodoscope at Mt.Norikura
43. Continuous observation of microbarographs at high mountains
44. Study of particle acceleration in electric field using X and gamma rays from lightning and thunderclouds
45. Observation of nightglow and its reflected and scattered light on the mountain
46. Adaptive strategies in community structure and leaf characteristics of alpine plants related to snow gradient
47. Field test of natural electric power supply at Mt. Norikura-dake
48. Observation of high-energy cosmic-ray electrons with emulsion chambers
49. A study of cosmic ray interactions by hybrid experiment on Mt. Chacaltaya
50. Study of Galactic Diffuse Gamma Rays
51. Observation of TeV gamma-ray spectra from galactic objects
52. Data Analysis of the UHECR data for the Auger Project

53. Basic Study for Cherenkov Telescopes of Next Generation
54. A R&D for a new atmospheric monitoring system
55. Study of the composition of cosmic-rays at the knee
56. CANGAROO-III Observation of gamma-rays in the southern sky
57. Study of the emission mechanism of unidentified TeV gamma-ray source based on the multi-wavelength spectrum
58. Observation with All-sky Survey High Resolution Air-shower detector Ashra
59. Experimental Study of High-energy Cosmic Rays in the Tibet AS γ experiment
60. Development of advanced photon counter for the future IACT
61. Sidereal daily variation of 10TeV galactic cosmic-ray intensity observed by the Tibet air shower array
62. Improvement of characteristics of the image sensor used in Ashra
63. Cosmic ray interactions in the knee and the highest energy regions
64. Bolivian Air Shower Joint Experiment
65. Application of Fast Image-delay Tube to Sky Survey for Cosmic Rays
66. Measurement of the temperature characteristics of YAP for TA fluorescence detectors
67. R&D for the Next Generation VHE Gamma-Ray Telescope
68. Observation of very-high-energy gamma-rays in Australia
69. Composition Study with the Telescope Array Data
70. Development of the optical fiber image transfer system for Ashra
71. A study on variation of interplanetary magnetic field with the cosmic-ray shadow by the sun
72. Workshop on '"High Energy Gamma-ray Astrophysics"
73. Optical observations of transient high-energy sources in the southern sky
74. Search for High Energy Gamma-ray Emission from Star Forming Regions and Theoretical Research
75. Improvement of the CANGAROO-III immediate data analysis system
76. Observation of UHE cosmic rays and TeV gamma rays with Ashra detector
77. Study of absolute energy calibration air shower by compact Electron LINAC
78. Study of radio detection of highest energy cosmic rays
79. Study of Extremely-high Energy Cosmic Rays by Telescope Array
80. Study on High Energy Cosmic-Ray source by Observation Using Long Duration Balloon
81. R&D and Design of large-scale cryogenic gravitational wave telescope (IX)
82. Study of effective thermal shielding method for the LCGT cryostat
83. Development of Sapphire Mirror Suspension for LCGT (IV)
84. Development of a high-power laser system for CLIO
85. Gravitational Wave Detector in Kamioka (VII)
86. digital Control of CLIO and Its Analysis
87. An research of the Earths free oscillations based on simultaneous observations with a laser strainmeter and a superconducting gravimeter

88. Evaluation of a fiber-coupled laser stabilization system
89. Evolution of the universe and particle physics
90. Deposition Rate variation of natural activities ^{7}Be and ^{210}Pb
91. Continuous Measurement of Underground Laboratory Environment
92. Chemical study for Antarctic micrometeorites
93. Determination of ^{26}Al in small Antarctic meteorite samples
94. Comprehensive Researches on Cosmic Dusts
95. Detection of time variations for cosmogenic Be-7, Na-22
96. Detection of low level radioisotopes in tree rings
97. Precise calculation of the atmospheric neutrino flux
98. Monte Carlo Simulation Data Generation for the IceCube experiment
99. Neutrino workshop

G. List of Committee Members

(a) Board of Councillors

KAJITA, Takaaki	ICRR, University of Tokyo
FUKUSHIMA, Masaki	ICRR, University of Tokyo
SUZUKI, Yoichiro	ICRR, University of Tokyo
KAWASAKI, Masayuki	ICRR, University of Tokyo
YAMAMOTO, Masayuki	University of Tokyo
HIRAO, Kimihiko	University of Tokyo
TAKASAKI, Tadafumi	KEK
EGUCHI, Toru	YITP, Kyoto university
MIYAMA, Shoken	National Astronomical Observatory
SATO, Fumitaka	Konan University
YAMAZAKI, Toshimitsu	University of Tokyo
MURAKI, Yasushi	Konan University
MIZUTANI, Kouhei	Saitama University
INOUE, Hajime	Institute of Space and Astronautical Science
KOMAMIYA, Yukio	ICEPP, University of Tokyo

(b) Advisory Committee

KAJITA, Takaaki	ICRR, University of Tokyo
TORII, Shoji	Waseda University
KAJINO, Fumiyoshi	Konan University
ITOW, Yoshitaka	STEL, Nagoya University
TERASAWA, Toshio	Tokyo Institute of Technology
SAITOH, Naoto	KEK
NISHIKAWA Koichiro	KEK
KODAMA, Hideo	KEK
AIHARA, Hiroaki	University of Tokyo
FUKUSHIMA, Masaki	ICRR, University of Tokyo
MORI, Masaki	ICRR, University of Tokyo
FUKUGITA, Masataka	ICRR, University of Tokyo
NAKAHATA, Masayuki	ICRR, University of Tokyo
SUZUKI, Yoichiro	ICRR, University of Tokyo
KURODA, Kazuaki	ICRR, University of Tokyo

(c) User's Committee

KAJINO, Fumiyoshi	Konan University
NISHIJIMA, Kyoshi	Tokai University
TORII, Shoji	Waseda University
OGIO, Shoichi	Osaka City University
MATSUBARA, Yutaka	Nagoya University
YOSHIDA, Shigeru	Chiba University
SAKURAI, Takahisa	Yamagata University
MUNAKATA, Kazuki	Shinshu University
OHASHI, Masataka	ICRR, University of Tokyo
HAYATO, Yosinari	ICRR, University of Tokyo
SAGAWA, Hiroyuki	ICRR, University of Tokyo
KANEYUKI, Kenji	ICRR, University of Tokyo
TAKITA, Masato	ICRR, University of Tokyo
HISANO, Junji	ICRR, University of Tokyo

H. List of Personnel

Director KAJITA Takaaki

Vice-Director FUKUSHIMA Masaki

Kamioka Observatory (Neutrino and Astroparticle Division)

Scientific Staff	SUZUKI Yoichiro,	NAKAHATA Masayuki,	MORIYAMA Shigetaka,
	TAKEUCHI Yasuo,	SHIOZAWA Masato,	HAYATO Yoshinari,
	YAMASHITA Masaki,	MIURA Makoto,	OBAYASHI Yoshihisa,
	KOSHIO Yusuke,	KAMEDA Jun,	TAKEDA Atsushi,
	ABE Ko,	SEKIYA Hiroyuki,	YAMADA Satoru,
	NAKAYAMA Shoei,	OGAWA Hiroshi,	KOBAYASHI Takashi
Chief Secretary	KAIZU Satoshi		
Technical Staff	MIZUHATA Minoru,	KANBE Tomio,	KUMAMARU Seiichi
Research Fellow	TAKENAGA Yumiko,	WATANABE Hideki	
Secretary	OKURA Youko,	MAEDA Yukari,	OKADA Eri

Research Center for Cosmic Neutrinos (Neutrino and Astroparticle Division)

Scientific Staff	KAJITA Takaaki,	KANEYUKI Kenji,	OKUMURA Kimihiro,
	SAKURAI Yoshihisa		
Technical Staff	SHINOHARA Masanobu		
Research Fellow	SHIMIZU Yuki,	TANIMOTO Naho,	KAJI Hiroshi,
	Athar Mohammad Sajjad		
Secretary	WATANABE Keiko,	KITSUGI Atsuko	

High Energy Cosmic Ray Division

Scientific Staff	FUKUSHIMA Masaki,	MORI Masaki,	
	ENOMOTO Ryoji,	YOSHIKOSHI Takanori,	TAKITA Masato,
	SASAKI Makoto,		
	TAKEDA Masahiro,	HAYASHIDA Naoaki,	SAKURAI Nobuyuki,
	OHISHI Michiko,	OHNISHI Munehiro,	ASAOKA Yoichi
Technical Staff	AOKI Toshifumi,	KOBAYASHI Takahide	
Research Fellow	TOKUNO Hisao,	SHIBATA Tatsunobu,	NONAKA Toshiyuki,
	KAWATA Kazumasa,	KONDO Yoshimi,	HUANG Jing,
	WANG Xiao,	KIUCHI Ryuta	
Secretary	SAWANO Sumiko,	KOKUBUN Yayoi,	YAMAKAWA Toshie,
	TATSUMI Fusako		

AKENO Observatory (High Energy Cosmic Ray Division)

Scientific Staff	SAGAWA Hiroyuki	
Technical Staff	OHOKA Hideyuki,	KAWAGUCHI Masami

Norikura (High Energy Cosmic Ray Division)

Technical Staff	YAMAMOTO Kuniyuki,	AGEMATSU Yoshiaki,	USHIMARU Tsukasa,
	ISHITSUKA Hideki,	SHIMODAIRA Hideaki	

Astrophysics and Gravity Division

Scientific Staff	FUKUGITA Masataka,	KURODA Kazuaki,	KAWASAKI Masahiro,
	OHASHI Masatake,	YASUDA Naoki,	HISANO Junji,
	MIYOKI Shinji,	UCHIYAMA Takashi	
Research Fellow	HIRAMATSU Teruaki,	ASANO Masaki,	SUYAMA Teruaki,
	AOKI Mayumi		
Secretary	KIKUCHI Rie		

Graduate Students

Doctor	IKEDA Daisuke,	KIDO Eiji,	TAKETA Akimichi,
	YUKAWA Yohei,		
	SAKO Takashi,		
	AITA Yuichi,	NODA Koji,	CHONAN Tsutomu,
	UESHIMA Kota,	IIDA Takashi,	MITSUKA Gaku,
	NISHINO Haruki,	ISHIHARA Chizue,	IKEDA Motoyasu,
	McLACHLAN Thomas Fukuei,		
	AGATSUMA Kazuhiro,		
	KANZAKI Toru,	TAKAYAMA Tsutomu,	SEKIGUCHI Toyokazu,
	NAKAYAMA Kazunori,		
	KONISHI Kohki		
Master	YAMAKAWA Yuichi,		
	KUNISAWA Toshiki,	RYOKI Shinichi,	NAKAYAMA Koichi,
	NAGAI Yuichiro,	INOUE Daisuke,	
	HIGASHI Yuhei,		
	UENO Koh,	NAKAJIMA Yuha,	KOHZUMA Yuki,
	YOKOZAWA Takaaki,		
	SAITOH Takanori,	MORIOKA Tomoko,	
	SAIKAWA Kenichi,	MIYAMOTO Koichi,	ARASHIBA Soichi,
	OKADA Takashi,	KAWAKAMI Etsuko,	YAMAMOTO Yusuke,
	YOKOZAWA Takaaki,	RYO Masaki	

Administration Division

Scientific Staff	ITOH Hideo		
Administrative Staff	NAGANEO Nobuyoshi,	SETO Mikako,	SASADA Takaaki,
	IRIE Makoto,	MATSUMOTO Kenichi,	ARIDOME Ryutaro,
	AKIYAMA Makiko,	NISHIMORI Tomoe,	YAMAGUCHI Akiko,
	SAITO Akiko,	MARUMORI Yasuko,	
	IIDA Nobuyuki		